University of South Florida

DIGITAL COMMONS
@ UNIVERSITY OF SOUTH FLORIDA

Digital Commons @ University of South Florida

USF Tampa Graduate Theses and Dissertations

USF Graduate Theses and Dissertations

10-7-2009

Theoretical Studies of Long-Range Interactions in Quasi-One Dimensional Cylindrical Structures

Kevin Tatur
University of South Florida

Follow this and additional works at: https://digitalcommons.usf.edu/etd

 Part of the American Studies Commons

Scholar Commons Citation

Tatur, Kevin, "Theoretical Studies of Long-Range Interactions in Quasi-One Dimensional Cylindrical Structures" (2009). *USF Tampa Graduate Theses and Dissertations.*
https://digitalcommons.usf.edu/etd/43

This Dissertation is brought to you for free and open access by the USF Graduate Theses and Dissertations at Digital Commons @ University of South Florida. It has been accepted for inclusion in USF Tampa Graduate Theses and Dissertations by an authorized administrator of Digital Commons @ University of South Florida. For more information, please contact digitalcommons@usf.edu.

Theoretical Studies of Long-Range Interactions in Quasi-One Dimensional Cylindrical Structures

by

Kevin Tatur

A dissertation submitted in partial fulfillment
of the requirements for the degree of
Doctor of Philosophy
Department of Physics
College of Arts and Sciences
University of South Florida

Major Professor: Lilia M. Woods, Ph.D.
Inna Ponomareva, Ph.D.
Sagar A. Pandit, Ph.D.
Norma A. Alcantar, Ph.D.

Date of Approval:
October 7, 2009

Keywords: Electromagnetic interactions, Casimir force, nanotechnology, mathematical methods, carbon nanotubes

© Copyright 2009, Kevin Tatur

Dedications

To my mother, father, Meenakshi and Tanushri.

ACKNOWLEDGMENTS

I would like to thank my family for all their support, love and encouragement throughout my Ph.D. studies. I had the pleasure of working and learning at the side of my Ph.D. advisor, Dr. Lilia Woods, who was an inspiration and a mentor during my studies. I would like to express my gratitude towards her for her patience and tutelage. I would also like to thank Dr. Sagar Pandit, Dr. Inna Ponomareva, Dr. Norma Alcantar and Dr. Razvan Theodorescu for agreeing to be in Ph.D. committee. Lastly, I would like to thank God for helping me achieve what I had set out to accomplish.

TABLE OF CONTENTS

LIST OF FIGURES

THEORETICAL STUDIES OF LONG-RANGE INTERACTIONS IN QUASI-ONE DIMENSIONAL CYLINDRICAL STRUCTURES

Kevin Tatur

ABSTRACT

Casimir forces originating from vacuum fluctuations of the electromagnetic fields are of increasing importance in many scientific and technological areas. The manifestations of these long-range forces at the nanoscale have led to the need of better understanding of their contribution in relation to the stability of different physical systems as well as the operation of various technological components and devices. This dissertation presents mathematical and theoretical methods to calculate the Casimir interaction in various infinitely long cylindrical nanostructures. A dielectric-diamagnetic cylindrical layer immersed in a medium is first considered. The layer has a finite thickness characterized with specific dielectric and magnetic properties. Another system considered is that of perfectly conducting concentric cylindrical shells immersed in a medium. The electromagnetic energy between two infinitely long straight parallel dielectric-diamagnetic cylinders immersed in a medium is also considered. The mode summation method is used to calculate the Casimir energy of all these systems. The energy dependence on the cylindrical radial curvature and dielectric response of the

cylinders is investigated. The fundamental effects of these long range interactions are studied in the form of exciton-plasmon interactions in carbon nanotubes and this is achieved by looking at the dielectric response of carbon nanotubes.

CHAPTER 1

INTRODUCTION AND BACKGROUND

1.1 Long Range Dispersion Forces

Long range dispersion forces are forces that originate from the electromagnetic interaction between electrically neutral objects with no permanent electric and/or magnetic moments and are quantum mechanical in nature [1-6]. H.B.G. Casimir was the first to explain the consequences of electromagnetic zero-point energy in real macroscopic objects [7]. He predicted the attraction between a pair of neutral, parallel conducting plates in vacuum. This attraction was a consequence of electromagnetic field fluctuations in vacuum and referred as the now well-known Casimir effect. The advent of dispersion forces is regarded as one of the most important achievements in quantum electrodynamics (QED), where the origin of the forces is explained by the ground-state (zero-point) fluctuations. These long range dispersion forces manifest themselves as van der Waals, Casimir-Polder, Casimir-Lifschitz, and Casimir forces.

The concept of long range dispersion forces was first explained by the Lifschitz's theory of the van der Waals forces [1] by considering objects as a distribution of neutral, polarizable atoms. By surface integration the contribution of all atoms on the object was obtained. However, dispersion forces are not additive and this prevents objects to be

treated as composed of elementary constituents. Although the Casimir effect can be explained by Lifschitz's theory of the van der Waals forces, modern quantum field theory offers a more basic explanation from first principles of the long range forces, due to a change of the vacuum energy. In other words, a deviation of the zero-point energy caused by the presence of boundaries gives rise to Casimir forces. The zero-point energy investigations have led to the physical vacuum energy of a quantized field to be calculated as the difference between the zero-point energy corresponding to the vacuum configuration with constraints and the free vacuum configuration with no constraints [1].

Dispersion forces exist on different scales and levels. For example, properties of weakly bound molecules are affected by dispersion forces on a microscopic level [8,9]. On a macroscopic level, properties of solids and liquids are influenced by dispersion forces [10-12]. Capillarity and flocculation are examples of such effects where atom-surface dispersion interactions influence atoms-surface properties, such as the wetting properties of liquids on surfaces [13-15]. In cosmology, the formation of planets around stars is a consequence of dust aggregation that is initiated by dispersion forces [16]. Dispersion forces have also become of significant importance to science and technology, predominantly nanotechnology. As devices are fabricated on the micron and submicron scale, the long range dispersion forces become more pronounced in this process of miniaturization. There are two sides to the importance of long range dispersion forces in nanotechnological devices. On one hand, the stability of many nanostructured materials relies on these long range forces. Cylindrically wrapped graphene sheets in carbon

nanotubes and boron nitride layers in boron nitride nanotubes are examples of such materials [17-19]. In addition, oscillating carbon nanotubes or buckyballs inside a stationary carbon nanotube have been demonstrated and related to those long range forces [20,21]. Also, with the advent of nanostructured devices and the increase in the number of experiments performed to demonstrate the Casimir effect, there is now the means to improve our fundamental knowledge and studies of long-range dispersion forces in non-trivial geometries as well as studying how these forces manifest themselves in practical devices. On the other hand, dispersion forces can become a hindrance and cause drastic effects causing undesired and permanent sticking of parts in nanostructures [22-24]. Micro- and nano electro-mechanical systems (MEMS and NEMS) are examples of such devices where the Casimir force can cause components to collapse and stick to one another and thereby resulting in the machines behaving erratically, a phenomenon called stiction.

Dispersion forces play a very important role in biology. These forces are found to be responsible for the interaction of molecules with cell membranes and for cell adhesion driven by mutual cell-membrane interactions [25]. The stability of hydrocarbon cylinders, viruses, muscle protein, and helical assemblies in aqueous solutions has been linked to long range forces. Another key role of long range dispersion forces is the interaction between colloids and solvents. The van der Waals forces have become recognized as the dominant interaction regarding the stability of colloids [26]. As colloids consist of many atoms, there are dispersion forces acting between them. Usually colloids are placed in

solvents and this results in colloid-solvent and solvent-solvent interactions due to dispersion forces. Therefore it can be seen that long range forces play a key role in various fields and as a result it becomes important to understand the behavior of long range interactions in nanostructures.

In this work, the goal is to provide a framework where one can obtain a better understanding of how long range interactions behave in cylindrical nanostructures by taking into account the finite speed of light and dielectric constant of the considered structures. We consider the theoretical studies of long range interactions originating from the electromagnetic field fluctuations in various cylindrical nanostructures, such as, a dielectric-diamagnetic cylindrical layer of finite thickness, multiple concentric cylindrical metallic shells, and between two parallel dielectric-diamagnetic cylinders, all immersed in an infinite medium. Such systems are of particular interest because they can serve as models to study the Casimir interaction in cylindrical tubular structures, such as carbon nanotubes, boron nitride nanotubes, nanowires, DNA, etc…It can also provide a test ground of how curvature effects coupled with dielectric and/or magnetic properties influence the mutual interaction in cylinders. We adapt an intuitive and elegant theoretical model to investigate the long range interactions in cylindrical nanostructures.

1.2 Dissertation Outline

Chapter 1 gives an overview of the motivation of the dissertation. More precisely, a background of how long range dispersion forces influence the behavior of nanostructured devices is given. The origin of long range dispersion forces is discussed and their manifestations in the form of Casimir effects and van der Waals forces are described in Chapter 2. A brief history of the theoretical and experimental milestones of long range interactions is given. The manifestation and use of long range interactions in quasi one-dimensional structures are described in Chapter 3.

In Chapter 4, a brief overview of the theoretical methods that have been used to calculate the Casimir energy of various systems is given and their limitation are explained. A more detailed explanation of the mode summation method is given since it is the method of choice in the Casimir energy calculations in this dissertation.

In Chapter 5, the Casimir energy of a system of a dielectric-diamagnetic cylindrical layer of finite thickness immersed in an infinite medium is calculated. Again, the methodology of applying the mode summation method is described and the techniques of how to remove the divergences are explained. Various limiting cases are investigated and numerical results presented.

Chapter 6 deals with the Casimir energy of N perfectly metallic cylindrical shells immersed in an infinite medium. Again the mode summation approach is explained with

regards to this particular model and limiting cases and numerical results are considered in terms of radial dimensions and material composition.

In Chapter 7, the Casimir energy of two straight and parallel dielectric-diamagnetic cylinders is calculated and the numerical results explained with respect to radial dimensions and material composition.

Chapter 8 describes the fundamental effects of long-range interactions in carbon nanotubes. These interactions exist in the form of exciton-photon coupling that result in exciton-plasmon coupling in small-diameter semiconducting carbon nanotubes. The plasmonic nature of nanotubes is explained in this chapter by investigating the dielectric response of carbon nanotubes using the random-phase approximation. Finally, Chapter 9 gives the conclusion to this dissertation.

CHAPTER 2

THEORETICAL RESULTS AND EXPERIMENTAL OBSERVATIONS

2.1 Important Theoretical Results

The history of dispersion forces can be traced back to the work of D. van der Waals [27] where the weak attractive forces between neutral molecules were introduced. Later, F. London [28] gave a precise formulation of the nature and strength of van der Waals forces as due to the interactions of the fluctuating electric dipole moments of the neutral molecules resulting in the neutral bodies attracting each other. He expressed the potential energy of two isotropic ground-state atoms as follows:

$$U(r) = -\frac{C}{r^6} \tag{2.1}$$

with

$$C = \frac{1}{24\pi^2\varepsilon_0^2}\sum_{kk'}\frac{\left|\langle 0|\hat{\mathrm{d}}|k\rangle\right|^2\left|\langle 0'|\hat{\mathrm{d}}'|k'\rangle\right|^2}{E_k + E_{k'} - (E_0 + E_{0'})} \tag{2.2}$$

where $\hat{\mathrm{d}}$ and $\hat{\mathrm{d}}'$ are the electric dipoles, $|k\rangle$ and $|k'\rangle$ are the eigenstates, E_k and $E_{k'}$ are the energies of the unperturbed atoms [1].

The works of Casimir and Polder addressed a more technical point, the fact that the polarization of the neighboring molecules or atoms induced by a given molecule or atom is delayed as a consequence of the velocity of light being finite. These forces are the long range retarded dispersion van der Waals forces. Casimir and Polder formulated the potential energy corresponding to two atoms separated by a distance *r* and with static polarizabilities α_1 and α_2 as:

$$U(r) = -\frac{23\hbar c}{4\pi}\frac{\alpha_1\alpha_2}{r^7} \tag{2.3}$$

This was then extended to macroscopic scale by performing surface integration to obtain the force per unit area between two neutral, parallel, perfectly conducting metallic plates in vacuum. This extension was done under the hypothesis that the macroscopic plates comprise of a distribution of neutral, polarizable atoms. Another formulation obtained by Casimir and Polder was that of the potential energy of a particle of polarizability α inside a cavity of a perfectly conducting material where the particle was separated from the flat wall by a distance *r*:

$$U(r) = -\frac{3\hbar c}{8\pi}\frac{\alpha}{r^4} \tag{2.4}$$

Two major difficulties arise from the works of London and Casimir and Polder. London's theory did not take into account the finite velocity of propagation of the electromagnetic interaction. Although this had been taken into account in the works of Casimir and Polder, there was still the fact that they viewed macroscopic objects as a

collection of neutral, polarizable atoms. This hypothesis is flawed since van der Waals forces are not additive thereby preventing us to treat macroscopic objects as a collection of neutral atoms. Lifschitz approached this problem by treating matter as a continuum with a well-defined, frequency-dependent dielectric susceptibility.

Lifschitz's theory was a closed theory that could deal with any kind of material bodies and it also explained in a precise way the transition from one power law to the other due to retardation effects. It also contained the formulas of London and that of Casimir and Polder. Lifschitz's expressed the formula for the force per unit area between two parallel infinitely conducting plates separated by a distance *r* as:

$$F = \frac{\hbar c \pi^2}{240 r^4} \tag{2.5}$$

For the case of two identical dielectrics of dielectric constant ε_0, the force per unit area was:

$$F = \frac{\hbar c \pi^2}{240 r^4} \left(\frac{\varepsilon_0 - 1}{\varepsilon_0 + 1} \right)^2 \varphi(\varepsilon_0) \tag{2.6}$$

where $\varphi(\varepsilon_0)$ is a function which has the following behavior for $\varepsilon_0 \to \infty$:

$$\varphi(\varepsilon_0) \approx 1 - \frac{1.11}{\sqrt{\varepsilon_0}} \ln \frac{\varepsilon_0}{7.6} \tag{2.7}$$

For the case of a metal and a dielectric of constant ε_0, the force per unit area is:

$$F = \frac{\hbar c \pi^2}{240 r^4} \left(\frac{\varepsilon_0 - 1}{\varepsilon_0 + 1} \right) \varphi(\varepsilon_0) \tag{2.8}$$

The important point about Lifschitz's theory is that the only information required to calculating the dispersion force is that of the dielectric properties of the body, in particular the dielectric susceptibility as a function of frequency.

2.2 Experimental Observations

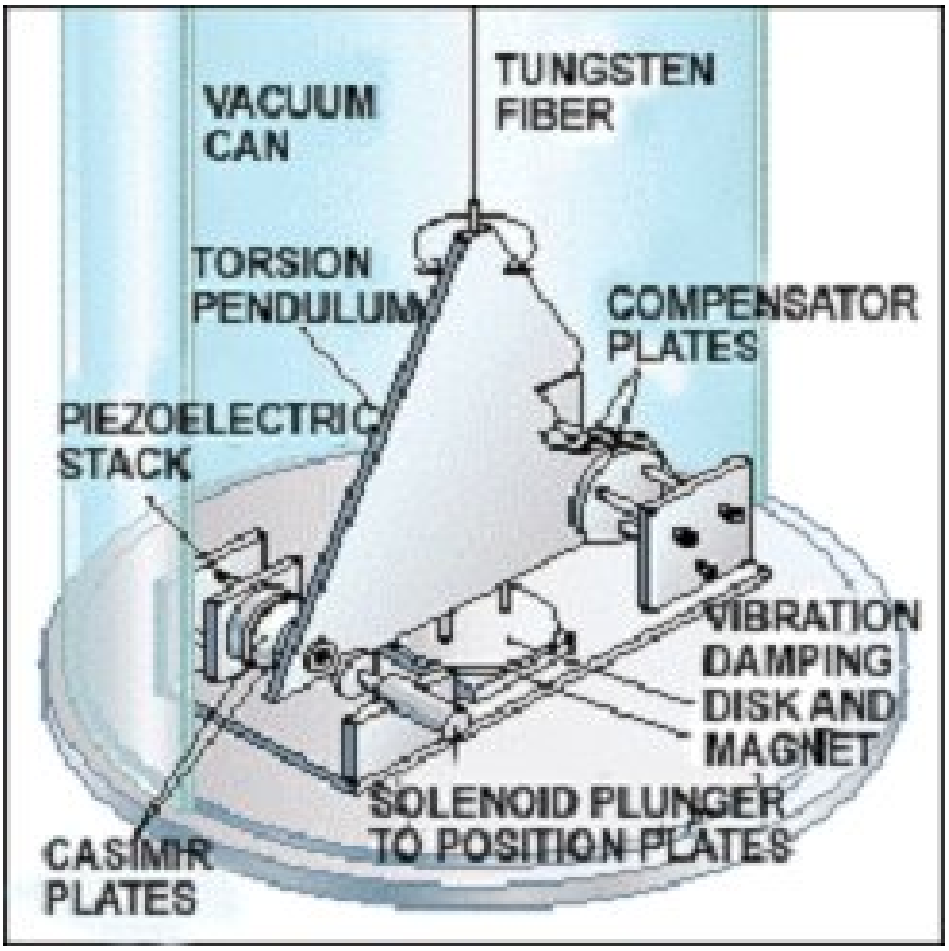

Figure 2.1 Schematic of Lamoreaux's experiment [29].

Although the Casimir effect was first proposed in 1948, its first experimental observation was shown by S. K. Lamoreaux in 1997 [29]. Very few experiments had been performed before to verify the Casimir effect mostly due to difficulty in keeping two plates parallel with each other. Also there was a lack of sensitive equipments available at the time to measure the Casimir force. Since those early days, sophisticated equipment has made it much easier to study the Casimir effect and a new generation of experiments and measurements began in 1997 with Lamoreaux. The experimental setup is shown in Figure 2.1. A gold coated spherical lens of 4cm diameter is brought close to a flat plate by means of a piezo stack. The flat plat is mounted on one arm of the torsion balance. The other arm of the torsion balance formed the central electrode of a pair of parallel plate capacitors. By applying voltages to the capacitors the restoring force required to compensate for any torque in the torsion balance could be measured, as a measure of the Casimir force. The Casimir force was measured by applying the voltage to the piezo stack through discrete and constant steps and at each step, the restoring force was measured. The relative displacement between the plates was measured as a function of the discrete steps by using a laser interferometer. It was found that the average displacement per 5.75 volt step was about 0.75μm and it was ensured that the system was in equilibrium between each measurement. The piezo stacks gave very accurate results for the relative plate separation and the absolute plate separation was determined by measuring the residual electrical attraction between the plates as a function of separation. The experimental results agreed with the theory to a level of 5%. The closest approach

between the plates was found to be 0.6μm and the experimental Casimir force measurements are shown in Figure 2.2.

Inspired by Lamoreaux's breakthrough, Mohideen and Roy performed an important experiment to estimate the Casimir force using atomic force microscope [30]. The experimental setup is shown in Figure 2.3 where the force between an aluminium coated polystyrene sphere 200μm in diameter and an optically polished flat sapphire disk, also aluminium coated, was measured by the deflection of a laser beam. An atomic force microscope (AFM) was used to measure the force between the sphere and plate and in the AFM, the force was measured by the deflection of its tip. A force on the sphere would cause the laser beam to be reflected from the cantilever on which the sphere is mounted due to deflection, and the position of the reflected beam determined by the output of a pair of photodiodes. A piezo stack is used to bring the flat disk close to the sphere in 3.6 nm steps. The Casimir force measurements obtained are shown in Figure 2.4. Here, the experimental results agreed with the theory to 1% when the sphere was brought to within 0.1μm to the plate. Other experimental demonstrations of the Casimir energy have been performed using atomic force microscope and a good review is available in references [31-36].

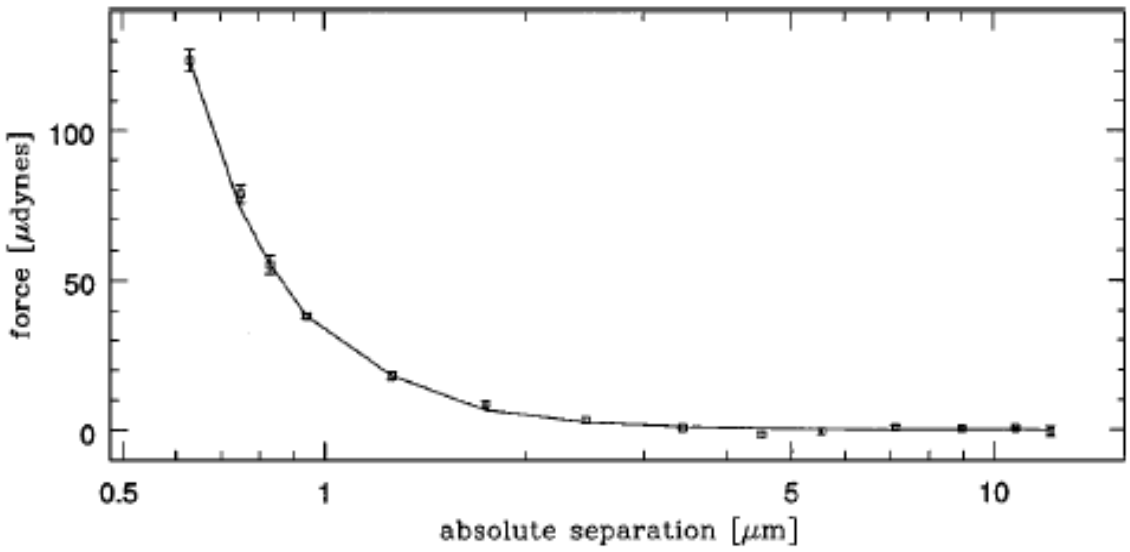

Figure 2.2 Measured force as a function of absolute separation [29].

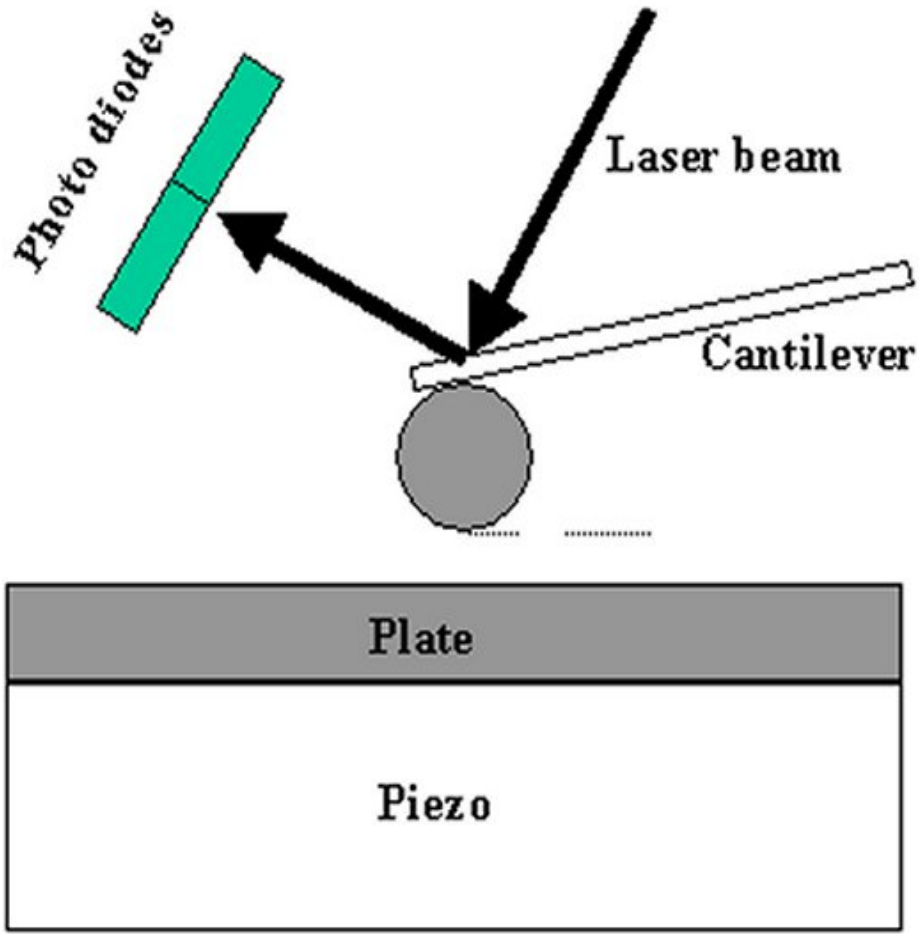

Figure 2.3 Schematic of Mohideen and Roy's experiment [30].

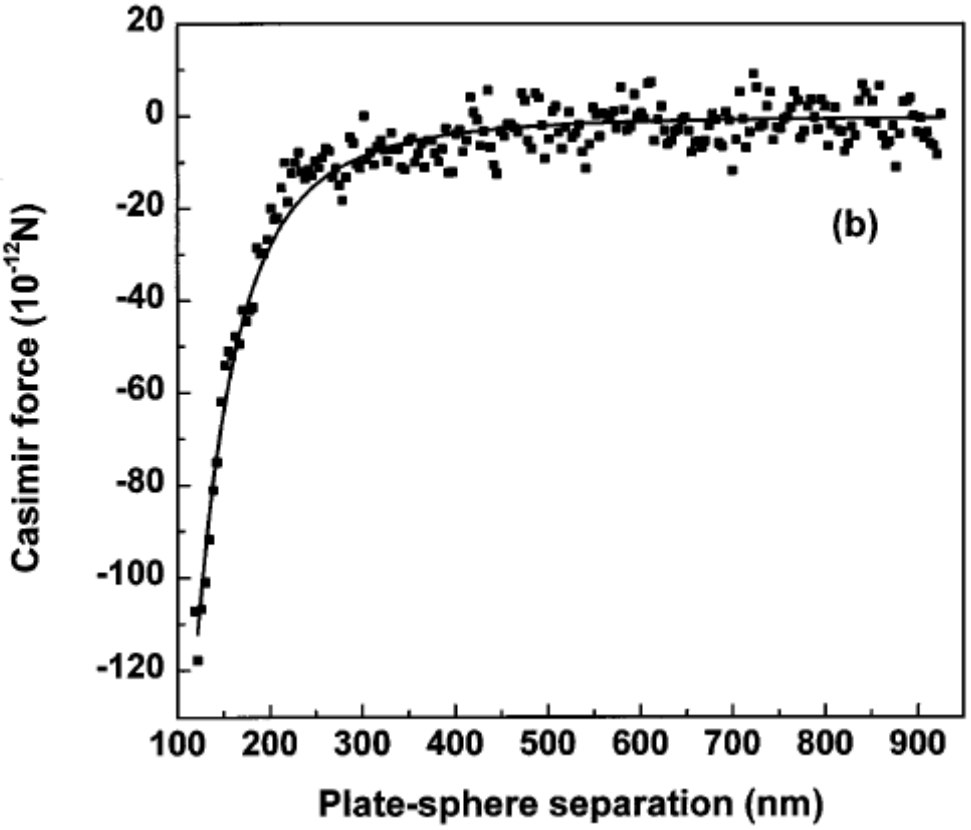

Figure 2.4 Measured Casimir force as a function of plate-sphere separation [30].

The first manifestation of the Casimir effect in micro-electromechanical sytems was demonstrated experimentally by Chan et al. at Bell Labs Lucient Technologies where they demonstrated the interaction of the Casimir force with a MEMS device in 2001 [37]. By bringing a 200 μm diameter gold coated sphere close to a polysilicon plate suspended 2 μm above a substrate, on thin torsional rods, they were able to rotate the plate when the sphere came to within a few 100 nm. The schematic of this experiment is shown in Figure 2.5. The attraction between the polysilicon plate and the sphere results in a torque that rotates the plate about the torsional rods. The capacitance between the plate and electrodes placed underneath the plate allows the rotation of the plate to be detected. In the presence of an external torque, the plate tilts causing an increase on one of the capacitances and a decrease on the other. This difference in capacitance gives the angle of rotation of the plate in response to the attractive force. The micromachined device is placed on a piezoelectric translation stage with the sphere close to one side of the plate and the plate is brought close to the sphere by extending the piezo. The measured angles of rotation and subsequent Casimir forces are shown in Figure 2.6.

The experiments performed for the Casimir force measurements in various systems have so far reported attractive interactions. However, recently J. N. Munday, F. Capasso and A. Parsegian have been able to demonstrate a repulsive Casimir force [38]. Repulsive Casimir energy has been predicted theoretically [39] but no experimental verifications had been performed until lately. The experimental setup is shown in Figure 2.7. The measurements are performed between a 39.8 μm gold coated sphere attached to

a cantilever and mounted on an atomic force microscope and a large silica plate separated by a fluid, bromobenzene. To detect the bending of the cantilever, light form a super luminescent diode is reflected off the back of the cantilever. An Asylum Research linear variable differential transformer is used to control a piezo column and this enables the sphere to be moved towards the plate. Any interaction between the sphere and the plate will result in the bending of the cantilever which in turn will cause a change in the detector signal that controls the difference in light intensity between the top half and the bottom half of the detector. The difference in signal is found to be proportional the force and repulsion is achieved when the dielectric response of the medium ε_3 is between the dielectric responses of the materials, ε_1 and ε_2, as shown in Figure 2.8.

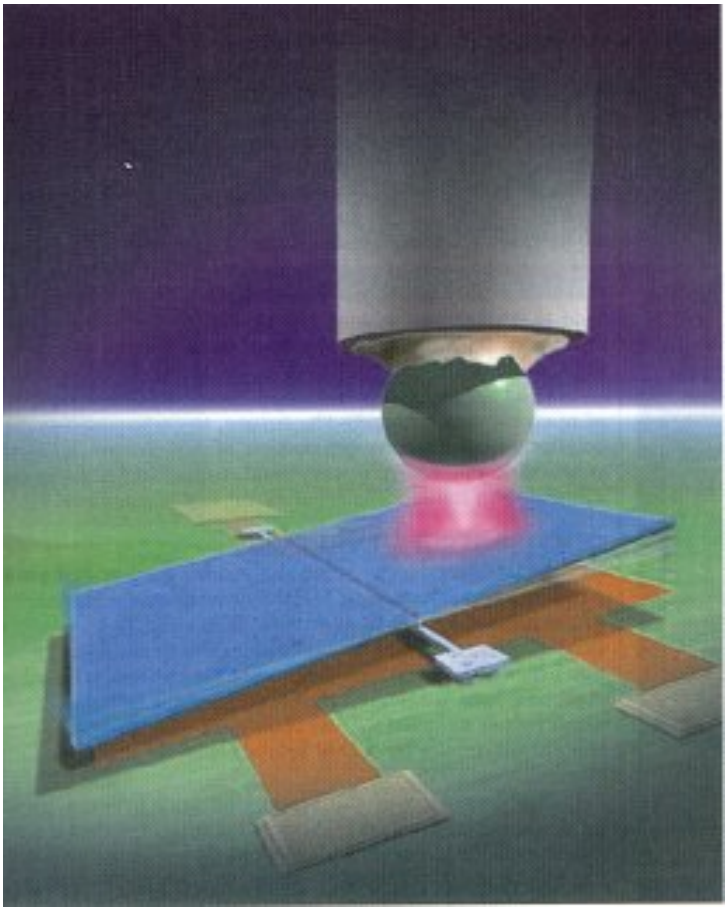

Figure 2.5 Schematic of Chan's experiment [37].

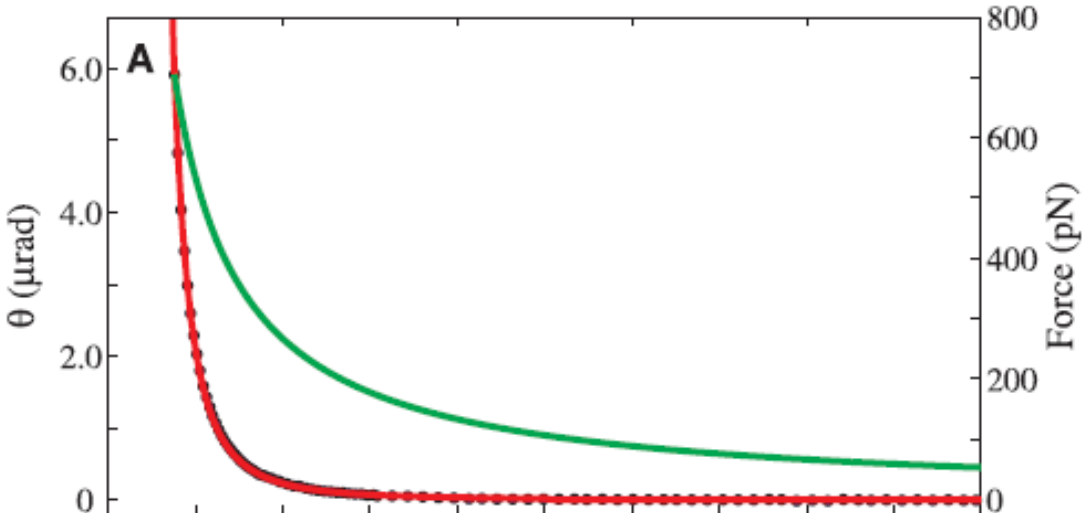

Figure 2.6 Measured angles of rotation of the plate and the Casimir force as a function of plate-sphere separation [37]. The red line represents the Casimir force after taking the roughness of metallic surfaces into account. The green line represents the electrostatic force to demonstrate the operation of the device.

(a)

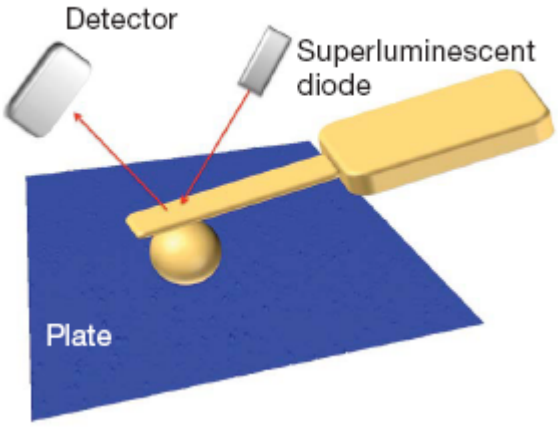

(b)

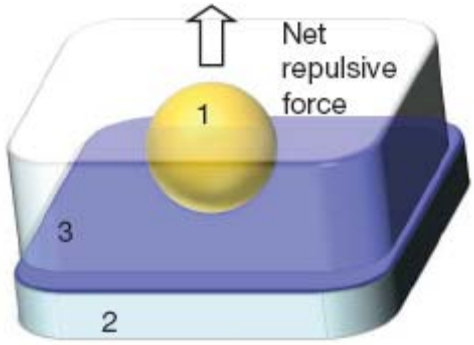

Figure 2.7 (a) Schematic of Munday's experiment. (b) Quantum levitation when $\varepsilon_1 > \varepsilon_3 > \varepsilon_2$ is satisfied. Repulsion is achieved when the dielectric response of the medium ε_3 is between the dielectric responses of the materials, ε_1 and ε_2 [38].

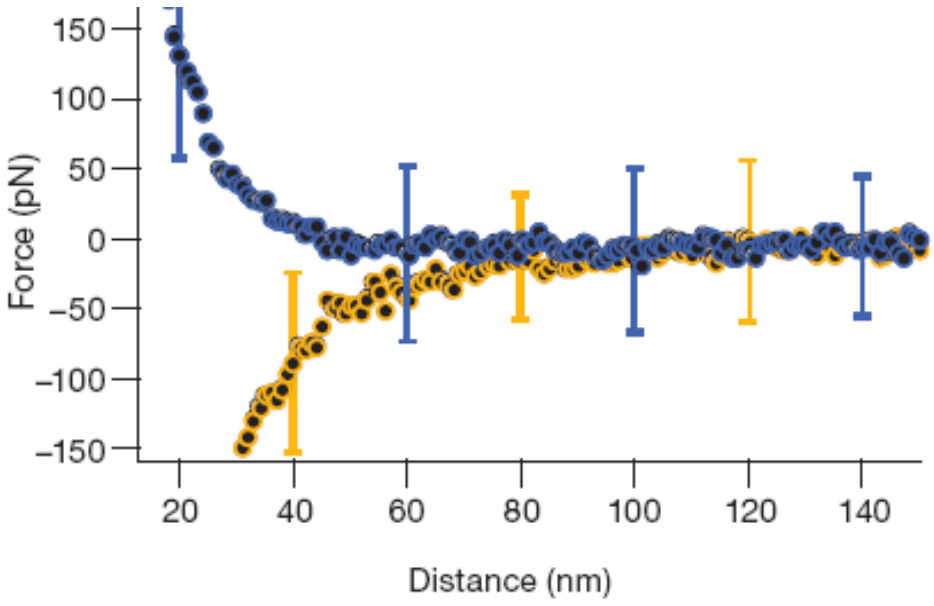

Figure 2.8 Measured Casimir force as a function of sphere-plate distance. The blue (orange) circles represent the force between the gold sphere and a silica (gold) plate in bromobenzene. Repulsion only occurs between the gold sphere and silica plate [38].

CHAPTER 3

QUASI ONE-DIMENSIONAL STRUCTURES

3.1 Cylindrical Nanostructures

The field of nanotechnology is rapidly growing and a multitude of cylindrical nanostructures have become key components in a wide variety of nanotechnological devices. The stability of many nanostructured materials is also found to be influenced by the long range dispersion forces. Cylindrically wrapped graphene sheets in carbon nanotubes, boron nitride layers in boron nitride nanotubes, nanotube bundles, and ropes are examples of such materials [17-19,20,40,41]. Carbon nanotubes have been shown to be applicable in the form of nano-oscillators [20] and nano-rotors [40]. They have also been proposed to be of importance in areas such as energy storage [41] and in optoelectronic device applications areas such as nanophotonics and cavity quantum electrodynamics [42,43].

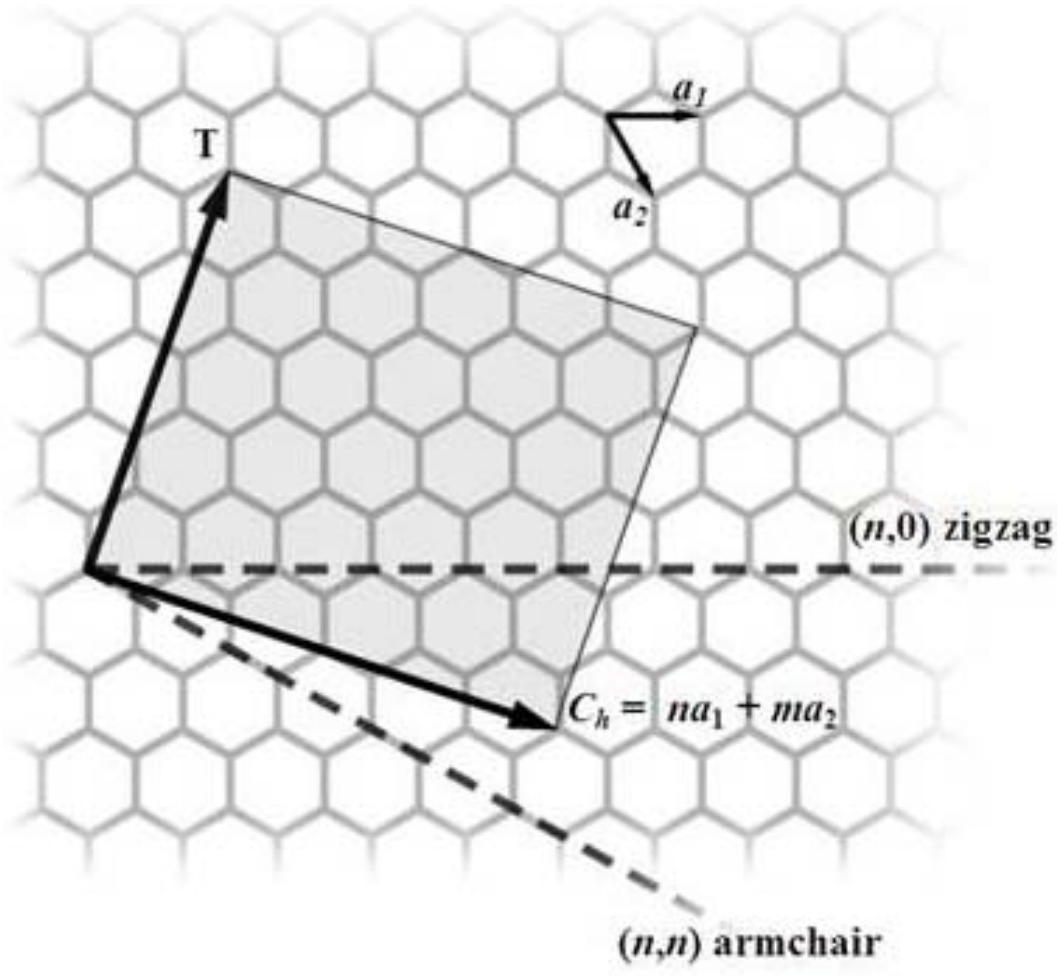

Figure 3.1 CNT structure is fully specified by a two-dimensional chiral vector $C_h = na_1 + ma_2$. T is the translational vector along the axial direction [44].

3.2 Carbon Nanotubes (CNTs) and Devices

A single wall (*n*, *m*) carbon nanotube is a rolled-up graphite sheet into a seamless cylinder, the structure of which is fully specified by a two-dimensional chiral vector $C_h = na_1 + ma_2$, where a_1 and a_2 are primitive lattice vectors of a graphite sheet and *n*, *m* are integers defining the structure of the nanotube as shown in Figure 3.1. A nanotube can be characterized as a metal or semiconductor depending on radius and chirality [45]. They have typical diameters of the order of ~1 nm to ~10 nm and are up to 1 cm in length [42]. As mentioned earlier, carbon nanotubes have been shown to be useful in nanotechnological devices such as nano-oscillators [20]. Nano-oscillators are designed using multiwalled carbon nanotubes, in which one nanotube is found to oscillate in an out of an outer nanotube, a process called telescoping. A nanomanipulator is brought into contact with the inner tube as shown in Figure 3.2 (C) and is spot-welded to the inner tube by means of a short, controlled electric pulse. In this way, the inner tube is brought in and out of the outer tube and thereby the atomic-scale nanotube surface wear and fatigue is studied. Finally, when the nanomanipulator is disengaged from the inner tube, the latter is brought back in by the innertube van der Waals force as seen in Figure 3.2 (E).

A nano-rotor is another device that has been demonstrated to make use of nanotubes [40]. The rotor consists basically of a gold rotor on a nanotube shaft that spins between electrodes. Such motors could be used in optical circuits to redirect light, a process called optical switching. The rotor could also be used to create a microwave

oscillator, and the spinning rotor could be used to mix liquids in microfluidic devices. Since these rotors make use of muti-wall nanotubes, friction between the nested nanotubes can become a major problem to the smooth running of the device and therefore a good understanding of how long range interactions influence those devices in needed.

Carbon nanotubes have also been proposed to be very useful in storing hydrogen atoms on the surface of nanotubes by adsorption [41]. Single-wall and multi-wall nanotubes have been found to be able to store significant amounts of hydrogen at room temperature. The hydrogen molecules are adsorbed on the walls of the nanotubes as shown in Figure 3.3 and interactions between the molecules and the surface rely on long range dispersion forces. It is clear that long range interactions play an important role in various nanotechnological devices which are cylindrical in geometry. Therefore one needs to study and understand the behavior of long-range interactions in cylindrical nanostructures so that there can be improvements leading to more efficient operation of nanotechnological devices. This is the goal of this dissertation where the Casimir energy in various cylindrical nanostructures, such as a dielectric-diamagnetic cylindrical layer, multiple concentric cylindrical metallic shells, and two parallel dielectric-diamagnetic cylinders, all immersed in an infinite medium will be calculated.

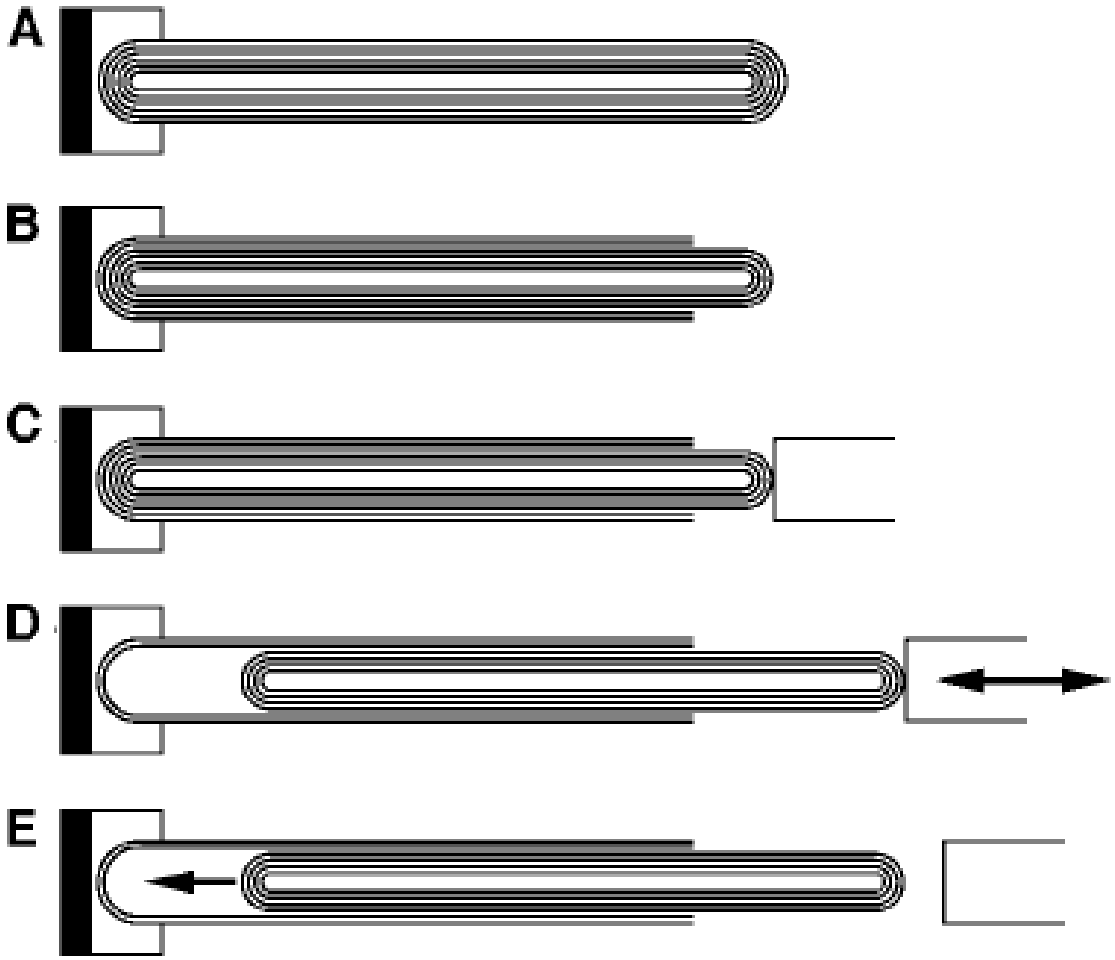

Figure 3.2 Schematic of a nano-oscillator. Figure E shows the inner tube being brought back in by van der Waals interaction [20].

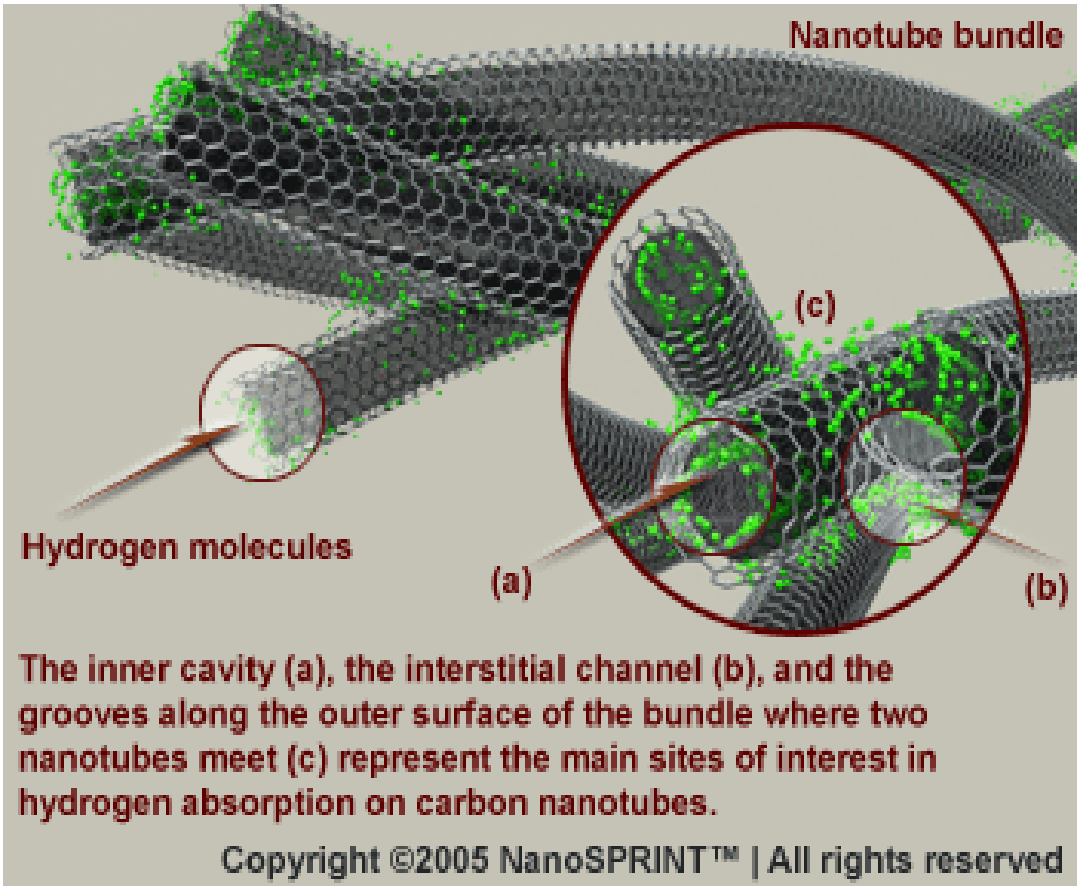

Figure 3.3 Bundles of carbon nanotubes used for hydrogen storage [41].

CHAPTER 4

ZERO POINT ENERGY AND MODE SUMMATION METHOD

4.1 Theoretical Investigations of Zero Point (Casimir) Energy

The importance of the Casimir effect in nanostructured devices and the increase in the number of experiments performed to demonstrate the Casimir effect have led to many theoretical investigations using a wide array of methods. These theoretical investigations have been performed on a variety of geometries and materials that closely resemble nanotechnological devices and components. The Casimir force is found to depend strongly on the shape, geometry/topology and material composition of the boundary or system under consideration. The magnitude and sign of the energy is found to change according to the geometry, topology and type of material constituting the system.

Depending on the system, the Casimir energy can be positive (repulsive), negative (attractive), or even zero. For systems in Ref. [7,27,46,47], the energy was found to be attractive. Similarly, for a metallic conducting cylindrical shell and eccentric metallic cylinders, the energy is also found to be attractive [3,5,6]. However, for a dielectric ball, the energy was calculated to be repulsive [48] and for a dielectric cylinder the energy came out to be zero [3,5]. There is an interesting case where the sign of the energy changes as a function of the dimensions of a box [49,50]. For a media of excited atoms,

the Casimir energy can be repulsive or attractive depending on the resonance frequency [51] and in the case of anisotropic and permeable rectangular plates, the force is repulsive [52].

By altering the material composition of the nano-structures, the sign of the Casimir force can be switched [38, 53]. It has been predicted that the interaction between planar materials immersed in a medium can be repulsive if the value of the dielectric constant of the medium is between the values of the dielectric constants of the materials [39]. Recent measurements of the Casimir force between a large sphere and a plate covered with a layer of silica, for which this condition for the dielectric properties is satisfied, demonstrate that the interaction can be repulsive [38]. Metamaterials can be used to modify the Casimir energy from attractive to repulsive by placing them between two conducting plates [38]. This can lead to a phenomenon called quantum levitation, where the repulsive Casimir force causes an object to "float" or levitate on top of the left-handed material. This can significantly reduce friction in nanostructured devices (MEMS and NEMS) and resulting in a smoother and more efficient operation of devices.

4.2 Overview of Theoretical Methods

There has been a variety of theoretical methods used to calculate long range forces in non-planar geometries. One of the methods used involved pairwise integration. The potential energies of interaction between two parallel, infinitely long carbon nanotubes of the same diameter in various arrangements were computed by making use

of pairwise integration [54]. A continuous distribution of atoms on the tube surface is assumed and the Lennard-Jones (LJ) carbon-carbon potential was used. Although this method was used to calculate the van der Waals interactions in graphitic structures for various configurations of C_{60} molecules interacting with carbon single walled nanotubes, it was flawed due to the fact that van der Walls energy is not additive.

Long range forces, in particular Casimir forces in certain systems can also be calculated using the semiclassical method. In this method, the limit $\hbar \to 0$ is taken and the energy is evaluated as a sum over the periodic orbits that reflect the surfaces of the system [4,55]. By considering periodic orbits that make contact with the boundary surface, the infinities never appear. This method has been used to calculate the Casimir energy in nonsymmetric configurations, between a plane and a sphere, and between concentric cylinders and spheres. However the semiclassical method is not purely quantum mechanical and as a result it does not give a very good approximation for the Casimir forces. Optical approximation is another theoretical method used to calculate Casimir forces [56]. The optical approximation takes into account the optical paths between surfaces, surfaces which are curved, and optical paths through points that do not lie on straight lines normal to one surface or the other. This method is mostly suitable when calculating the Casimir energy between planar structures.

Proximity force approximation (PFA) is yet another technique used for Casimir energy calculations [57]. This method is valid for surfaces where the separation is much

smaller than typical local curvatures. It has been successfully used to calculate the Casimir energy of a sphere and cylinder in front of a plane. Roughly speaking, the proximity force approximation maps the Casimir effect of an arbitrary geometry onto Casimir's parallel-plate configuration. The major problem with this approach is that curvature effects are being neglected and thereby limiting the Casimir force calculations.

One of the most advanced and a recent approach is based on macroscopic quantum electrodynamics of dispersing and absorbing media [see Ref. [1] for latest review. There, the vacuum electric and magnetic fields are considered as primary physical observables whose quantum mechanical operators are given by the convolution of the Green tensor of the Fourier-domain Maxwell equations with appropriately chosen bosonic field operators for creation and annihilation of the medium-assisted electromagnetic field quanta. In this approach, the Green tensor and the (complex) medium-assisted dielectric and magnetic permeabilities for a particular geometry are responsible for the dissipation processes. Although this approach allows one to use to take into account realistic properties of materials such as frequency-dependent dielectric permittivities, the problem becomes far too complicated for cylindrical geometries where the Green tensor used becomes too big to keep track of. This method had been successfully utilized in dealing with spherical geometries where the Green tensor is not as huge.

4.3 Mode Summation Method Applied to Cylindrical Geometries

The theoretical approach that gives us an exact Casimir energy for geometries with curvature effects is the mode summation method. The mode summation approach involves representing the Casimir energy in a very intuitive manner as a sum of the zero-point energies of the electromagnetic excitations supported by the system. One obtains these photon energies from the dispersion relation that corresponds to the system under consideration. The photon energies or electromagnetic modes are obtained by solving the Maxwell's equations with appropriate boundary conditions. The Casimir energy can then be expressed by the sum over all modes, as follows [3-6]:

$$E_C = \frac{\hbar}{2}\sum_{\{p\}} \omega_p \tag{4.1}$$

The term ω_p represents the eigenfrequencies satisfying the dispersion relation supported by the system. Here $\{p\}$ are the complete set of quantum numbers determined by the geometry of system under consideration. For a cylindrical structure, $\{p\} = (n, m, k_z)$ where n is the order of the appropriate Bessel functions, m denotes the number of roots of the dispersion relation, and k_z is continuous corresponding to wave vector along the infinite axial direction of the cylinder. When solving Maxwell's equations with respect to cylindrical geometries, the dispersion relations are found to contain Bessel functions and the order of the appropriate Bessel functions is denoted by n.

The sum in Equation (4.1) is an infinite one and in order to remove the occurring divergence, the zero-point energy of the infinite homogeneous space is subtracted off from the energy of the system [3]:

$$E_C = \frac{\hbar}{2}\sum_{\{p\}}\left(\omega_p - \widetilde{\omega}_p\right) \tag{4.2}$$

The term $\widetilde{\omega}_p$ represents the eigenfrequencies corresponding to the reference vacuum with no boundaries present. Since k_z is continuous, we can express the Casimir energy per unit length as:

$$E_C = \frac{\hbar}{2}\int_{-\infty}^{\infty}\frac{dk_z}{2\pi}\sum_{n,m}\left[\omega_{n,m}(k_z) - \widetilde{\omega}_{n,m}(k_z)\right] \tag{4.3}$$

Both sums in Equation (4.3) are divergent and each sum will be treated individually and means to remove any occurring divergences will be explained. For the sum over *m*, we will make use of Residue's theorem to treat the divergence, and depending on the system, the sum over *n* will be evaluated correspondingly. For instance in the case of a cylindrical dielectric-diamagnetic layer, the Riemann Zeta function regularization procedure is used whereas in the case of multiple perfectly conducting cylindrical shells, the energy of isolates metallic shells is subtracted from the energy of the whole system. Before we do any of these regularizations, we first introduce the parameter *s* and express the Casimir energy as follows:

$$E_C(s) = \frac{\hbar}{2}\int_{-\infty}^{\infty}\frac{dk_z}{2\pi}\sum_{n,m}\left[\omega_{n,m}^{-s}(k_z) - \widetilde{\omega}_{n,m}^{-s}(k_z)\right] \tag{4.4}$$

$$E_C = \lim_{s\to -1} E_C(s) \tag{4.5}$$

where s in general is a complex number, allowing one to perform the regularization procedure rigorously. By using $\chi^2 = \varepsilon\mu\omega^2 - k_z^2$, where ε and μ are the dielectric and magnetic function of the system respectively, Casimir energy $E_C(s)$ can be expressed as:

$$E_C(s) = \frac{\hbar c^{-s}}{2}\int_{-\infty}^{+\infty}\frac{dk_z}{2\pi}\sum_{n=-\infty}^{\infty}\sum_{m=1}^{\infty}\left\{\left[\chi_{nm}^2(\Re)+k_z^2\right]^{-s/2}-\left[\chi_{nm}^2(\Re\to\infty)+k_z^2\right]^{-s/2}\right\} \tag{4.6}$$

The term $\Re$ denotes the radius of the cylindrical nanostructures. For a cylinder, we have $\Re = R_1$, whereas for N multiple cylinders, $\Re = R_1, R_2, ..., R_N$.

Using the Residue's theorem, the infinite sum over m can be converted in terms of a contour integral in the complex plane for any given value of n and k_z [3-5, 58, 59]:

$$E_C(s) = \frac{\hbar c^{-s}}{4\pi i}\int_{-\infty}^{+\infty}\frac{dk_z}{2\pi}\sum_{n=-\infty}^{\infty}\oint_{\mathscr{C}}d\chi(\chi^2+k_z^2)^{-s/2}\frac{d}{d\chi}\ln\frac{f_n^{TE}(\chi\Re)\,f_n^{TM}(\chi\Re)}{f_n^{TE}(\infty)\,f_n^{TM}(\infty)} \tag{4.7}$$

where the contour $\mathscr{C}$ is along the imaginary axis $(-i\infty,+i\infty)$ and an infinite semicircle closed in the right half of the complex plane with poles on the real axis as shown in Figure 4.1. $f_n^{TE,TM}(\chi\Re)$ are the dispersion relations of the system whereas $f_n^{TE,TM}(\infty)$ are the dispersion relations when there is no boundaries in the system. The only contribution from the contour integration comes from the imaginary y-axis. Therefore, making the substitution $y = \mathrm{Im}\,\chi$, $E_C(s)$ is reduced to:

$$E_C(s) = \frac{\hbar c^{-s}}{2\pi^2}\sin\frac{\pi s}{2}\sum_{n=-\infty}^{\infty}\int_0^{\infty}dk_z\int_{k_z}^{\infty}dy(y^2-k_z^2)^{-s/2}\frac{d}{dy}\ln\frac{f_n^{TE}(i\Re y)\,f_n^{TM}(i\Re y)}{f_n^{TE}(i\infty)\,f_n^{TM}(i\infty)} \tag{4.8}$$

The order of integration in Equation (4.8) is changed and the integration over the k_z-variable is performed, giving:

$$E_C(s) = \frac{\hbar c^{-s}}{4\sqrt{\pi}\Gamma\left(\frac{s}{2}\right)\Gamma\left(\frac{3-s}{2}\right)} \sum_{n=-\infty}^{\infty} \int_0^{\infty} dy y^{1-s} \frac{d}{dy} \ln \frac{f_n^{TE}(i\Re y) f_n^{TM}(i\Re y)}{f_n^{TE}(i\infty) f_n^{TM}(i\infty)} \tag{4.9}$$

where $\Gamma(s)$ is the gamma function. The exact Casimir energy is obtained by taking the limit $E_C = \lim_{s\to -1} E_C(s)$.

Equation (4.9) represents the Casimir energy expression in terms of the electromagnetic modes of the system. The electromagnetic modes are obtained by solving the Maxwell's equation with appropriate boundary conditions. We will make use of Equation (4.9) to calculate the Casimir energy for the system of a cylindrical dielectric-diamagnetic layer, multiple concentric metallic shells, and two parallel dielectric cylinders.

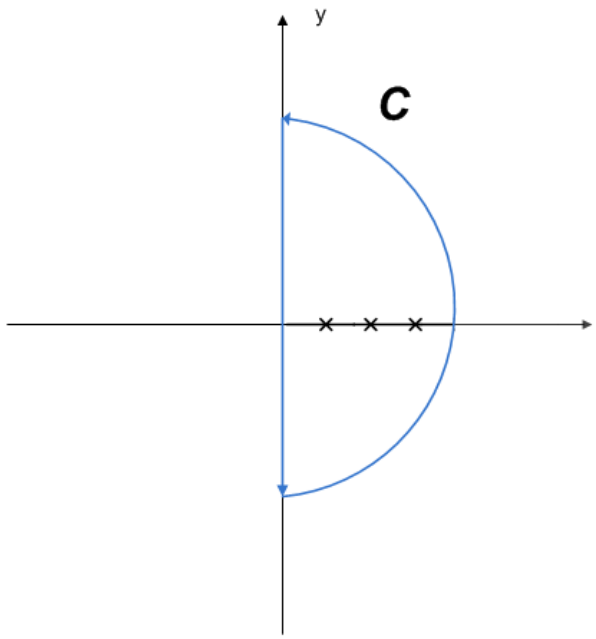

Figure 4.1 Contour in the complex frequency plane with poles along the real axis.

4.3.1 Zeta Function Regularization

As mentioned in the previous section, the zero-point energy is divergent and a means of regularization is required to change the infinite quantity into a finite one. Some of the most important regularization schemes are the frequency cutoff, point splitting, zeta function, heat kernel, proper time, and Fujikawa method [60, 61]. In regards to the cylindrical geometries used in this dissertation, the zeta function regularization procedure is found to be convenient. In the zeta function regularization, the Casimir energy in Equation (4.1) becomes temporarily of the form:

$$E_C(s) = \frac{\hbar}{2}\sum_{\{p\}} \omega_p{}^{-s} \tag{4.10}$$

where the exact Casimir energy is obtained on removing the regularization in the limit $s \to -1$. This regularization is called the Riemann zeta function regularization because the zero-point energy $E_C(s)$ is given by:

$$E_C(s) = \frac{\hbar}{2}\zeta(s) \tag{4.11}$$

Equation (4.11) is expressed in terms of the Riemann zeta function as follows:

$$\zeta(s) = \sum_{\{p\}} \omega_p{}^{-s} \tag{4.12}$$

The parameter s is considered to belong in the region of the complex s-plane where $\mathrm{Re}\, s > 1$. An analytic continuation of Equation (4.12) to the point $s = -1$ should therefore be constructed.

The calculations involving the zeta functions have all been performed at zero temperature. However, standard cosmology predicts matter at extremely high temperatures in the early universe [60]. Dolan and jackiw [62] have been the first to study the symmetry behavior of Quantum Field Theory at finite temperature. They showed that in massless electrodynamics in two dimensions, the gauge boson acquired a mass which was independent of temperature. Reuter and Dittrich [63] rederived these results by utilizing the zeta function procedure. A good review of finite temperature formalism in Quantum Field Theory is found in reference [64].

CHAPTER 5

CYLINDRICAL DIELECTRIC-DIAMAGNETIC LAYER OF FINITE THICKNESS

5.1 Cylindrical Model

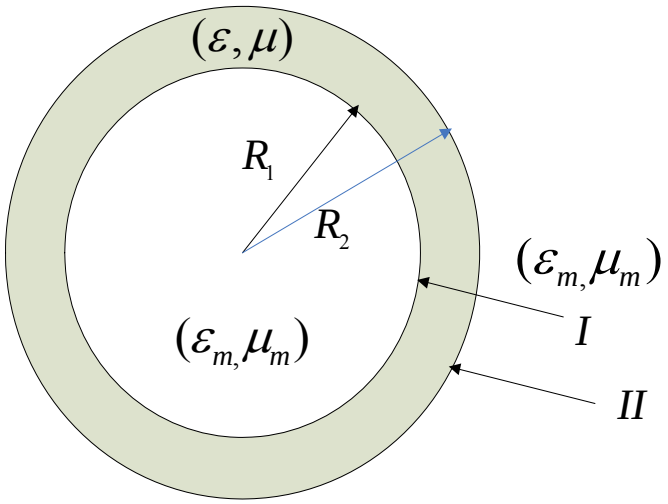

Figure 5.1 Cylindrical layer of finite thickness with its axial direction perpendicular to the page is immersed in an infinite medium. The layer has permittivity and permeability (ε,μ), respectively, and the medium - (ε_m,μ_m). The interfaces are denoted as *I* and *II*.

The first model we consider is that of a dielectric-diamagnetic cylindrical layer immersed in an infinite medium. Here, we apply the mode summation method to calculate the Casimir energy of such a layer. The system under consideration is a cylindrical layer with an inner radius R_1 and outer radius R_2 with an infinite axial direction perpendicular to the page. The dielectric layer has dielectric and magnetic functions ε and μ respectively, and it is placed in an infinite medium of dielectric and magnetic functions ε_m and μ_m respectively, as illustrated in Figure 5.1.

5.2 Electromagnetic Modes

The electromagnetic modes supported by the dielectric-diamagnetic layer imbedded in an infinite medium are obtained by solving the Maxwell's equations [65] with appropriate boundary conditions across interfaces *I* and *II*. Once the electromagnetic modes are obtained, one can then make use of the mode summation method for the Casimir energy calculations. The Maxwell's equations are defined as:

$$\vec{\nabla}.\vec{B} = 0 \tag{5.1}$$

$$\vec{\nabla}.\vec{E} = 0 \tag{5.2}$$

$$\vec{\nabla} \times \vec{E} = -\frac{\partial \vec{B}}{\partial t} \tag{5.3}$$

$$\vec{\nabla} \times \vec{B} = \varepsilon\mu \frac{\partial \vec{E}}{\partial t} \tag{5.4}$$

Solving the Maxwell's equations will give us the electric and magnetic fields supported by the system. The components of the electric (*E*) and magnetic fields (*B*) are expressed in cylindrical coordinates (ρ,θ,z) as follows [65]:

$$E_\rho^j(\rho,\theta,z)=\sum_{n=-\infty}^{\infty}\left\{\frac{n\omega}{\rho\chi^2}\left[C_n^j J_n+D_n^j H_n^{(1)}\right]-\frac{ik}{\chi}\left[A_n^j J_n'+B_n^j H_n'^{(1)}\right]\right\}e^{in\theta}e^{i(k_z z-\omega t)} \tag{5.5}$$

$$E_\theta^j(\rho,\theta,z)=\sum_{n=-\infty}^{\infty}\left\{\frac{nk}{\rho\chi^2}\left[A_n^j J_n+B_n^j H_n^{(1)}\right]+\frac{i\omega}{\chi}\left[C_n^j J_n'+D_n^j H_n'^{(1)}\right]\right\}e^{in\theta}e^{i(k_z z-\omega t)} \tag{5.6}$$

$$E_z^j(\rho,\theta,z)=\sum_{n=-\infty}^{\infty}\left\{A_n^j J_n+B_n^j H_n^{(1)}\right\}e^{in\theta}e^{i(k_z z-\omega t)} \tag{5.7}$$

$$B_\rho^j(\rho,\theta,z)=\sum_{n=-\infty}^{\infty}\left\{-\frac{n\omega\varepsilon\mu}{\rho\chi^2}\left[A_n^j J_n+B_n^j H_n^{(1)}\right]-\frac{ik}{\chi}\left[C_n^j J_n'+D_n^j H_n'^{(1)}\right]\right\}e^{in\theta}e^{i(k_z z-\omega t)} \tag{5.8}$$

$$B_\theta^j(\rho,\theta,z)=\sum_{n=-\infty}^{\infty}\left\{\frac{nk}{\rho\chi^2}\left[C_n^j J_n+D_n^j H_n^{(1)}\right]-\frac{i\varepsilon\mu\omega}{\chi}\left[A_n^j J_n'+B_n^j H_n'^{(1)}\right]\right\}e^{in\theta}e^{i(k_z z-\omega t)} \tag{5.9}$$

$$B_z^j(\rho,\theta,z)=\sum_{n=-\infty}^{\infty}\left\{C_n^j J_n+D_n^j H_n^{(1)}\right\}e^{in\theta}e^{i(k_z z-\omega t)} \tag{5.10}$$

where $j=1,2,3$ stands for the three regions separated by the interfaces *I* and *II* in Figure 5.1, k_z is the wave-vector along the *z* direction, ω is the frequency of the electromagnetic excitations and $\chi^2=\varepsilon\mu\omega^2-k_z^2$. Also, $J_n\equiv J_n(\chi\rho)$ and $H_n^{(1)}\equiv H_n^{(1)}(\chi\rho)$ are the Bessel function of first kind of order *n* and the Hankel functions of the first kind of order *n*, respectively. In addition, $J_n'=J_n'(x)=\frac{dJ_n(x)}{dx}$, and $H_n'^{(1)}=H_n'^{(1)}(x)=\frac{dH_n^{(1)}(x)}{dx}$.

The unknown coefficients $A_n^j, B_n^j, C_n^j, D_n^j$ are related by imposing the boundary conditions for the continuity of $\varepsilon_j E_\rho^j, E_\theta^j, E_z^j, \frac{1}{\mu_j} B_z^j$ across each interface of the cylindrical layer giving the dispersion relation for the electromagnetic modes supported by this system. It is important to note that the permittivity ε and permeability μ for the layer, and the permittivity ε_m and permeability μ_m for the medium are taken to be constants. To account for the dielectric properties in the Casimir energy turns out to be difficult even for arbitrary dispersionless permittivity and permeability. This situation also occurs when calculating the Casimir effect for a ball [5, 48] or a cylinder [3, 5], where the condition of constant light velocity across the interface is imposed. Here we also impose the same condition $\varepsilon\mu = \varepsilon_m \mu_m = c^{-2}$, where c is the speed of light. The $\varepsilon\mu = \varepsilon_m \mu_m = c^{-2}$ condition is referred to as the dielectric-diamagnetic case as opposed to the purely dielectric one in which $\mu_1 = \mu_2 = 1$. The physical implication of this condition is that the electric and magnetic fields are treated in a symmetric way, thus there is no preference for the electric field as it occurs for the dielectric cylinder [66-68].

Now that we have applied the boundary conditions across each interface of the cylindrical layer to the electric and magnetic fields, we obtain after imposing the constant speed of light condition the following expressions:

$$\varepsilon_m A_n^1 J_n'(\chi R_1) = \varepsilon[A_n^2 J_n'(\chi R_1) + B_n^2 H_n'^{(1)}(\chi R_1)] \tag{5.11}$$

$$\varepsilon_m B_n^3 H_n'^{(1)}(\chi R_2) = \varepsilon[A_n^2 J_n'(\chi R_2) + B_n^2 H_n'^{(1)}(\chi R_2)] \tag{5.12}$$

$$A_n^1 J_n(\chi R_1) = A_n^2 J_n(\chi R_1) + B_n^2 H_n^{(1)}(\chi R_1) \tag{5.13}$$

$$B_n^3 H_n^{(1)}(\chi R_2) = A_n^2 J_n(\chi R_2) + B_n^2 H_n^{(1)}(\chi R_2) \tag{5.14}$$

$$\mu C_n^1 J_n'(\chi R_1) = \mu_m [C_n^2 J_n'(\chi R_1) + D_n^2 H_n'^{(1)}(\chi R_1)] \tag{5.15}$$

$$\mu D_n^3 H_n'^{(1)}(\chi R_2) = \mu_m [C_n^2 J_n'(\chi R_2) + D_n^2 H_n'^{(1)}(\chi R_2)] \tag{5.16}$$

$$C_n^1 J_n(\chi R_1) = C_n^2 J_n(\chi R_1) + D_n^2 H_n^{(1)}(\chi R_1) \tag{5.17}$$

$$D_n^3 H_n^{(1)}(\chi R_2) = C_n^2 J_n(\chi R_2) + D_n^2 H_n^{(1)}(\chi R_2) \tag{5.18}$$

In general, the dispersion equation for cylindrical structures can be defined in terms of a determinant of a 4 x 4 matrix where separation between pure magnetic (TE) and pure electric (TM) modes is not possible except for the *n*=0 case [69,70]. Equations (5.11-5.14) are the expressions for the transverse magnetic (TM) modes whereas Equations (5.15-5.18) are those for the transverse electric (TE) modes. After some algebra, Equations (5.11-5.18) can be reduces to two expressions:

$$f_n^{TE}(\chi, R_1, R_2) = \Delta_1(\chi R_1)\Delta_2(\chi R_2) + (\mu - \mu_m)^2 J_n(\chi R_1) J_n'(\chi R_1) H_n(\chi R_2) H_n'(\chi R_2) = 0 \tag{5.19}$$

$$f_n^{TM}(\chi, R_1, R_2) = \delta_1(\chi R_1)\delta_2(\chi R_2) + (\varepsilon - \varepsilon_m)^2 J_n(\chi R_1) J_n'(\chi R_1) H_n(\chi R_2) H_n'(\chi R_2) = 0 \tag{5.20}$$

for each $n = 0, \pm 1, \pm 2, \ldots$

We have used the following notations:

$$\Delta_r(\chi R_r) = \mu J_n(\chi R_r) H_n'(\chi R_r) - \mu_m J_n'(\chi R_r) H_n(\chi R_r) \tag{5.21}$$

$$\delta_r(\chi R_r) = \varepsilon J_n(\chi R_r) H_n'(\chi R_r) - \varepsilon_m J_n'(\chi R_r) H_n(\chi R_r) \tag{5.22}$$

where r=1, 2.

Here $f_n^{TE}(\chi, R_1, R_2) = 0$ and $f_n^{TM}(\chi, R_1, R_2) = 0$ are the dispersion relations for the transverse electric (TE) and transverse magnetic (TM) modes respectively. Now that we have the dispersion relations, we can proceed in applying the mode summation method. Using Equation (4.9), the Casimir energy for a dielectric-diamagnetic cylindrical layer of finite thickness is expressed as:

$$E_C(s) = \frac{\hbar c^{-s}}{4\sqrt{\pi}\Gamma\left(\frac{s}{2}\right)\Gamma\left(\frac{3-s}{2}\right)} \sum_{n=-\infty}^{\infty} \int_0^{\infty} dy y^{1-s} \frac{d}{dy} \ln \frac{f_n^{TE}(iR_1 y, iR_2 y) f_n^{TM}(iR_1 y, iR_2 y)}{f_n^{TE}(i\infty) f_n^{TM}(i\infty)} \tag{5.23}$$

with the dispersion relations $f_n^{TE,TM}$ given by Equations (5.19) and (5.20).

5.3 Casimir Energy of Dielectric-Diamagnetic Cylindrical Layer

In order to perform the calculations of the Casimir energy for the dielectric-diamagnetic cylindrical layer, it is convenient to first introduce the parameter $\xi = \frac{\varepsilon - \varepsilon_m}{\varepsilon + \varepsilon_m}$. This parameter allows the Casimir energy of the cylindrical layer to be represented as an infinite series in terms of powers of ξ^2 in analogy to the calculations of the Casimir

energy for a solid ball or cylinder [3,5]. The ξ^2 expansion allows one to consider explicitly each term in the series, and thus establish various limiting cases. By introducing the parameter $\xi = \frac{\varepsilon - \varepsilon_m}{\varepsilon + \varepsilon_m}$, we can follow the works done for compact dielectric-diamagnetic cylinders and spherical balls [3,5,71,72]. The parameter ξ can be categorized into two very important cases for the cylindrical layer: the $\xi << 1$ case and the $\xi = 1$ case.

The $\xi << 1$ case corresponds to an optically dilute dielectric-diamagnetic cylindrical layer with properties not very different from the dielectric and magnetic properties of the medium. The $\xi = 1$ case corresponds to two perfectly conducting concentric cylindrical shells. Introducing the parameter ξ also allows us to apply the Riemann Zeta function regularization procedure to remove the occurring divergences in the considered ξ^2 terms thus extending its application to cylindrical layer systems.

5.3.1 The case of $\xi = \frac{\varepsilon - \varepsilon_m}{\varepsilon + \varepsilon_m} << 1$

This case corresponds to the case when the dielectric (magnetic) properties of the surrounding medium and material of the layer do not differ much. After using standard properties of the Bessel functions [73], the dispersion relations are expressed as follows:

$$f_n^{TE}(iR_1y,iR_2y)\,f_n^{TM}(iR_1y,iR_2y)=\frac{16\mu^2\varepsilon_m^2}{\pi^4}\left[\frac{1}{y^4R_1^{\,2}R_2^{\,2}}\left(\frac{1-\xi}{1+\xi}\right)^2+\frac{4\xi^2(1-\xi)}{(1+\xi)^3}\mathrm{X}_1+\frac{16\xi^4}{(1+\xi)^4}\mathrm{X}_2\right] \tag{5.24}$$

The terms X_1 and X_2 are defined as follows:

$$\mathrm{X}_1=\frac{2I_n(yR_1)I_n'(yR_1)K_n(yR_2)K_n'(yR_2)}{(y^2R_1R_2)}-\frac{I_n(yR_1)I_n'(yR_1)K_n(yR_1)K_n'(yR_1)}{(yR_2)^2}-\frac{I_n(yR_2)I_n'(yR_2)K_n(yR_2)K_n'(yR_2)}{(yR_1)^2} \tag{5.25}$$

$$\mathrm{X}_2=I_n(yR_1)I_n'(yR_1)K_n(yR_2)K_n'(yR_2)\left[I_n(yR_2)K_n(yR_1)-I_n(yR_1)K_n(yR_2)\right]\times\left[I_n'(yR_2)K_n'(yR_1)-I_n'(yR_1)K_n'(yR_2)\right] \tag{5.26}$$

Here the functions $J_n(iRy)$ and $H_n(iRy)$ have been replaced by the modified Bessel functions using $I_n(y)=i^{-n}J_n(iy)$ and $K_n(y)=i^{n+1}\frac{\pi}{2}H_n(iy)$. Now we can perform a series expansion of Equation (5.23) with respect to ξ. Taking into consideration that $I_n=I_{-n}$ and $K_n=K_{-n}$, and retaining only the leading term in the expansion $\sim\xi^2$, the exact energy E_C is expressed in the following way:

$$E_C \cong \frac{\hbar c \xi^2}{4\pi} \lim_{s \to -1} [\mathrm{Y}_1(s) + \mathrm{Y}_2(s)] \tag{5.27}$$

The Casimir energy has been separated into two parts, $\mathrm{Y}_1(s)$ and $\mathrm{Y}_2(s)$. Since the sum over *n* in Equation (5.23) is still present, we find it convenient to break it into the $n = 0$ term and the $n \neq 0$ term. $\mathrm{Y}_1(s)$ collects the $n = 0$ terms from the summation:

$$\mathrm{Y}_1(s) = \int_0^\infty dy\, y^{-s} \Big[4y^2 R_1 R_2 I_0(yR_1) I_0'(yR_1) K_0(yR_2) K_0'(yR_2)$$

$$- 2\left(\frac{1}{R_1^{1-s}} + \frac{1}{R_2^{1-s}} \right) \left(y^2 I_0(y) I_0'(y) K_0(y) K_0'(y) + 1 \right) + e^{2y(R_1 - R_2)} \Big] \tag{5.28}$$

$\mathrm{Y}_2(s)$ collects all $n \neq 0$ terms from the summation:

$$\mathrm{Y}_2(s) = \sum_{n=1}^\infty \int_0^\infty dy\, y^{-s} \Big[8y^2 R_1 R_2 I_n(yR_1) I_n'(yR_1) K_n(yR_2) K_n'(yR_2)$$

$$- 4\left(\frac{1}{R_1^{1-s}} + \frac{1}{R_2^{1-s}} \right) y^2 I_n(y) I_n'(y) K_n(y) K_n'(y) + 2e^{2y(R_1 - R_2)} \Big] \tag{5.29}$$

We evaluate the terms in $\mathrm{Y}_1(s)$ and $\mathrm{Y}_2(s)$ by making use of uniform asymptotic expansion of Bessel functions and applying Riemann Zeta function. We start by evaluating the terms in $\mathrm{Y}_2(s)$. The first term in $\mathrm{Y}_2(s)$ is evaluated by making use of the change of variables $y = nz, n = 1,2,3,...$ The uniform asymptotic expansion of the Bessel

functions [73] is performed and the dominant term is retained. We obtain for the first term of $\mathrm{Y}_2(s)$:

$$8\sum_{n=1}^{\infty}\int_0^{\infty} y^{2-s} R_1 R_2 I_n(yR_1) I_n'(yR_1) K_n(yR_2) K_n'(yR_2) dy \cong -2\sum_{n=1}^{\infty} n^{1-s} \int_0^{\infty} y^{-s} e^{2n(\eta_1-\eta_2)} dy \qquad (5.30)$$

where $\eta_i = \sqrt{1+(R_i y)^2} + \ln\left[\dfrac{R_i y}{1+\sqrt{1+(R_i y)^2}}\right]$ for $i = 1, 2$. Interchanging the integration and the summation in Equation (5.30) and taking the limit $s \to -1$, one obtains:

$$\frac{1}{4}\int_0^{\infty} y \frac{\partial^2}{\partial(\eta_1-\eta_2)^2} \sum_{n=1}^{\infty} e^{2n(\eta_1-\eta_2)} dy = \int_0^{\infty} y \frac{e^{2|\eta_1-\eta_2|}(e^{2|\eta_1-\eta_2|}+1)}{(e^{2|\eta_1-\eta_2|}-1)^3} dy \qquad (5.31)$$

The second term in $\mathrm{Y}_2(s)$ is also evaluated by making use of the change of variables $y = nz, n = 1,2,3,...$ Again, we perform the uniform asymptotic expansion valid for the Bessel functions of large order [73] and this time we retain the first three terms ($\sim 1/n^4$) of the expansion. This leads to the expression:

$$-2\left(\frac{1}{R_1^{1-s}}+\frac{1}{R_2^{1-s}}\right)\left(2\sum_{n=1}^{\infty} n^{-1-s}+1\right)\int_0^{\infty}\left(y^{2-s} I_n(y) I_n'(y) K_n(y) K_n'(y)\right) dy$$

$$\approx -\frac{1}{8}\left(\frac{1}{R_1^{1-s}}+\frac{1}{R_2^{1-s}}\right)\left(2\sum_{n=1}^{\infty} n^{-1-s}+1\right)\int_0^{\infty} z^{-s}\left(\frac{1}{1+z^2}-\frac{2}{(1+z^2)^2}+\frac{1}{(1+z^2)^3}\right) dz$$

$$= -\frac{1}{8}\left(\frac{1}{R_1^{1-s}}+\frac{1}{R_2^{1-s}}\right)\left(2\sum_{n=1}^{\infty} n^{-1-s}+1\right)\left[\frac{1}{2}\Gamma\left(\frac{s+1}{2}\right)\Gamma\left(\frac{1-s}{2}\right)-\Gamma\left(\frac{s+3}{2}\right)\Gamma\left(\frac{1-s}{2}\right)+\frac{1}{4}\Gamma\left(\frac{s+5}{2}\right)\Gamma\left(\frac{1-s}{2}\right)\right]$$

(5.32)

The term $\sum_{n=1}^{\infty} n^{-1-s}$ in Equation (5.32) is the Riemann Zeta function:

$$\sum_{n=1}^{\infty} n^{-1-s} = \zeta(1+s) \tag{5.33}$$

Also, we have added 1 to $2\sum_{n=1}^{\infty} n^{-1-s}$ in Equation (5.32). This is compensated by subtracting the appropriate terms from $\mathrm{Y}_1(s)$ later. Now it can be seen how the divergent sum over *n* can be regularized using the Riemann Zeta function as mentioned earlier. It follows that:

$$\begin{aligned}\left(2\sum_{n=1}^{\infty} n^{-1-s}+1\right)\Gamma\left(\frac{s+1}{2}\right) &= \lim_{s\to -1}\left[(2\zeta(s+1)+1)\Gamma\left(\frac{s+1}{2}\right)\right] \\ &= \lim_{s\to -1}\left[2\zeta(0)+2\zeta'(0)(s+1)+\mathcal{O}((s+1)^2)+1\right] \\ &\quad \times\left[\frac{2}{s+1}-\gamma+\mathcal{O}(s+1)\right] \\ &= -2\ln(2\pi).\end{aligned} \tag{5.34}$$

where γ is the Euler constant and $\mathcal{O}(s+1)$ represents the higher order terms. In Equation (5.34), $\zeta(1+s)$ is expanded in Taylor series and we make use of the properties of the Riemann Zeta function, $\zeta(0) = -\frac{1}{2}, \zeta'(0) = -\frac{1}{2}\ln(2\pi)$. This technique allows us to remove the divergences from the poles of the Gamma function that come up in the calculations of the Casimir energy for a dielectric cylinder. The remaining terms in

Equation (5.32) are finite. The last term in $\mathrm{Y}_2(s)$ is solved exactly in the $s \to -1$ limit resulting in:

$$2\sum_{n=1}^{\infty}\int_0^{\infty} dyye^{2(yR_1-yR_2)} = \frac{\zeta(0)}{2(R_1-R_2)^2} \tag{5.35}$$

where $\zeta(0) = -\frac{1}{2}$.

Therefore, we were able to remove the occurring divergences in $\mathrm{Y}_2(s)$ with all the terms in Equation (5.29) being finite and convergent:

$$\mathrm{Y}_2(s \to -1) = \int_0^{\infty} y\frac{e^{2|\eta_1-\eta_2|}(e^{2|\eta_1-\eta_2|}+1)}{(e^{2|\eta_1-\eta_2|}-1)^3}dy + \frac{\ln(2\pi)}{4}\left(\frac{1}{R_1^2}+\frac{1}{R_2^2}\right) - \frac{1}{4(R_1-R_2)^2} \tag{5.36}$$

Now that we have evaluated all the terms in $\mathrm{Y}_2(s)$, we can evaluate the terms in $\mathrm{Y}_1(s)$. The first and second terms have in $\mathrm{Y}_1(s)$ cannot be evaluated analytically and numerical methods need to be used. The third term however can be solved analytically in the limit $s \to -1$ giving:

$$\int_0^{\infty} dyye^{2(yR_1-yR_2)} = \frac{1}{4(R_1-R_2)^2} \tag{5.37}$$

We can therefore write $\mathrm{Y}_1(s \to -1)$ as follows:

$$\mathrm{Y}_1(s\to -1) = 4\int_0^\infty dy\, y^3 R_1 R_2 I_0(yR_1) I_0'(yR_1) K_0(yR_2) K_0'(yR_2)$$

$$-\left(\frac{1}{R_1^2}+\frac{1}{R_2^2}\right)\int_0^\infty dy\left\{2y^3 I_0(y) I_0'(y) K_0(y) K_0'(y) - \frac{y}{8}\left[\frac{1}{1+y^2} - \frac{2}{\left(1+y^2\right)^2} + \frac{1}{\left(1+y^2\right)^3}\right] + \frac{y}{2}\right\}$$

$$+\frac{1}{4(R_1-R_2)^2}$$

(5.38)

All the terms in Equation (5.38) are finite and convergent. Combining Equations (5.36) and (5.38) into Equation (5.27), we obtain an expression for the Casimir energy for an optically dilute cylindrical layer:

$$E_C \cong -\frac{\hbar c \xi^2}{2\pi}\left[\int_0^\infty dy\left\{\frac{y e^{2|\eta_1-\eta_2|}(e^{2|\eta_1-\eta_2|}+1)}{2(e^{2|\eta_1-\eta_2|}-1)^3} + 2y^3 R_1 R_2 I_0(yR_1) I_0'(yR_1) K_0(yR_2) K_0'(yR_2)\right.\right.$$

$$\left.-\left(\frac{1}{R_1^2}+\frac{1}{R_2^2}\right)\left[y^3 I_0(y) I_0'(y) K_0(y) K_0'(y) - \frac{y}{16}\left(\frac{1}{1+y^2} - \frac{2}{\left(1+y^2\right)^2} + \frac{1}{\left(1+y^2\right)^3}\right) + \frac{y}{4}\right]\right\}$$

$$\left.+\frac{\ln(2\pi)}{8}\left(\frac{1}{R_1^2}+\frac{1}{R_2^2}\right)\right]$$

(5.39)

It is very important to note that all terms in Equation (5.39) are finite and convergent. This shows that we were able to apply the mode summation technique to the

system of cylindrical layer and our endeavor of removing occurring divergences was a successful one. The sum over *m* was treated using Residue's theorem described in section 4.3 while the sum over *n* was evaluated using the Riemann Zeta function by introducing two parameters, ξ and *s*, as described in section 5.3.

5.3.1.1 Limiting Cases

In this section, the Casimir energy for various limits of the cylindrical layer is considered. We first start by investigating the limit for a layer of very small thickness, $\alpha \sim 1$ where $\alpha = R_2 / R_1$. In this limit, we find that the dominant contribution in Casimir energy comes from the term in Equation (5.31) and in this limit the Casimir energy per unit length behaves as:

$$E_C \approx \frac{-0.076\hbar c\xi^2}{R_1^2(\alpha-1)^3} \tag{5.40}$$

On the other hand, in the limit of large radii $R_1, R_2 \to \infty$, while keeping the separation between the two cylinders fixed, $d = R_2 - R_1 = const$ we obtain a system that corresponds to an infinite dielectric- diamagnetic plate. In this limit, the Casimir energy per unit area behaves as:

$$E_C \approx \frac{-\hbar c\xi^2}{8\pi^2 d^3} \tag{5.41}$$

This result is exactly what Klich et al. reported in Ref. [74].

In the limit $R_2 \to \infty$, we have a system that corresponds to a compact dielectric cylinder of radius R_1 and dielectric and magnetic properties (ε, μ) imbedded in an infinite medium with dielectric and magnetic properties (ε_m, μ_m) with the speed of light being constant across the interface at R_1. In this case, only the terms $\sim 1/R_1^2$ in the expressions for Y_1 and Y_2 contribute to E_C. However, we find it essential to evaluate the next term $(\sim 1/n^6)$ in the Bessel functions asymptotic uniform expansion in the calculation of Equation (5.32). Due to the occurring cancellations the value of the Casimir energy the latter becomes zero in the limit of $R_2 \to \infty$, thus recovering the results reported in Refs. [3,5].

It can be seen that we are able to recover some very important results by considering various limiting cases in our cylindrical layer. All these recovered results were performed theoretically and now we can move onto the numerical implementation of the Casimir energy and confirm those limits we just obtained.

5.3.1.2 Numerical Results

After implementing Equation (5.39) numerically and varying the thickness of the layer, α we find that the Casimir energy behaves as shown in Figure 5.2. It can be seen that in the limit $\alpha \to 1$, the energy behaves as:

$$| E_C | \sim \frac{1}{(\alpha - 1)^3} \tag{5.42}$$

This clearly resembles the theoretical result obtained in the same limit in Equation (5.40). Another case observed is that for $\alpha \geq 7$ the layer is already in the limit of large α and $E_C \to 0$, thus the system behaves as a compact cylinder with (ε, μ) characteristics imbedded in an infinite medium with (ε_m, μ_m) characteristics. Again this confirms the theoretical result obtained in Section 5.3.1.1. Another important observation is that the Casimir energy is negative implying an attractive energy.

Next, the interaction energy as a function of the inner radius is investigated. By changing the thickness of the layer, we can see how the Casimir energy behaves and the result is depicted in Figure 5.3. The most significant changes are found when the thickness of the layer is small due to the fact that for small thicknesses the dominant contribution comes from Equation (5.31). As the thickness is increased, the system behaves more like a compact cylinder of radius R_1 and dielectric and magnetic properties (ε, μ) imbedded in an infinite medium with dielectric and magnetic properties (ε_m, μ_m) with the speed of light being constant across the interface at R_1. Here it is clear that $E_C \to 0$ again confirming our theoretical calculations.

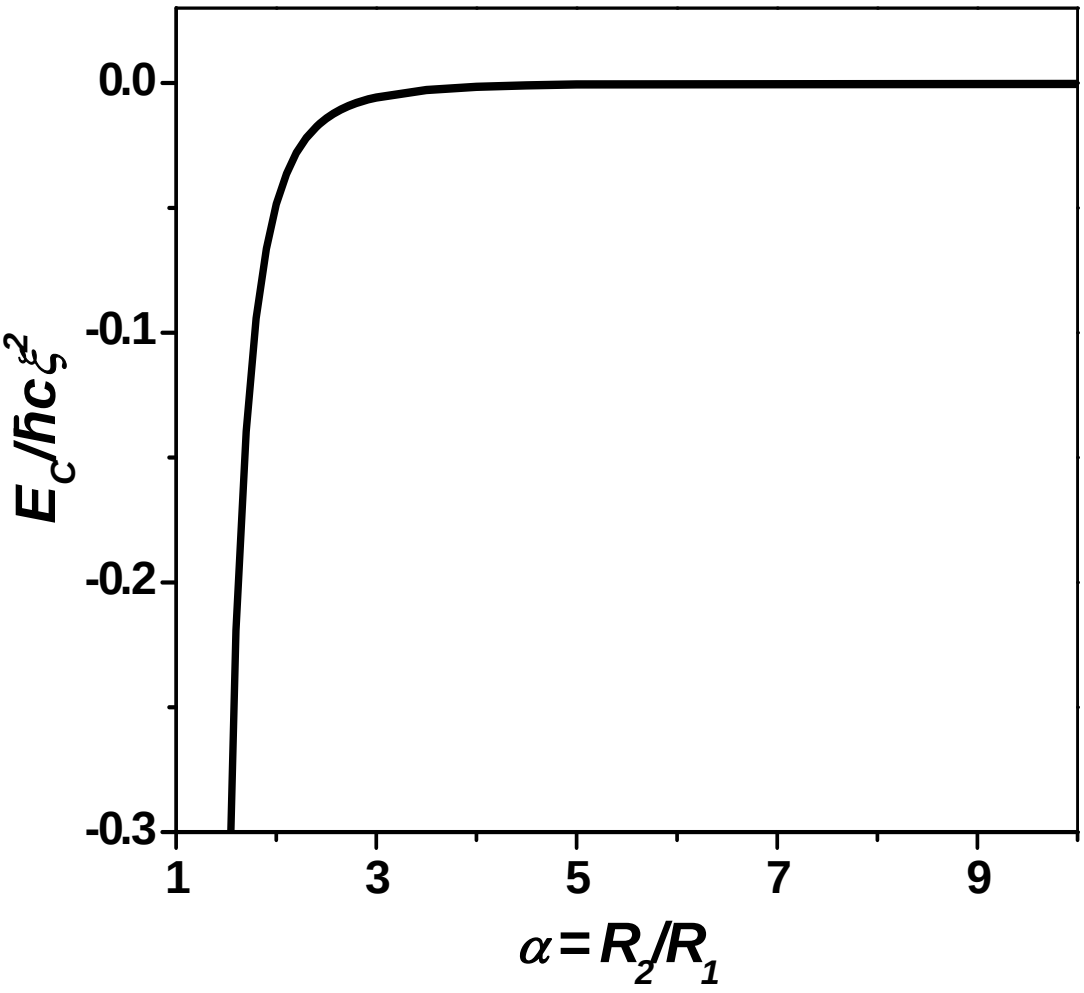

Figure 5.2 The Casimir energy per unit length for a cylindrical dielectric-diamagnetic layer as a function of R_2/R_1.

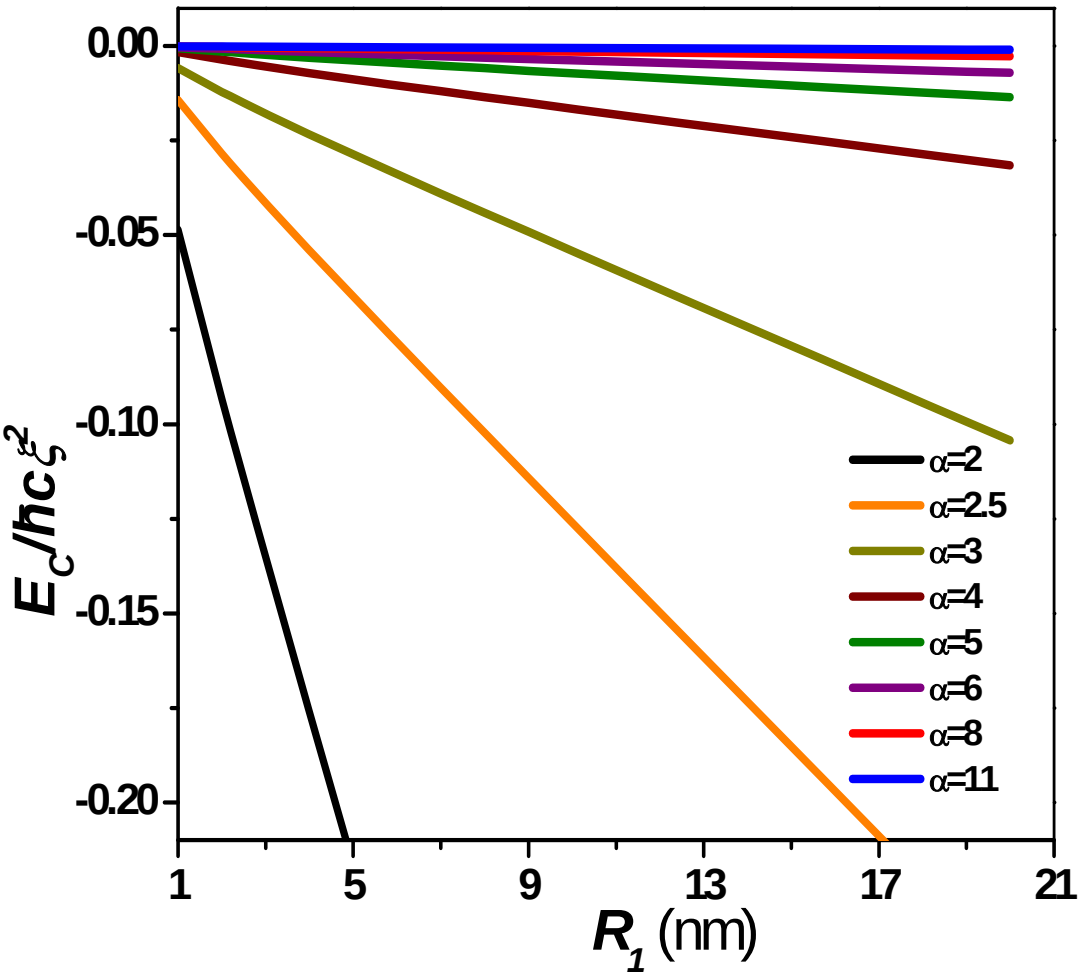

Figure 5.3 The Casimir energy per unit length for the same layer as a function of inner radius R_1.

5.3.2 The case of $\xi = \frac{\varepsilon - \varepsilon_m}{\varepsilon + \varepsilon_m} = 1$

This case corresponds to two perfectly conducting cylindrical shells if one takes c=1. In this model, the expression for the Casimir energy is given by:

$$E_C(s \to -1) = -\frac{\hbar c}{8\pi} \sum_{n=-\infty}^{\infty} \int_0^{\infty} dy y^2 \frac{d}{dy} \ln \frac{f_n^{TE}(iR_1 y, iR_2 y) f_n^{TM}(iR_1 y, iR_2 y)}{f_n^{TE}(i\infty) f_n^{TM}(i\infty)} \tag{5.43}$$

As seen in Equation (5.43) we still have the infinite sum over n which is divergent. In order to remove this divergence, we find it convenient to consider the difference between the energy of the concentric cylindrical shells and the energy of a single isolated shell. In our case, since we have two isolated cylindrical shells, we use the following:

$$\widetilde{E}_C(s \to -1) = E_C(s \to -1) - E_C^{(1)}(s \to -1) - E_C^{(2)}(s \to -1) \tag{5.44}$$

where $E_C(s \to -1)$ is given by Equation (5.43) and $E_C^{(1,2)}(s \to -1)$ are the energies for the single isolated cylindrical shells with radius R_1, R_2, respectively. The energies for the isolated shells are already known from Ref. [3,5],

$$E_C^{(1,2)}(s \to -1) = \frac{-0.01356\hbar c}{R_{1,2}^2} \tag{5.45}$$

Therefore, all we need to figure out is $\widetilde{E}_C(s \to -1)$ using the dispersion relations of the system of cylindrical shells. Using the dispersion relations $\widetilde{E}_C(s \to -1)$ becomes:

$$\widetilde{E}_C(s\to -1) = -\frac{\hbar c}{8\pi}\sum_{n=-\infty}^{\infty}\int_0^{\infty} dy y^2 \frac{d}{dy}\ln\frac{f_n^{TE}(iR_1 y, iR_2 y) f_n^{TM}(iR_1 y, iR_2 y)(f_{n,1}^{TE}(i\infty) f_{n,1}^{TM}(i\infty))^2}{f_{n,1}^{TE}(iR_1 y) f_{n,1}^{TM}(iR_1 y) f_{n,1}^{TE}(iR_2 y) f_{n,1}^{TM}(iR_2 y) f_n^{TE}(i\infty) f_n^{TM}(i\infty)} \quad (5.46)$$

Here $f_n^{TE}(iR_1 y, iR_2 y)$ $f_n^{TM}(iR_1 y, iR_2 y)$ are the dispersion relations defined with $\xi = 1$. In this case only the term containing the X_2 expression in Equation (5.24) remain. X_2 is the dispersion relation for the electromagnetic modes for two infinitely thin concentric perfectly conducting cylindrical shells and this result agrees with Ref.[4, 65]. Therefore we have the dispersion relation as:

$$f_n^{TE}(iR_1 y, iR_2 y) f_n^{TM}(iR_1 y, iR_2 y) =$$

$$I_n(yR_1) I_n'(yR_1) K_n(yR_2) K_n'(yR_2)\left[I_n(yR_2) K_n(yR_1) - I_n(yR_1) K_n(yR_2)\right] \quad (5.47)$$

$$\times\left[I_n'(yR_2) K_n'(yR_1) - I_n'(yR_1) K_n'(yR_2)\right]$$

$f_{n,1}^{TE,TM}(iR_1 y), f_{n,1}^{TE,TM}(iR_2 y)$ are the dispersion relations for a single isolated cylinder with radii R_1, R_2, respectively. When $\xi = 1$ and $c = 1$, $f_{n,1}^{TE,TM}(iR_{1,2} y)$ become equivalent to the dispersion relations of a single infinitely thin perfectly conducting shell as shown in Ref. [3,5]. $f_n^{TE,TM}(i\infty)$ and $f_{n,1}^{TE,TM}(i\infty)$ are the dispersion relations with no boundaries present.

Inserting all the dispersion relations into Equation (5.46), we end up with:

$$\widetilde{E}_C(s\to -1)=\frac{\hbar c}{4\pi}\left\{\int_0^\infty y\ln\left(\left(1-\frac{I_0(yR_1)K_0(yR_2)}{I_0(yR_2)K_0(yR_1)}\right)\left(1-\frac{I_0'(yR_1)K_0'(yR_2)}{I_0'(yR_2)K_0'(yR_1)}\right)\right)dy\right.$$
$$\left.+2\sum_{n=1}^{\infty}\int_0^\infty y\ln\left(\left(1-\frac{I_n(yR_1)K_n(yR_2)}{I_n(yR_2)K_n(yR_1)}\right)\left(1-\frac{I_n'(yR_1)K_n'(yR_2)}{I_n'(yR_2)K_n'(yR_1)}\right)\right)dy\right\} \tag{5.48}$$

Now we have to evaluate the terms in Equation (5.48). The first term is evaluated numerically while the second term can be evaluated analytically. For the second term, we first make use of the uniform asymptotic expansion of the Bessel functions for large orders followed by a Taylor series expansion of the logarithmic function. This results in the following:

$$2\sum_{n=1}^{\infty}\int_0^\infty y\ln\left[\left(1-\bar{I}_n\bar{K}_n\right)\left(1-\bar{I}_n'\bar{K}_n'\right)\right]dy\sim -4\sum_{m=1}^{\infty}\int_0^\infty\frac{y}{m(e^{2m|\eta_1-\eta_2|}-1)}dy \tag{5.49}$$

Equation (5.48) now becomes:

$$\widetilde{E}_C(s\to -1)=\frac{\hbar c}{4\pi}\left\{\int_0^\infty y\ln\left(\left(1-\frac{I_0(yR_1)K_0(yR_2)}{I_0(yR_2)K_0(yR_1)}\right)\left(1-\frac{I_0'(yR_1)K_0'(yR_2)}{I_0'(yR_2)K_0'(yR_1)}\right)\right)dy\right.$$
$$\left.-4\sum_{m=1}^{\infty}\int_0^\infty\frac{y}{m(e^{2m|\eta_1-\eta_2|}-1)}dy\right\} \tag{5.50}$$

Now that $\widetilde{E}_C(s\to -1)$ has been evaluated, using Equations (5.50) and (5.45) into Equation (5.44), we obtain an expression for the Casimir energy of perfectly conducting cylindrical shells:

$$E_C(s\to -1)=\frac{\hbar c}{4\pi}\left[\int_0^\infty y\ln\left[\left(1-\bar{I}_0\bar{K}_0\right)\left(1-\bar{I}_0'\bar{K}_0'\right)\right]dy - 4\sum_{m=1}^{\infty}\int_0^\infty \frac{y}{m(e^{2m|\eta_1-\eta_2|}-1)}dy\right] \tag{5.51}$$
$$-0.01356\hbar c\left(\frac{1}{R_1^2}+\frac{1}{R_2^2}\right)$$

All the terms in Equation (5.51) are physically convergent and finite. The integrals present can be solved numerically.

5.3.2.1 Numerical Results

Equation (5.51) is implemented numerically and the behavior of the energy as a function of the separation of the cylindrical shells is investigated. The behavior is shown in Figure 5.4. When the separation between the shells is small, $\alpha\to 1$ where $\alpha = R_2/R_1$ the energy can be expressed analytically in the following form:

$$E_C\approx\frac{-\hbar c 0.0862}{R_1^2(\alpha-1)^3} \tag{5.52}$$

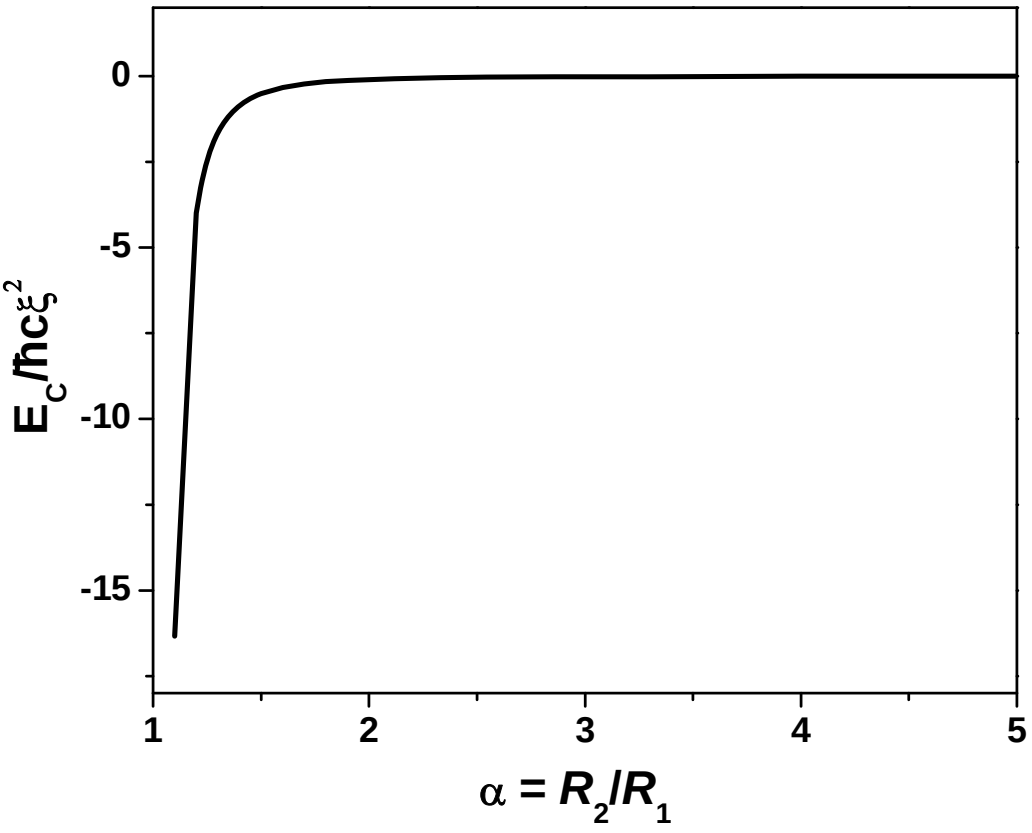

Figure 5.4 The Casimir energy per unit length for the same layer as a function of $\alpha = R_2 / R_1$

In the case where the radii of the shells are very large, $R_1, R_2 \to \infty$ and the separation between the shells is kept fixed, $d = R_2 - R_1 = const$, the system now corresponds to two parallel perfectly conducting plates, similar the system studied by Casimir [7]. In this case, we are able to recover the well-known formula for the Casimir energy per unit area for two perfectly conducting plates:

$$E_C \approx \frac{-\hbar c \pi^2}{720 d^3} \tag{5.53}$$

As the radius of the second shell is increased, the system now behaves as a conducting cylindrical shell immersed in a medium and we see from Figure 5.4 that the energy converges to a constant. For large α, the only non-zero term in Equation (5.51) is $\sim 1/R_1^2$, thus giving the energy for one perfectly conducting cylindrical shell.

Therefore, we have been able to calculate the Casimir energy for a dielectric-diamagnetic cylindrical layer immersed in an infinite medium by making use of the mode summation method. Two separate cases have been investigated, one where the system behaves like an optically dilute dielectric-diamagnetic cylindrical layer with properties not very different from the dielectric and magnetic properties of the medium and one where the system corresponds to that of two perfectly conducting cylindrical shells. In both cases, the divergences were removed and the numerical values obtained were physically finite and convergent.

The case of two perfectly conducting concentric cylinders might be of particular interest as a qualitative model of the Casimir interactions in a double-wall metallic carbon nanotube system. Previous theoretical studies, however, have shown that the perfectly conducting metallic cylinder model does not describe correctly the electrodynamical processes closely related to the Casimir interaction, such as atomic spontaneous decay [75,76], atom-nanotube van der Waal coupling [77], atomic light absorption [78], and atomic entanglement [79]) near carbon nanotubes. This means that one needs to take into account realistic electromagnetic properties and the strong modification of the photonic density of states due to the increasing role of the interface photonic modes near the nanotube surface. For example, in Carbon nanotubes, the interface photonic modes in the longitudinal direction are plasmons. These plasmons couple strongly with the excitons in the nanotube by long range interactions [43]. The perfect-conductor case might serve as a qualitative model of a double-wall metallic nanotube system in the limit of largely different radii, as the role of the interface photonic modes decreases with increasing inter-tube separation. This model serves as a formulation for future more advanced theoretical techniques which should be able to reproduce the results obtained in this work. The results described here have been published in the paper [80].

CHAPTER 6

N PERFECTLY CONDUCTING CYLINDRICAL SHELLS

6.1 Cylindrical Model

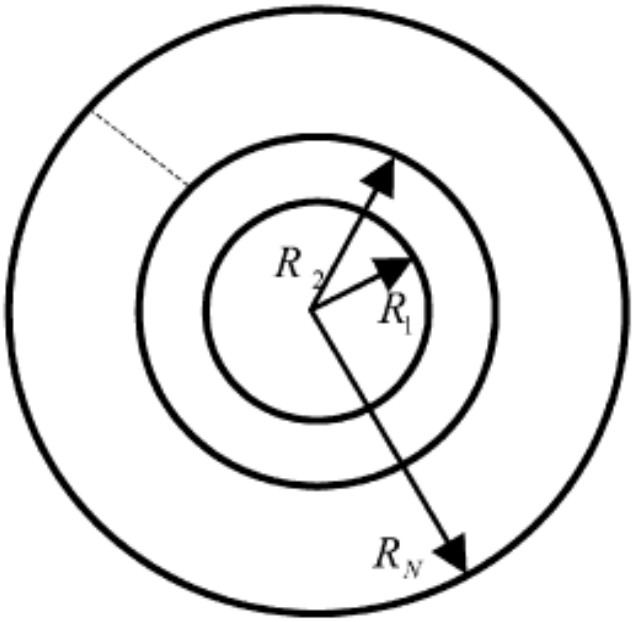

Figure 6.1 Infinitely long perfectly conducting and concentric cylindrical shells immersed in an infinite medium. The axial direction is perpendicular to the page. The radii of the shells are R_i where $i=1,2,\ldots N$.

In this work, the Casimir energy for a system of infinitely long, infinitely thin, and perfectly conducting concentric cylindrical shells immersed an infinite medium is calculated using the mode summation method. The system consists of *N* multiple shells with radii R_i where *i=1,2,…N*, as shown in Figure 6.1. This kind of system is of interest to us because it resembles cylindrical structures made of metallic shells, such as metallic multiwall nanotubes [81,82].

6.2 Electromagnetic Modes

To calculate the Casimir energy of this system of multiple concentric metallic shells, we again make use of the mode summation method. This requires us to find the electromagnetic modes of the system by solving Maxwell's equations with appropriate boundary conditions across each interface of the shells [65]. It follows that the z-component of the electric and magnetic fields in cylindrical coordinates are respectively given as:

$$E_z = \sum_{n=-\infty}^{\infty} \left[A_n J_n(\chi\rho) + B_n H_n^{(1)}(\chi\rho) \right] e^{in\theta} e^{i(k_z z - \omega t)} \tag{6.1}$$

$$B_z = \sum_{n=-\infty}^{\infty} \left[C_n J_n(\chi\rho) + D_n H_n^{(1)}(\chi\rho) \right] e^{in\theta} e^{i(k_z z - \omega t)} \tag{6.2}$$

where k_z is the wave-vector along the *z* direction, ω is the frequency of the electromagnetic excitations and $\chi^2 = \omega^2 - k_z^2$. Also, $J_n(\chi\rho)$ and $H_n^{(1)}(\chi\rho)$ are the

Bessel function of first kind of order *n* and the Hankel functions of the first kind of order *n*, respectively.

The remaining components of the electric and magnetic fields can be derived from Maxwell's equations [65]. The Dirichlet and Neumann boundary conditions are used here to find the unknown coefficients A_n, B_n, C_n, D_n. These boundary conditions require that the z-component of the electric field and the normal component of the magnetic field to vanish at each surface, respectively [65,83]. After applying the boundary conditions, we obtain the following:

$$A_n J_n(\chi R_i) + B_n H_n^{(1)}(\chi R_i) = 0 \tag{6.3}$$

$$C_n J_n'(\chi R_i) + D_n H_n'^{(1)}(\chi R_i) = 0 \tag{6.4}$$

where $i=1,2,\ldots N$ and $J_n'(x) = \frac{dJ_n(x)}{dx}$, $H_n'^{(1)}(x) = \frac{dH_n^{(1)}(x)}{dx}$.

The dispersion relations for this system are obtained by solving Equations (6.3) and (6.4). The electromagnetic modes can then be classified as transverse electric (TE) and transverse magnetic (TM) modes [69,70]. For the TE modes, the frequency $\omega(k_z)$ is found by solving:

$$\begin{aligned} &J_n(\chi R_1) = 0, \quad r < R_1 \\ &J_n(\chi R_j) H_n^{(1)}(\chi R_{j+1}) - J_n(\chi R_{j+1}) H_n^{(1)}(\chi R_j) = 0, \quad R_j < r < R_{j+1} \\ &H_n^{(1)}(\chi R_N) = 0, \quad r > R_N \end{aligned} \tag{6.5}$$

where $j = 1,2,\ldots,N-1$.

For the TM modes, the frequency $\omega(k_z)$ is found by solving:

$$J_n'(\chi R_1) = 0, \quad r < R_1$$

$$J_n'(\chi R_j)H_n'^{(1)}(\chi R_{j+1}) - J_n'(\chi R_{j+1})H_n'^{(1)}(\chi R_j) = 0, \quad R_j < r < R_{j+1} \tag{6.6}$$

$$H_n'^{(1)}(\chi R_N) = 0, \quad r > R_N$$

Thus the dispersion relations for the electromagnetic modes for the N perfectly conducting metallic shells are obtained as follows:

$$f_n^{TE}(\chi, R_1, R_2, \ldots R_N) = J_n(\chi R_1)H_n^{(1)}(\chi R_N)\left[\prod_{j=1}^{N-1}\left(J_n(\chi R_j)H_n^{(1)}(\chi R_{j+1}) - J_n(\chi R_{j+1})H_n^{(1)}(\chi R_j)\right)\right] \tag{6.7}$$

$$f_n^{TM}(\chi, R_1, R_2, \ldots R_N) = J_n'(\chi R_1)H_n'^{(1)}(\chi R_N)\left[\prod_{j=1}^{N-1}\left(J_n'(\chi R_j)H_n'^{(1)}(\chi R_{j+1}) - J_n'(\chi R_{j+1})H_n'^{(1)}(\chi R_j)\right)\right] \tag{6.8}$$

Now that the dispersion relations are obtained, we can now make use of Equation (4.9) to express the Casimir energy for the system of multiple concentric metallic shells:

$$E_C = -\frac{\hbar c}{8\pi}\sum_{n=-\infty}^{\infty}\int_0^{\infty} dy y^2 \frac{d}{dy}\ln\frac{f_n^{TE}(iR_1 y, iR_2 y, \ldots, iR_N y)\, f_n^{TM}(iR_1 y, iR_2 y, \ldots, iR_N y)}{f_n^{TE}(i\infty)\, f_n^{TM}(i\infty)} \tag{6.9}$$

Here, the functions $J_n(iyR)$ and $H_n^{(1)}(iyR)$ are replaced by the modified Bessel functions using $I_n(y) = i^{-n} J_n(iy)$ and $K_n(y) = i^{n+1}(\pi/2)H_n^{(1)}(iy)$.

6.3 Casimir Energy of *N* Perfectly Metallic Cylindrical Shells

In order to proceed with the calculation of the Casimir energy, we still need to deal with the infinite sum over *n* in Equation (6.9). To treat this divergence, we find it convenient to take the difference between the energy of the system of concentric shells and the energy of the individual isolated cylindrical shells. In this way the Casimir energy is expressed in a more transparent way and the remaining divergences are cancelled out [4,80]. Thus for a system of *N* infinitely long metallic cylindrical shells we consider

$$\widetilde{E}_C = E_C - \left(\sum_{i=1}^{N} E_C^{(i)} \right) \tag{6.10}$$

where E_C is given by Equation (6.9) and $E_C^{(i)}$ are the energies of the single isolated cylindrical shells with radii $R_1, R_2, ..., R_N$. The energies $E_C^{(i)}$ have already been derived [3,5] and here we use their final result - $E_C^{(i)} = -0.01356\hbar c / R_i^2$. From Equations. (6.9) and (6.10) one obtains:

$$\widetilde{E}_C = -\frac{\hbar c}{8\pi} \sum_{n=-\infty}^{\infty} \int_0^{\infty} dy y^2 \frac{d}{dy} \ln \frac{f_n^{TE}(iR_1 y, iR_2 y, ..., iR_N y) f_n^{TM}(iR_1 y, iR_2 y, ..., iR_N y) \left[f_{n,i}^{TE}(i\infty) f_{n,i}^{TM}(i\infty) \right]^N}{\prod_{i=1}^{N} \left[f_{n,i}^{TE}(iR_i y) f_{n,i}^{TM}(iR_i y) \right] f_n^{TE}(i\infty) f_n^{TM}(i\infty)} \tag{6.11}$$

Here $f_n^{TE,TM}(iR_1 y, iR_2 y, ..., iR_N y)$ are the dispersion relations defined by Equations (6.7) and (6.8) with $y = \mathrm{Im}\,\chi$. $f_{n,i}^{TE,TM}(iR_i y)$ are the dispersion relations for a single cylindrical shell with radius R_i and $f_{n,i}^{TE,TM}(i\infty)$ are the dispersion relations with no boundaries present.

Making the appropriate substitutions into Equation (6.11) for the dispersion relations from Equations (6.7), (6.8) and for the dispersion relations of single isolated cylindrical shells, we obtain:

$$\widetilde{E}_C = \frac{\hbar c}{4\pi}\left\{\int_0^\infty dy y \ln\left[\prod_{j=1}^{N-1}\left(\left(1-\frac{I_0(yR_j)K_0(yR_{j+1})}{I_0(yR_{j+1})K_0(yR_j)}\right)\left(1-\frac{I_0'(yR_j)K_0'(yR_{j+1})}{I_0'(yR_{j+1})K_0'(yR_j)}\right)\right)\right]\right.$$
$$\left. + 2\sum_{n=1}^{\infty}\int_0^\infty dy y \ln\left[\prod_{j=1}^{N-1}\left(\left(1-\frac{I_n(yR_j)K_n(yR_{j+1})}{I_n(yR_{j+1})K_n(yR_j)}\right)\left(1-\frac{I_n'(yR_j)K_n'(yR_{j+1})}{I_n'(yR_{j+1})K_n'(yR_j)}\right)\right)\right]\right\} \quad (6.12)$$

where the $n = 0$ and $n \neq 0$ terms in the modified Bessel functions have been separated.

For a given number of cylindrical shells *N*, the first term in the expression of $\widetilde{E}_C$ can be evaluated numerically. The evaluation of the second term is facilitated by the use of the uniform asymptotic expansion of the modified Bessel functions for large orders [73] and also by using the Taylor series expansion of the logarithmic function $\ln(1-x_j)$ for $x_j < 1$, where $x_j = e^{-2n|\eta_j - \eta_{j+1}|}$ [4,80]. This leads to the second term being expressed as:

$$2\sum_{n=1}^{\infty}\int_{0}^{\infty}dyy\ln\left[\prod_{j=1}^{N-1}\left(\left(1-\frac{I_n(yR_j)K_n(yR_{j+1})}{I_n(yR_{j+1})K_n(yR_j)}\right)\left(1-\frac{I_n'(yR_j)K_n'(yR_{j+1})}{I_n'(yR_{j+1})K_n'(yR_j)}\right)\right)\right]$$

$$\sim -4\sum_{m=1}^{\infty}\int_{0}^{\infty}dy\left(\sum_{j=1}^{N-1}\frac{y}{m(e^{2m|\eta_j-\eta_{j+1}|}-1)}\right) \tag{6.13}$$

Combining Equations (6.13), (6.12) and $E_C^{(i)}=-0.01356\hbar c/R_i^2$ into Equation (6.10), the Casimir energy of the considered system of concentric conducting shells is found to be:

$$E_C=\frac{\hbar c}{4\pi}\left\{\int_{0}^{\infty}dyy\ln\left[\prod_{j=1}^{N-1}\left(\left(1-\frac{I_0(yR_j)K_0(yR_{j+1})}{I_0(yR_{j+1})K_0(yR_j)}\right)\left(1-\frac{I_0'(yR_j)K_0'(yR_{j+1})}{I_0'(yR_{j+1})K_0'(yR_j)}\right)\right)\right]\right.$$

$$\left.-4\sum_{m=1}^{\infty}\int_{0}^{\infty}dy\left(\sum_{j=1}^{N-1}\frac{y}{m(e^{2m|\eta_j-\eta_{j+1}|}-1)}\right)\right\}-0.01356\hbar c\left(\sum_{i=1}^{N}\frac{1}{R_i^2}\right) \tag{6.14}$$

for $j=1,2,...,N-1$ where $\eta_j=\sqrt{1+(R_jy)^2}+\ln\left(\frac{R_jy}{1+\sqrt{1+(R_jy)^2}}\right)$.

All the terms in Equation (6.14) can be evaluated numerically. They are convergent and provide finite, physically meaningful values for the Casimir energy for the perfectly conducting system considered here. This demonstrates that we were successful in applying the mode summation method to calculate the Casimir energy of infinitely long, perfectly conducting concentric cylindrical shells.

6.3.1 Limiting Cases

In this section we investigate various limiting cases for the Casimir energy with respect to the separation of the shells. First when $N = 2$, we recover the energy obtained in Refs. [4,6,80] for the case of two perfectly conducing concentric shells described by Equation (5.51). Furthermore, in the limit of infinitely close cylinders, the dominant term comes from Equation (6.13), and we find that:

$$E_C \approx -0.0862\hbar c \sum_{j=1}^{N-1} \frac{1}{R_j^2 (\alpha_j - 1)^3} \tag{6.15}$$

where $\alpha_j = R_{j+1} / R_j$. Thus for *j=1*, we obtain the result for two infinitely close shells [4,80].

The limit of large radii and constant shell separation, $R_j \to \infty$ and $d_j = R_{j+1} - R_j = const$ for all *j*, we have a system that corresponds to *N* infinite parallel conducting plates. For this limit, we obtain the Casimir energy per unit area as:

$$E_C \approx -\hbar c \pi^2 \sum_{j=1}^{N-1} \frac{1}{720 d_j^{\,3}} \tag{6.16}$$

thereby recovering the well known formula for the Casimir energy per unit area of two perfectly conducting plates (*j=1*) same as Equation (5.53)- $E_C \approx -\hbar c \pi^2 / (720 d^3)$ [7].

6.3.2 Numerical Results

The considered system implies that as *N* increases, greater possibilities for radial size and curvature variations of one or more cylindrical shells become available. We illustrate this point by showing numerical results for *N=3* shells. One particular case is when the radii of the shells are varied in such a way as to keep the distance between each shell constant. In Figure 6.2 we show the behavior of the Casimir energy when the separation of the shells are fixed, $\alpha_1 = \alpha_2$. Here, $\alpha_1 = R_2 / R_1$ and $\alpha_2 = R_3 / R_2$. In the limit of $R_1, R_2, R_3 \to \infty$ and $d_1 = d_2 = const$ where $d_1 = R_2 - R_1$ and $d_2 = R_3 - R_2$, we obtain the Casimir energy per unit area as $E_C \approx -\hbar c \pi^2 \left(1/720 d_1^{\,3} + 1/720 d_2^{\,3}\right)$ confirming a result obtained in Ref. [84].

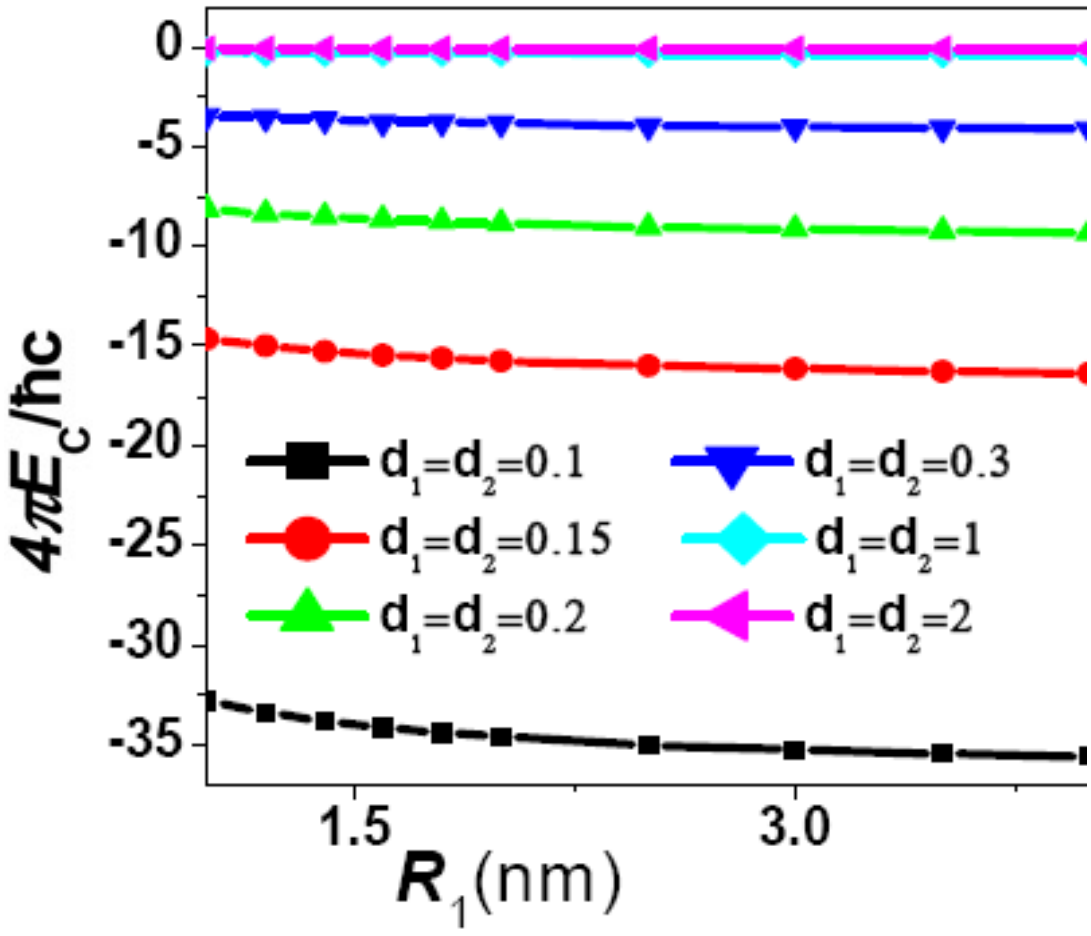

Figure 6.2 The Casimir energy for the case of $N=3$ shells as a function of the inner radius R_1.

Increasing the radius of the outer two shells, their separation being constant, while keeping the inner radius fixed provides us with a very interesting case for the Casimir energy. This is illustrated in Figure 6.3 where $R_1 = 1\,nm$ and R_2 increasing with $\alpha_2 = const$. We see that $|E_C|$ is larger for smaller α_2 indicating the dominant term from Equation (6.13). As R_2 increases, the Casimir energy becomes practically a constant with our system behaving more like a single cylindrical shell and two perfectly conducting plates. The electromagnetic interactions between the inner shell and the outer shells become smaller as the separation increases and therefore this leads to a constant value for the Casimir energy.

Another interesting case involves keeping the two inner radii constant and the outer one R_3 is varied. Figure 6.4 shows the behavior of the Casimir energy in such a case. For the $R_3 \to \infty$ limit, the energy approaches that of two perfectly conducting cylindrical shells infinitely separated from a conducting parallel plate. Again, we see that $|E_C|$ is large for small α_1 due to the main contribution from Equation (6.13). As α_2 increases, the Casimir energy becomes practically a constant approaching the limit for two cylindrical shells and a parallel plate.

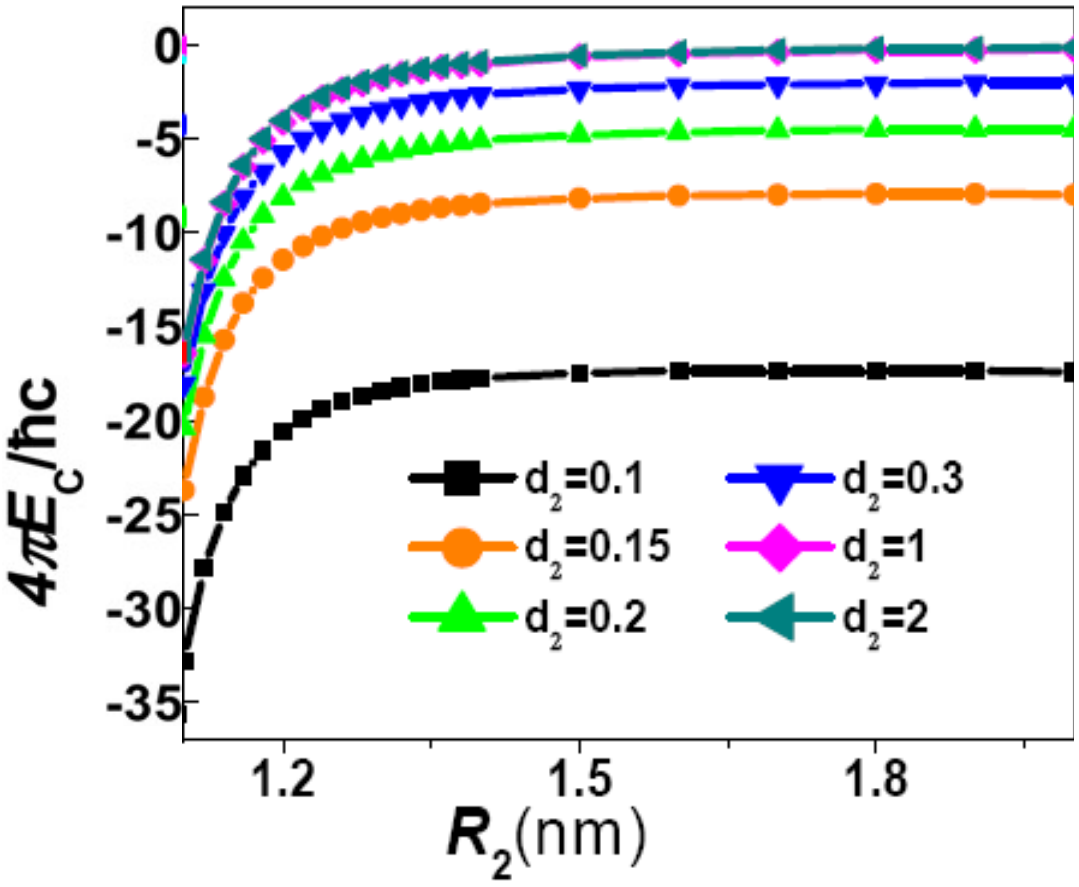

Figure 6.3 The Casimir energy for the case of $N=3$ shells as a function of the radius of the second shell R_2.

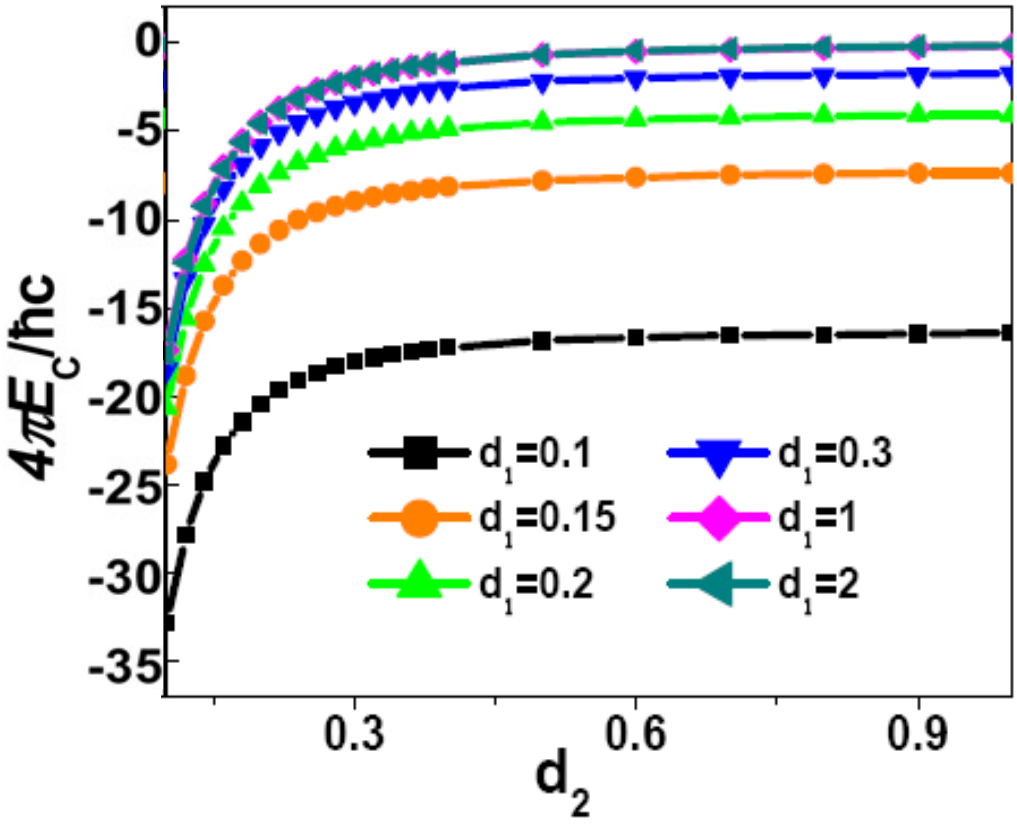

Figure 6.4 The Casimir energy for the case of $N=3$ shells as a function of the separation between the outer two shells.

Finally, we investigate the relationship between the number of shells N and the corresponding Casimir energy. In Figure 6.5, we show results E_C for various α_i as a function of N. We find that $|E_C|$ increases non-linearly and it is larger for smaller $\alpha's$ indicating the dominant contribution from Equation (6.13). The higher the number of shells implies that there are more electromagnetic interactions between the surfaces resulting in a higher Casimir energy. The closer the shells will result in a higher Casimir energy due to high electromagnetic interaction and the dominant contribution of Equation (6.13). As the separation between the shells becomes larger, $|E_C|$ decreases and it approaches the limit of the sum of energies of single cylindrical shells with the appropriate radii [3,5].

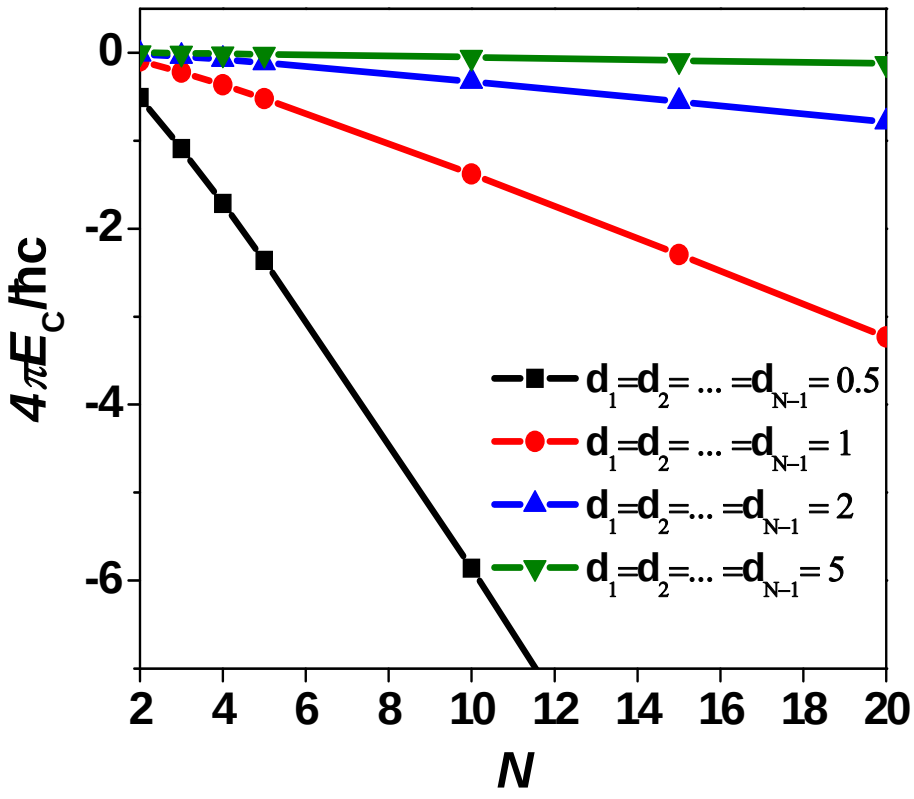

Figure 6.5 The Casimir energy as a function of the number of concentric cylindrical shells.

CHAPTER 7

TWO PARALLEL DIELECTRIC-DIAMAGNETIC CYLINDERS

7.1 Cylindrical Model

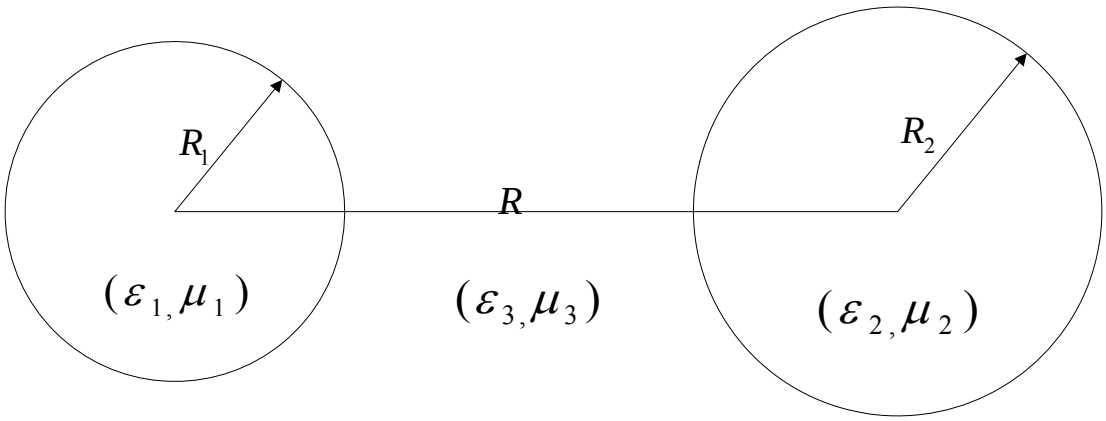

Figure 7.1 Two infinitely long parallel cylinders of radii R_1 and R_2 with center-to-center separation R immersed in an infinite medium. The cylindrical axis is perpendicular to the page.

The system under consideration consists of two infinitely long straight parallel circular cylinders of radii R_1 and R_2 , with center-to-center separation R . The permittivity and permeability of the first cylinder is ε_1 and μ_1 respectively and for the second cylinder the permittivity and permeability is ε_2 and μ_2 respectively. The cylinders are placed in an infinite medium of dielectric and magnetic functions ε_3 and μ_3. All dielectric and magnetic characteristics are taken to be constants.

In this work, we consider the interaction originating from the electromagnetic field fluctuations between infinitely long parallel circular dielectric-diamagnetic cylinders immersed in a medium. Such a system is of particular interest because it can serve as a model to study the Casimir interaction between cylindrical tubular structures, such as carbon nanotubes, boron nitride nanotubes, nanowires, DNA, etc…It can also provide a test ground of how curvature effects coupled with dielectric and/or magnetic properties influence the mutual interaction between the cylinders.

7.2 Electromagnetic Modes

In order to utilize the mode summation method, one needs to find the electromagnetic modes by solving the Maxwell's equations [65] with the appropriate boundary conditions across the interfaces of each cylinder. In this problem, the electric and magnetic fields are expressed with respect to two separate sets of cylindrical coordinates, one for each cylinder. The solution to the wave equation is satisfied in three

regions and consequently, the z-component of the electric and magnetic fields (axial direction perpendicular to the page) is defined in these three regions:

$$\rho_1 < R_1,\ \rho_2 > R_2 \tag{7.1}$$

$$\rho_1 > R_1,\ \rho_2 < R_2 \tag{7.2}$$

$$\rho_1 > R_1,\ \rho_2 > R_2 \tag{7.3}$$

Therefore, we can write the z-component of the electric and magnetic fields as follows:

$$E_z^{(1)} = \sum_{n=-\infty}^{\infty} \left\{ A_n^{(1)} J_n(\chi_1 \rho_1) e^{in\theta_1} + B_n^{(3)} H_n^{(1)}(\chi_3 \rho_2) e^{in\theta_2} \right\} e^{i(k_z z - \omega t)} \tag{7.4}$$

$$B_z^{(1)} = \sum_{n=-\infty}^{\infty} \left\{ C_n^{(1)} J_n(\chi_1 \rho_1) e^{in\theta_1} + D_n^{(3)} H_n^{(1)}(\chi_3 \rho_2) e^{in\theta_2} \right\} e^{i(k_z z - \omega t)} \tag{7.5}$$

$$E_z^{(2)} = \sum_{n=-\infty}^{\infty} \left\{ A_n^{(2)} J_n(\chi_2 \rho_2) e^{in\theta_2} + B_n^{(4)} H_n^{(1)}(\chi_3 \rho_1) e^{in\theta_1} \right\} e^{i(k_z z - \omega t)} \tag{7.6}$$

$$B_z^{(2)} = \sum_{n=-\infty}^{\infty} \left\{ C_n^{(2)} J_n(\chi_2 \rho_2) e^{in\theta_2} + D_n^{(4)} H_n^{(1)}(\chi_3 \rho_1) e^{in\theta_1} \right\} e^{i(k_z z - \omega t)} \tag{7.7}$$

$$E_z^{(3)} = \sum_{n=-\infty}^{\infty} \left\{ B_n^{(4)} H_n^{(1)}(\chi_3 \rho_1) e^{in\theta_1} + B_n^{(3)} H_n^{(1)}(\chi_3 \rho_2) e^{in\theta_2} \right\} e^{i(k_z z - \omega t)} \tag{7.8}$$

$$B_z^{(3)} = \sum_{n=-\infty}^{\infty} \left\{ D_n^{(4)} H_n^{(1)}(\chi_3 \rho_1) e^{in\theta_1} + D_n^{(3)} H_n^{(1)}(\chi_3 \rho_2) e^{in\theta_2} \right\} e^{i(k_z z - \omega t)} \tag{7.9}$$

where k_z is the wave-vector along the z direction, ω - the frequency of the electromagnetic excitations, and $\chi_j^{\,2} = \varepsilon_j \mu_j \omega^2 - k_z^2$ with $j=1,2,3$. $J_n(\chi_j \rho)$ and $H_n^{(1)}(\chi_j \rho)$ are the Bessel functions of first kind of order n and the Hankel functions

of the first kind of order *n*, respectively. Also, regions (1), (2) and (3) are defined by Equations (7.1), (7.2) and (7.3) respectively.

It can be seen that there are two cylindrical coordinate systems associated with each cylinder - (ρ_i, θ_i, z) with *i=1, 2* in Equations (7.4-7.9). In order to be able to solve for the unknown coefficients, we need to be able to express the electric and magnetic fields with respect to a single cylindrical coordinate system. This is achieved by making use of the addition theorem [73]:

$$H_n^{(1)}(\chi_3\rho_2)e^{in\theta_2} = \sum_{j=-\infty}^{\infty} H_{n+j}^{(1)}(\chi_3 R)J_j(\chi_3\rho_1)e^{ij\theta_1} \tag{7.10}$$

Equation (7.10) enables us to express the second coordinate system in terms of the first coordinate system and a similar relation is used with $\rho_1 \leftrightarrow \rho_2$, $\theta_1 \leftrightarrow \theta_2$ to express the first coordinate system in terms of the second coordinate system. We can now express the electric and magnetic fields in terms of only one coordinate system as follows with

i=1, 2:

$$E_z^{(i)} = \sum_{n=-\infty}^{\infty}\left\{A_n^{(i)}J_n(\chi_i\rho_i)e^{in\theta_i} + B_n^{(i+2)}\sum_{j=-\infty}^{\infty}H_{n+j}^{(1)}(\chi_3 R)J_j(\chi_3\rho_i)e^{ij\theta_i}\right\}e^{i(k_z z-\omega t)} \tag{7.11}$$

$$B_z^{(i)} = \sum_{n=-\infty}^{\infty}\left\{C_n^{(i)}J_n(\chi_i\rho_i)e^{in\theta_i} + D_n^{(i+2)}\sum_{j=-\infty}^{\infty}H_{n+j}^{(1)}(\chi_3 R)J_j(\chi_3\rho_i)e^{ij\theta_i}\right\}e^{i(k_z z-\omega t)} \tag{7.12}$$

$$E_z^{(3)} = \sum_{n=-\infty}^{\infty}\left\{B_n^{(4)}H_n^{(1)}(\chi_3\rho_1)e^{in\theta_1} + B_n^{(3)}H_n^{(1)}(\chi_3\rho_2)e^{in\theta_2}\right\}e^{i(k_z z-\omega t)} \tag{7.13}$$

$$B_z^{(3)} = \sum_{n=-\infty}^{\infty} \left\{ D_n^{(4)} H_n^{(1)}(\chi_3 \rho_1) e^{in\theta_1} + D_n^{(3)} H_n^{(1)}(\chi_3 \rho_2) e^{in\theta_2} \right\} e^{i(k_z z - \omega t)} \tag{7.14}$$

The electric $E_z^{(3)}$ and magnetic $B_z^{(3)}$ fields for the medium contain one term expressed in the coordinate set of one cylinder and another term – in the coordinate system of the other cylinder. Again using the addition theorem, we can express the fields in terms of a single coordinate system. The ρ- and θ-components of the fields can be easily obtained using Maxwell's equations [65]. The unknown coefficients $A_n^{(i)}, B_n^{(i)}, C_n^{(i)}, D_n^{(i)}, B_n^{(i+2)}, D_n^{(i+2)}$ are related by imposing the boundary conditions for the continuity of $\varepsilon_j E_{\rho_i}^{(j)}, E_{\theta_i}^{(j)}, E_z^{(j)}, B_z^{(j)} / \mu_j$ across the interface of each cylinder giving the dispersion relation for the electromagnetic modes supported by this system. In the general case, the dispersion relation is complicated and the calculations of the interaction energy are not feasible, however significant simplifications occur when the speed of light *c* is constant everywhere.

The dispersion relations can now be obtained by applying the boundary conditions and keeping $\varepsilon_j \mu_j = c^{-2}$. This leads to the dispersion relations defined by:

$$f_1(i\nu, R_1, R_2, R) = Det(1 - \widetilde{\Gamma}) = 0 \tag{7.15}$$

$$f_2(i\nu, R_1, R_2, R) = Det(1 - \widetilde{\Delta}) = 0 \tag{7.16}$$

where the substitution $\nu = \mathrm{Im}\,\chi$ has been made. $\widetilde{\Gamma}$ and $\widetilde{\Delta}$ are matrices with elements:

$$\Gamma_{nl} = \sum_{j=-\infty}^{\infty} \frac{(\varepsilon_3 - \varepsilon_1)(\varepsilon_3 - \varepsilon_2) i^{n-l} K_{n+j}(\nu R) K_{j+l}(\nu R)}{\left[\varepsilon_2 \frac{K_n'(\nu R_2)}{I_n'(\nu R_2)} - \varepsilon_3 \frac{K_n(\nu R_2)}{I_n(\nu R_2)} \right] \left[\varepsilon_1 \frac{K_j'(\nu R_1)}{I_j'(\nu R_1)} - \varepsilon_3 \frac{K_j(\nu R_1)}{I_j(\nu R_1)} \right]} \tag{7.17}$$

$$\Delta_{nl} = \sum_{j=-\infty}^{\infty} \frac{(\varepsilon_3 - \varepsilon_1)(\varepsilon_3 - \varepsilon_2) i^{n-l} K_{n+j}(\nu R) K_{j+l}(\nu R)}{\left[\varepsilon_3 \frac{K_n'(\nu R_2)}{I_n'(\nu R_2)} - \varepsilon_2 \frac{K_n(\nu R_2)}{I_n(\nu R_2)} \right] \left[\varepsilon_3 \frac{K_j'(\nu R_1)}{I_j'(\nu R_1)} - \varepsilon_1 \frac{K_j(\nu R_1)}{I_j(\nu R_1)} \right]} \tag{7.18}$$

where $I'_{n,j}(x) = dI_{n,j}(x)/dx$ and $K'_{n,j}(x) = dK_{n,j}(x)/dx$.

The electromagnetic modes supported by the system of two straight, parallel dielectric-diamagnetic cylinders are obtained from Equations (7.15) and (7.16). Using Equation (4.9), the Casimir energy of two straight, parallel dielectric-diamagnetic cylinders is given as:

$$E_C = -\frac{\hbar c}{8\pi} \int_0^{\infty} d\nu \nu^2 \frac{d}{d\nu} \ln \frac{f_1(i\nu, R_1, R_2, R) f_2(i\nu, R_1, R_2, R)}{f_1(i\infty) f_2(i\infty)} \tag{7.19}$$

where $f_1(i\infty)$ and $f_2(i\infty)$ are the dispersion relations with no boundaries present.

7.3 Casimir Energy of Two Straight Parallel Cylinders

In order to evaluate Equation (7.19), we find it convenient to use the log-det approximation [85]:

$$\ln\{f_1(i\nu, R_1, R_2, R)\} = \ln\{Det(1-\widetilde{\Gamma})\} \approx -Tr\{\widetilde{\Gamma}\} = -\sum_n \Gamma_{nn} \tag{7.20}$$

$$\ln\{f_2(i\nu, R_1, R_2, R)\} = \ln\{Det(1-\widetilde{\Delta})\} \approx -Tr\{\widetilde{\Delta}\} = -\sum_n \Delta_{nn} \tag{7.21}$$

$$\ln\{f_1(i\infty)\} = \ln\{Det(1-\widetilde{\Gamma}(\infty))\} \approx -Tr\{\widetilde{\Gamma}(\infty)\} = -\sum_n \Gamma_{nn}(\infty) \tag{7.22}$$

$$\ln\{f_2(i\infty)\} = \ln\{Det(1-\widetilde{\Delta}(\infty))\} \approx -Tr\{\widetilde{\Delta}(\infty)\} = -\sum_n \Delta_{nn}(\infty) \tag{7.23}$$

We use only the leading term of the log-det approximation since it gives the contribution to the leading order. This expansion gives the leading term when $R_1, R_2 < R$, which is the case here. The Casimir energy can now be expressed in the following form:

$$E_C \approx \frac{\hbar c}{8\pi}\int_0^\infty d\nu\nu^2 \frac{d}{d\nu}\left[\sum_{n=-\infty}^{\infty}\left(\Gamma_{nn}+\Delta_{nn}-\Gamma_{nn}(\infty)-\Delta_{nn}(\infty)\right)\right] \tag{7.24}$$

Here, since we are dealing with the traces of the matrices, n=l. For all terms occurring in Equation (7.24), we find it convenient to arrange them into four parts, $(n=0,\ j=0)$, $(n=0,\ j\neq 0)$, $(n\neq 0,\ j=0)$, and $(n\neq 0,\ j\neq 0)$ groups. The terms with $(n=0,\ j\neq 0)$ are evaluated by making use of the change of variables, $\nu = jz,\ j = 1,2,3,...,$ and performing the uniform asymptotic expansion of the Bessel functions [73]. The terms with $(n\neq 0,\ j=0)$ are evaluated by making use of the change of variables, $\nu = nz, n = 1,2,3,...,$ and again performing the uniform asymptotic expansion of the Bessel functions. The terms with $n\neq 0,\ j\neq 0$ are evaluated using large order expansion for the Bessel functions. This is a technique used in other works for the interaction energy in cylindrical structures [2,3,80,86]. After doing the appropriate changes, we obtain the following convergent expression for the zero-point energy per unit length l, for the case of two parallel cylinders:

$$E_C = -\frac{\hbar c}{4\pi}\left\{\int_0^\infty d\nu\nu\left[\frac{(\varepsilon_3-\varepsilon_1)(\varepsilon_3-\varepsilon_2)K_0{}^2(\nu R)}{\left[\varepsilon_2\dfrac{K_0'(\nu R_2)}{I_0'(\nu R_2)}-\varepsilon_3\dfrac{K_0(\nu R_2)}{I_0(\nu R_2)}\right]\left[\varepsilon_1\dfrac{K_0'(\nu R_1)}{I_0'(\nu R_1)}-\varepsilon_3\dfrac{K_0(\nu R_1)}{I_0(\nu R_1)}\right]}+\right.\right.$$

$$\left.\left.+\frac{(\varepsilon_3-\varepsilon_1)(\varepsilon_3-\varepsilon_2)K_0{}^2(\nu R)}{\left[\varepsilon_3\dfrac{K_0'(\nu R_2)}{I_0'(\nu R_2)}-\varepsilon_2\dfrac{K_0(\nu R_2)}{I_0(\nu R_2)}\right]\left[\varepsilon_3\dfrac{K_0'(\nu R_1)}{I_0'(\nu R_1)}-\varepsilon_1\dfrac{K_0(\nu R_1)}{I_0(\nu R_1)}\right]}\right]\right.$$

$$\left.+\frac{2}{\pi}\frac{(\varepsilon_3-\varepsilon_1)(\varepsilon_3-\varepsilon_2)}{(\varepsilon_3+\varepsilon_1)(\varepsilon_3+\varepsilon_2)}\int_0^\infty\frac{d\nu\nu}{\sqrt{1+\nu^2R^2}}\left[\frac{e^{2(\eta-\eta_1-\nu R_2)}}{(e^{2(\eta-\eta_1-\nu R_2)}-1)^2}+\frac{e^{2(\eta-\eta_2-\nu R_1)}}{(e^{2(\eta-\eta_2-\nu R_1)}-1)^2}+2\sum_{\substack{n=1\\j=1}}^{\infty}\frac{e^{-2n(\eta-\eta_2)}e^{-2j(\eta-\eta_1)}}{(n+j)}\right]\right\}$$

(7.25)

where

$$\eta=\sqrt{1+(R\nu)^2}+\ln\left[R\nu/1+\sqrt{1+(R\nu)^2}\right]$$

and

$$\eta_{1,2}=\sqrt{1+(R_{1,2}\nu)^2}+\ln\left[R_{1,2}\nu/1+\sqrt{1+(R_{1,2}\nu)^2}\right].$$

7.3.1 Limiting Cases

In this section we evaluate the Casimir energy for two straight parallel cylinders in the limit for largely separated cylinders, $R >> R_1, R_2$. This particular limit can be used as a qualitative model to investigate the interaction of two tubular systems separated by large distances. To simplify the evaluations, we take the cylinders to have equal radii $R_1 = R_2$ and the same dielectric $\varepsilon_1 = \varepsilon_2$ and magnetic $\mu_1 = \mu_2$ properties. When $R >> R_1 = R_2$, the first two terms in Equation (7.25) are approximated by taking a small argument expansion with respect to $\nu R_{1,2}$ in the denominators.

After making the appropriate modifications, we obtain the first term of the Casmir energy from Equation (7.25) to be:

$$\int_0^\infty d\nu\nu \frac{(\varepsilon_3-\varepsilon_1)^2 K_0{}^2(\nu R)}{\left[\varepsilon_1 \frac{K_0'(\nu R_1)}{I_0'(\nu R_1)} - \varepsilon_3 \frac{K_0(\nu R_1)}{I_0(\nu R_1)}\right]^2} \approx \frac{(\varepsilon_3-\varepsilon_1)^2}{4\varepsilon_1{}^2} R_1{}^4 \left\{ \int_0^\infty d\nu\nu^5 K_0{}^2(\nu R) + \right.$$

$$\left. \frac{\varepsilon_3}{2\varepsilon_1} R_1{}^2 \left[\int_0^\infty d\nu\nu^7 K_0{}^2(\nu R)\ln\nu + \int_0^\infty d\nu\nu^7 K_0{}^2(\nu R)\ln R_1 \right] \right\} \tag{7.26}$$

The integrals in Equation (7.26) can be evaluated using the following identities [82]:

$$\int_0^\infty d\nu\nu^{s-1} K_\mu{}^2(\nu R) = 2^{s-3} R^{-s} \left[\Gamma\left(\frac{1}{2}s\right)\right]^2 B\left(\frac{1}{2}s+\mu, \frac{1}{2}s-\mu\right) \tag{7.27}$$

$$\int_0^\infty d\nu \nu^{s-1} \ln(\nu) K_\mu{}^2(\nu R) = \frac{\partial}{\partial s} \int_0^\infty d\nu \nu^{s-1} K_\mu{}^2(\nu R) \tag{7.28}$$

where B is a beta function.

After doing the modifications, the first term ends up as:

$$\int_0^\infty d\nu \nu \frac{(\varepsilon_3 - \varepsilon_1)^2 K_0{}^2(\nu R)}{\left[\varepsilon_1 \frac{K_0'(\nu R_1)}{I_0'(\nu R_1)} - \varepsilon_3 \frac{K_0(\nu R_1)}{I_0(\nu R_1)}\right]^2} \approx \frac{(\varepsilon_3 - \varepsilon_1)^2}{4\varepsilon_1{}^2} R_1{}^4 \left\{\frac{16}{15} R^{-6} + \frac{288}{35} \frac{\varepsilon_3}{\varepsilon_1} R_1{}^2 R^{-8} \left[\ln\left(\frac{2R_1}{R}\right) - \gamma + \frac{451}{420}\right]\right\} \tag{7.29}$$

where γ is Euler's constant.

In similar fashion, the second term of the Casimir energy in Equation (7.25) is found to be:

$$\int_0^\infty d\nu \nu \frac{(\varepsilon_3 - \varepsilon_1)^2 K_0{}^2(\nu R)}{\left[\varepsilon_3 \frac{K_0'(\nu R_1)}{I_0'(\nu R_1)} - \varepsilon_1 \frac{K_0(\nu R_1)}{I_0(\nu R_1)}\right]^2} \approx \frac{(\varepsilon_3 - \varepsilon_1)^2}{4\varepsilon_3{}^2} R_1{}^4 \left\{\frac{16}{15} R^{-6} + \frac{288}{35} \frac{\varepsilon_1}{\varepsilon_3} R_1{}^2 R^{-8} \left[\ln\left(\frac{2R_1}{R}\right) - \gamma + \frac{451}{420}\right]\right\} \tag{7.30}$$

The third and the fourth term of Equation (7.25) become the same when $R_1 = R_2$ and in the limit of $R >> R_1, R_2$, we have:

$$\frac{4}{\pi}\int_0^\infty \frac{\nu e^{2(\eta-\eta_1-\nu R_2)}}{\sqrt{1+\nu^2 R^2}\,(e^{2(\eta-\eta_1-\nu R_2)}-1)^2}dz \approx \frac{1}{4}\frac{R_1^{\,2}}{\pi R^4} \tag{7.31}$$

The last term of the Casimir energy in Equation (7.25) becomes:

$$\frac{4}{\pi}\sum_{n=1}^{\infty}\sum_{j=1}^{\infty}\int_0^\infty \frac{\nu e^{-2n(\eta-\eta_2)(n+j)}}{\sqrt{1+\nu^2 R^2}\,(n+j)}d\nu \approx \frac{3R_1^{\,4}}{526\pi}\frac{1}{R^6}+\frac{5R_1^{\,6}}{23328\pi}\frac{1}{R^8}+..... \tag{7.32}$$

where we have retained only the n=1, j=1,2 terms.

Combining Equations (7.29) - (7.32) into Equation (7.25), we have for the limit $R >> R_1, R_2$, where $R_1 = R_2$, the energy per unit length of the system defined as:

$$E_C \approx -\frac{\hbar c}{8\pi}(\varepsilon_3-\varepsilon_1)^2\left\{\frac{1}{2\pi(\varepsilon_1+\varepsilon_3)^2}\frac{R_1^{\,2}}{R^4}+\left[\frac{8}{15}\left(\frac{1}{\varepsilon_1^{\,2}}+\frac{1}{\varepsilon_3^{\,2}}\right)+\frac{3}{512\pi}\frac{1}{(\varepsilon_1+\varepsilon_3)^2}\right]\frac{R_1^{\,4}}{R^6}\right\} \tag{7.33}$$

The energy is expressed as a sum of terms proportional to powers of the R_1/R ratio and we have considered the first two dominant terms. The other terms in E_C have higher powers of R_1/R^2 indicating that their contribution is small.

7.3.2 Numerical Results

In this section we evaluate the Casimir energy for two straight parallel cylinders numerically and we present numerical and analytical results for various interesting cases by modifying the radial dimension, curvature, and material composition of our system. In order to have a better understanding of how the Casimir energy behaves for a system of two straight, parallel dielectric-diamagnetic cylinders, it is essential to investigate the

dependence of the interaction energy on the radial dimensions of the cylinders and their separation. This is achieved by evaluating Equation (7.25) numerically.

First we investigate the dependence of the Casimir energy over the surface-to-surface separation. Figure 7.2 shows the behavior of the interaction energy as a function of surface-to-surface separation d with $R_1 = 1\,\text{nm}$. One sees that as R_2 is increased the energy diverges slower as a function of d when compared to the one for $R_1 \sim R_2$. At larger d separations, $|E_C|$ decreases slower when $R_2 >> R_1$ as displayed in the inset of Figure 7.2. The crossover occurs at d~0.4 nm. The calculations reveal that the dominant contribution for the cases of $R_1 \sim R_2$ comes from the third and fourth terms of Equation (7.25). As R_2 becomes larger, the fourth term in Equation (7.25) remains dominant, while the third one becomes less important. The reason for the crossover (inset in Figure 5.2) for small and large R_2 can be traced to the exponential distance dependences in these terms. There is a faster decrease in $|E_C|$ for small d when $R_2 >> R_1$ as compared to the cases of small d and $R_1 \sim R_2$ due to the faster decrease in the exponential factors. But for large d, the situation is reversed as indicated by the inset of Figure 7.2. When $d \sim R_2 >> R_1$ there are two large distance scales. Because of their dominance through the η and $\eta_{1,2}$ factors (which are subtracted), the exponential decrease in the fourth term is actually slower than the case for $d >> R_2 \sim R_1$. The results shown in Figure 7.2 are independent of the choices for the dielectric responses of the cylinders and medium.

Another very important case study concerns the dependence of the interaction energy with respect to the dielectric responses of the cylinders and medium. This study can provide us with very important information about how material composition influences the Casimir energy of a system. It has been predicted that the interaction between planar materials 1 and 2 immersed in medium 3 can be repulsive if the value of the dielectric constant of the medium is between the values of the dielectric constants of the materials [39]. Recent measurements of the Casimir force between a large sphere and a plate covered with a layer of silica, for which this condition for the dielectric properties is satisfied, demonstrate that the interaction can be repulsive [38].

We first investigated the case when the dielectric constant of the environment is changed while the dielectric constants of the cylinders $\varepsilon_{1,2}$ are constant and secondly when the dielectric constant of one of the cylinders is varied and $\varepsilon_{2,3}$ are constant. The results are shown in Figures 7.3 and 7.4.

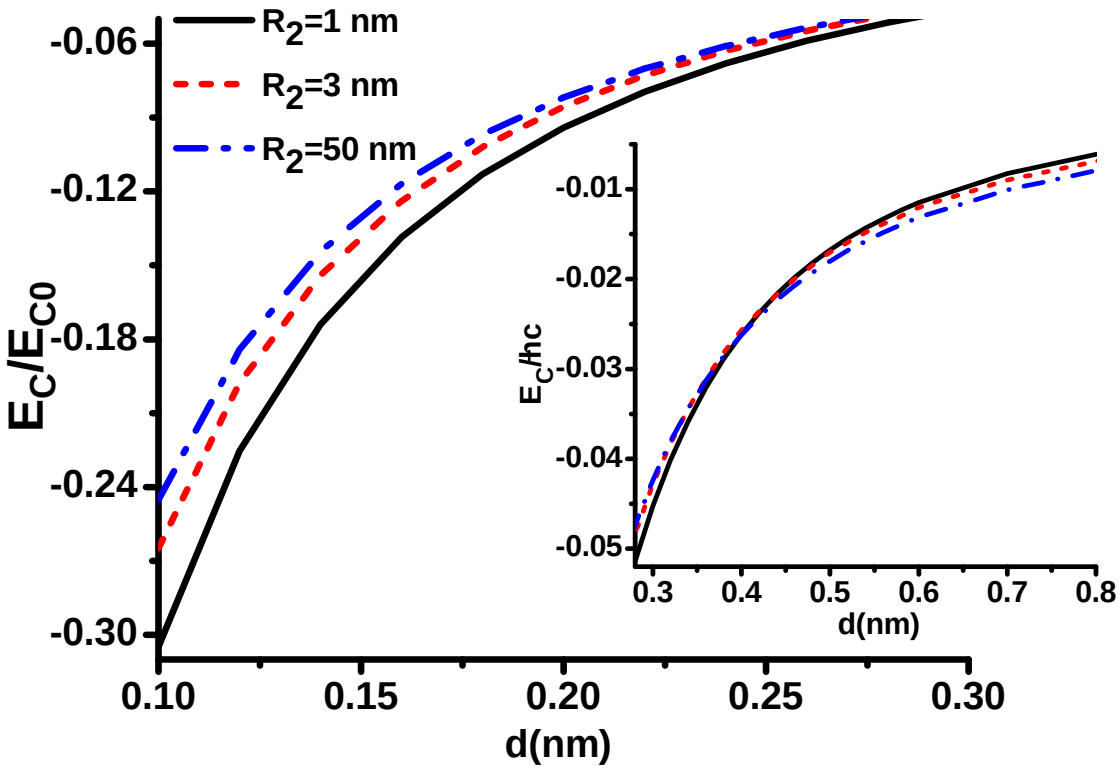

Figure 7.2 Dimensionless interaction energy as a function of surface-to-surface separation defined as $d = R - R_1 - R_2$. E_{C0} is defined as $\hbar cl / \pi R_1^2$. For all cases, $\varepsilon_1 = \varepsilon_2 = 2$ and $\varepsilon_3 = 15$.

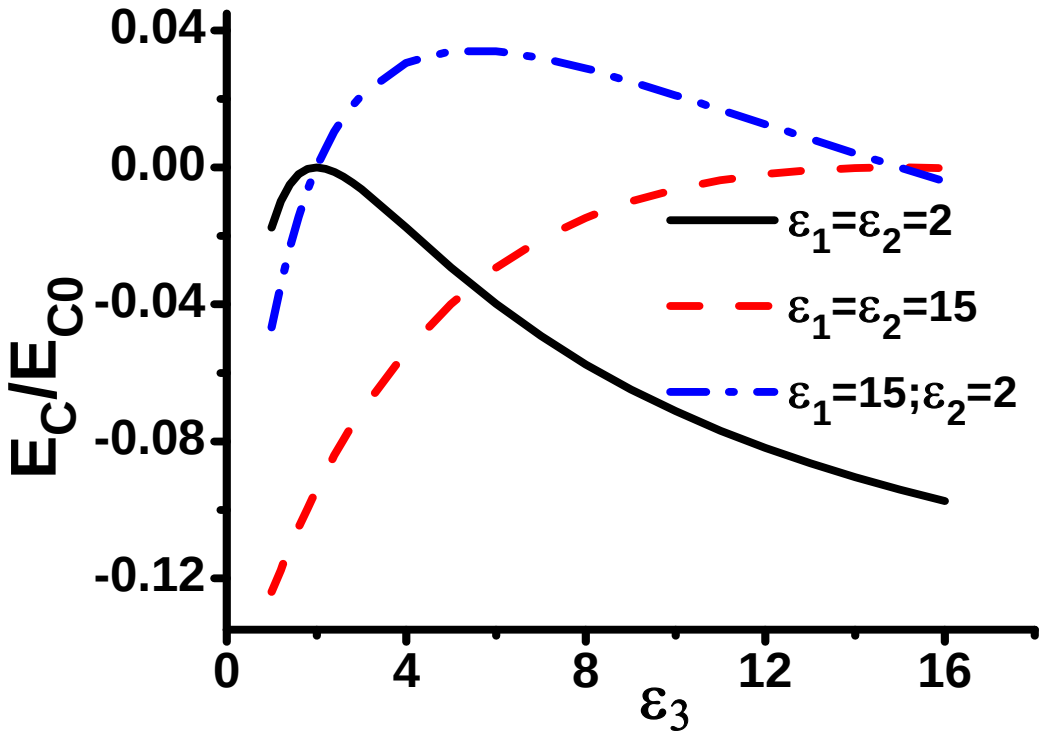

Figure 7.3 Dimensionless interaction energy as a function of the dielectric function of the medium. E_{C0} is defined as $\hbar cl / \pi R_1^2$. The cylinders have equal radii, $R_1 = R_2 = 1\,\text{nm}$ and center-to-center separation, $R = 2.2\,\text{nm}$.

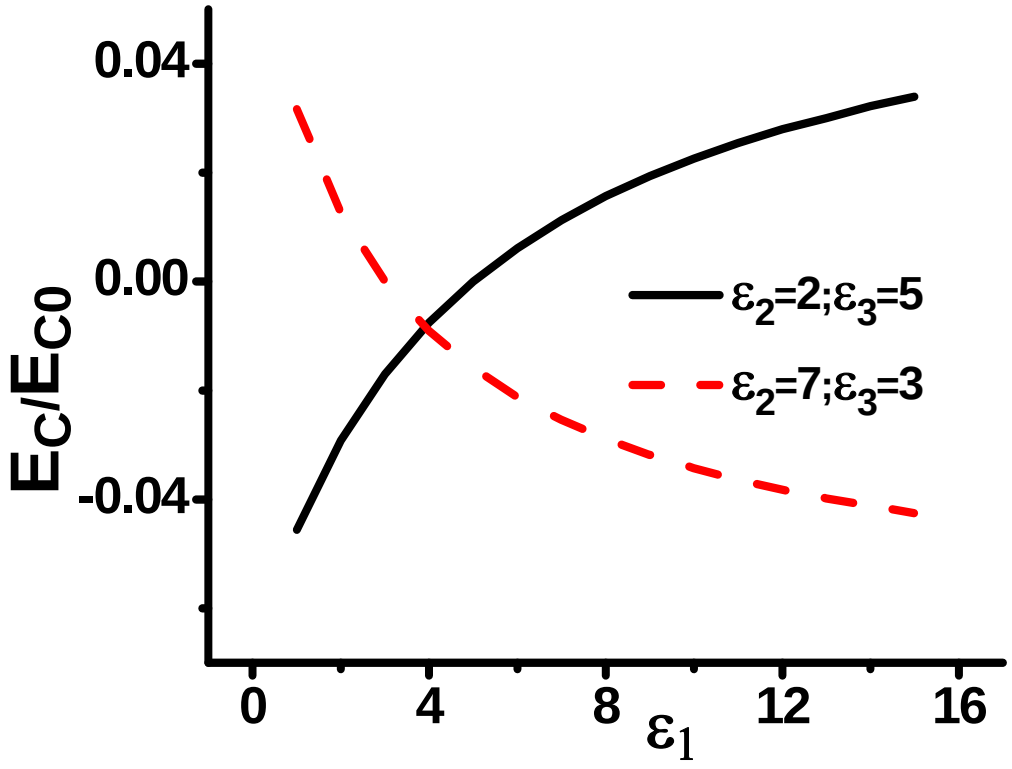

Figure 7.4 Dimensionless interaction energy as a function of the dielectric function of one cylinder. E_{C0} is defined as $\hbar cl / \pi R_1^2$. The cylinders have equal radii, $R_1 = R_2 = 1$ nm and center-to-center separation, $R = 2.2$ nm .

The results in Figures 7.3 and 7.4 are easily understood by realizing that the dominant contribution in E_C comes from the third and fourth terms in Equation (7.25) since $R_1 = R_2$. The rest of the terms are found to be at least one or more orders smaller. Thus the interaction energy will be dominated by the pre-factor $\xi = (\varepsilon_3 - \varepsilon_1)(\varepsilon_3 - \varepsilon_2)/(\varepsilon_1 + \varepsilon_3)(\varepsilon_2 + \varepsilon_3)$. For $\varepsilon_1 = \varepsilon_2$, ξ is always positive meaning that $E_C < 0$ and the corresponding force is attractive. This is what is shown in Figure 7.3 for $\varepsilon_1 = \varepsilon_2 = 2{,}15$. On the other hand, when $\varepsilon_1(\varepsilon_2) > \varepsilon_3 > \varepsilon_2(\varepsilon_1)$, the pre-factor ξ becomes negative, thus $E_C > 0$ which corresponds to a repulsive force. The maximum in E_C as a function of ε_3 is found when $\varepsilon_{3,\max} = \sqrt{\varepsilon_1 \varepsilon_2}$. This is seen on Figure 7.3, which shows that $\varepsilon_{3,\max} \approx 5.5$ for $\varepsilon_1 = 15, \varepsilon_2 = 2$.

Another very important scenario that yields positive Casimir energy is when we change the composition of one (or both) cylinders while keeping the medium fixed. This case is shown in Figure 7.4 where for $\varepsilon_2 = 2$ and $\varepsilon_3 = 5$ $E_C > 0$ as long as $\varepsilon_1 > \varepsilon_3 > \varepsilon_2$ is satisfied. Also, for $\varepsilon_2 = 7$ and $\varepsilon_3 = 3$, $E_C > 0$ when $\varepsilon_2 > \varepsilon_3 > \varepsilon_1$ is satisfied. Furthermore, since the pre-factor ξ controls the magnitude of the interaction energy, when the dielectric constants of the cylinders and the environment are such that $\varepsilon_1 - \varepsilon_3$ and $\varepsilon_2 - \varepsilon_3$ are small, $|E_C|$ is also small in magnitude. However, when the dielectric properties are very different in value, then $|E_C|$ becomes large.

CHAPTER 8

EXCITON-PLASMON INTERACTION IN CARBON NANOTUBES

8.1 Fundamental Effects of Long Range Interactions

An emerging area of research in carbon nanotubes is that of opto-electronics. The interest in carbon nanotube opto-electronics arises because nanotubes have several properties that make them excellent opto-electronic materials. For instance, an important characteristic of opto-electronic materials is the presence of a direct bandgap which allows electronic transitions between the valence and conduction bands to proceed without the intervention of phonons. Carbon nanotubes are materials possessing direct band gaps, thereby allowing multiple bands to participate in opto-electronic events spanning a wide range of energies. The purpose of this chapter is to investigate the viability of carbon nanotubes as candidates for novel opto-electronic devices. The work is characterized in three aspects: (1) the problem is formulated by bringing an excited atom in the vicinity of a carbon nanotube; (2) the electronic structure of carbon nanotubes, and (3) the dielectric response of carbon nanotubes. The first part is conceived by defining a Hamiltonian and this was done by Dr. Igor Bondarev [43]. The second and third parts were my work and helped us gain an understanding to carbon nanotubes used in opto-electronic devices.

Quasi-one dimensional structures such as nanowires and carbon nanotubes exhibit many-body effects that dominate their optical properties. The most important aspect of many-body effects in optical properties are excitons, which are electron-hole pairs bound by the Coulomb interaction. The excitation of an electron across the bandgap by the absorption of a photon leaves behind a positively charged hole and they both experience a Coulomb interaction that leads to a bound state where the exciton and hole are separated by the exciton radius. The evidence of the importance of excitons in carbon nanotubes has come from both experiment and theory. On the theoretical front, *ab initio* calculations of the optical spectra of carbon nanotubes including electron-hole interactions within the Bethe_Salpeter approach [88] has indicated a large exciton binding energy in semiconducting carbon nanotubes and even in metallic nanotubes. The optical absorption spectrum of semiconducting carbon nanotubes show a series of sharp and pronounced excitonic lines corresponding to bound excitons. The excitation exciton energies for different carbon nanotubes have already been reported [88], and we will be making use of the lowest exciton energies in this project. With the presence of excitons in carbon nanotubes already established, we proceed in investigating the contribution of long range interactions in carbon nanotubes.

In this section, we aim to demonstrate the fundamental effects of long-range interactions in carbon nanotubes, more specifically in the form of exciton-plasmon interactions in carbon nanotubes. The proposed interactions of excitonic states with surface electromagnetic modes of small-diameter semiconducting single-walled carbon

nanotubes can produce strong exciton-surface-plasmon coupling. Understanding of electromagnetic interactions between excitons and plasmons in molecular systems and spatially confined quantum systems, such as carbon nanotubes, is both of fundamental interest and of importance in the development of photonic and opto-electronic devices [89]. The interaction strength determines the absorption and emission properties of molecules coupled to nanostructures. The manufacture of nanostructures and control of their interaction in devices are some of the challenges researchers are facing today. Organic semiconductors, hybrid semiconductor-metal nanoparticle molecules and carbon nanotubes support excitonic states, created by the absorption of photons. Carbon nanotubes also support surface electromagnetic modes, both transversely polarized and longitudinally polarized. The longitudinally polarized surface electromagnetic modes are generated by the electronic Coulomb potential and result in the plasmonic excitations [90]. Due to the quasi-one dimensionality of the nanotube, the exciton quasi-momentum vector is directed predominantly along the nanotube axis and this corresponds to the longitudinal exciton. Since the surface plasmons are also directed along the propagation direction, they couple with the longitudinal excitons on the nanotube surface. It is therefore essential to consider the correct electronic structure of the carbon nanotube since the plasmonic nature of the nanotubes is related to their dielectric function.

8.2 Electronic Structure of Carbon Nanotubes (CNTs)

The electronic structure of any nanotube can be obtained within the π-band tight-binding (TB) model of graphene by folding the π-band along a certain direction [91].

However, experimental and theoretical calculations [92] suggest that hybridization of graphitic σ- and π- states should occur because of the curvature of the tubes. The curvature effects induce the mixing of the π- and σ- bands and these effects are found to alter significantly the electronic structure of nanotubes compared to the π-TB model [93].

The electronic structure of carbon nanotubes is studied within the sp^3 tight-binding model [91,94,95] and the random-phase approximation (RPA) [96]. More specifically, we use the sp^3 tight-binding model to calculate the electronic structure, and the random-phase approximation to evaluate the dielectric function. The $2p_z$ and ($2s$, $2p_x$, $2p_y$) orbitals in a CNT, respectively form the π- and σ- bands. The curvature effects result in the misorientation of the orbitals and therefore the mixing of the orbitals need to be taken into account in the calculations of the band structure.

The electron wavefunction of a carbon nanotube $\psi_{k,J}(r)$ can be represented as linear combinations of basis functions $\phi_{k,J}(r)$. In the tight-binding method, the basis functions are expressed by atomic orbitals which are centered on atoms with different position vectors. The representation of the electron wavefunction is expressed as:

$$\psi_{k,J}(r) = \sum_i c_{ki,J}\phi_{ki,J}(r) \tag{8.1}$$

Using the above representation in the one-electron equation of Schrodinger, one obtains the matrix equation for the coefficients $c_{ki,J}$:

$$\sum_{r'}(H_{klrr'} - E_{kl}^{J}S_{klrr'})c_{klr'} = 0 \tag{8.2}$$

In the orthogonal tight-binding models (π-TB), the overlap of the atomic orbitals centered on different atoms is ignored and the overlap matrix $S_{klr'}$ is approximated by a unit matrix [91]. However, it is clear that the overlap of orbitals on different atoms is not always negligible due to the curvature effects and the mixing of the orbitals. Here, the overlap is included in the non-orthogonal TB model and only nearest neighbors are taken into account [92]. Only zig-zag nanotubes are considered in our calculations and diagonalizing the matrix defined by Equation (8.2) yields the band structure of the nanotubes under consideration.

In this work, we consider the following semiconducting zig-zag nanotubes: (8,0), (10,0) and (11,0). After diagonalizing the matrix equations for these nanotubes, we obtained their respective band structures shown in Figures (8.1) – (8.3).

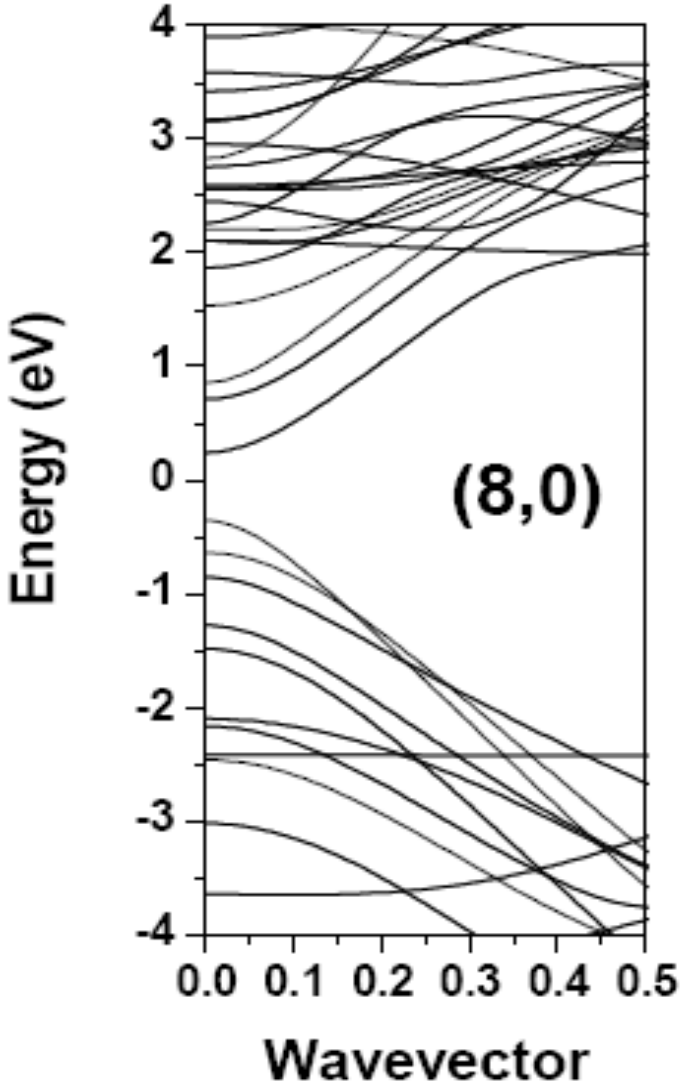

Figure 8.1 Band Structure of the (8,0) CNT.

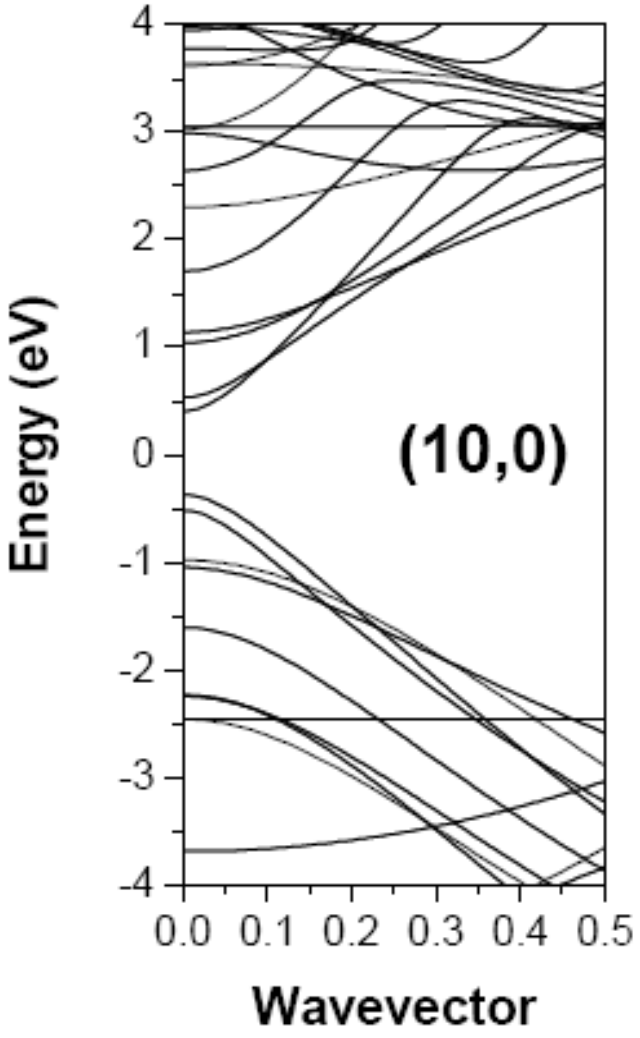

Figure 8.2 Band Structure of the (10,0) CNT.

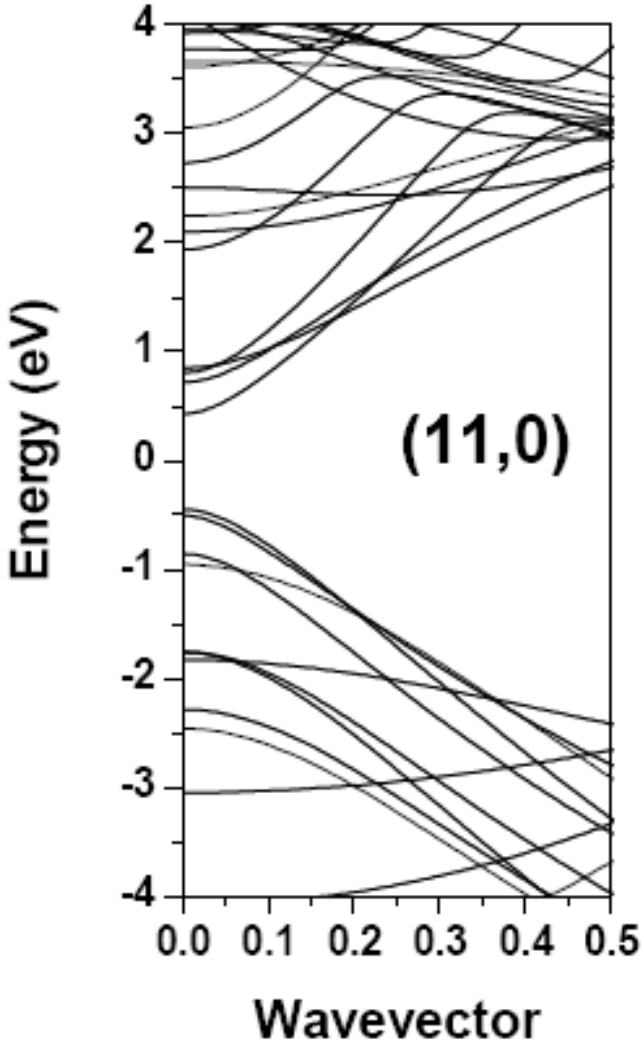

Figure 8.3 Band Structure of the (11,0) CNT.

8.3 Dielectric Response of Carbon Nanotubes (CNTs)

Now we have obtained the band structure of the nanotubes, we can make use of the eigenstates and energies to calculate the dielectric response using the random phase approximation (RPA). RPA is one of the most often used methods for describing the dynamic electronic response of systems. It is responsible for effects such as screening of external potentials (those responsible for scattering in the system) as well as for collective excitations of the free electron gas (plasmons in many body theory). The dielectric function within RPA is given as [96]:

$$\varepsilon(q,w,J) = \varepsilon_o - 4\pi e^2 I_J(qr)K_J(qr)\sum_{k,J}\frac{\left|\left\langle k+q,J\left|e^{-iq..r}\right|k,J\right\rangle\right|^2\left(n^F_{k+q,J}-n^F_{k,J}\right)}{E^J_{k+q}-E^J_k-\left(\hbar\omega+i\Gamma\right)} \tag{8.3}$$

where ε_o is the background dielectric constant; $I_J(qr), K_J(qr)$ are the modified Bessel functions of first and second kind of order *J* respectively; q is the momentum with dimensions *1/r*; *r* is the nanotube radius; ω is the frequency; Γ is the level broadening parameter; $\left|k,J\right\rangle$ is the electronic state described by energies E^J_k; and $n^F_{k,J}$ is the Fermi-Dirac distribution.

The electronic bands of single wall carbon nanotubes have been assigned by line group symmetry and their corresponding selection rules have already been derived [97]. The angular momentum *J* is found to be a good quantum number and serves as a band index as well [94]. According to the line group theory, the selection rules for the angular momentum *J* depend on the direction of the polarization. In the direction parallel to the

tube, the selection rule imposes $\Delta J = 0$ and in the direction perpendicular to the tube we have $|\Delta J| = 1$. Since only the interactions between longitudinally polarized surface electromagnetic modes and longitudinal excitons are considered in our calculations, due to the quasi-one dimensionality of the nanotubes, only the condition $\Delta J = 0$ is used in the evaluation of the dielectric function. The dielectric function, evaluated in both the real and imaginary realms, is expected to strongly depend on q and J. Electrons are excited from the occupied valence bands to the unoccupied conduction bands of the same J's. The results for both the real and imaginary parts of the dielectric function for the zig-zag nanotubes are shown in Figures (8.4) – (8.6).

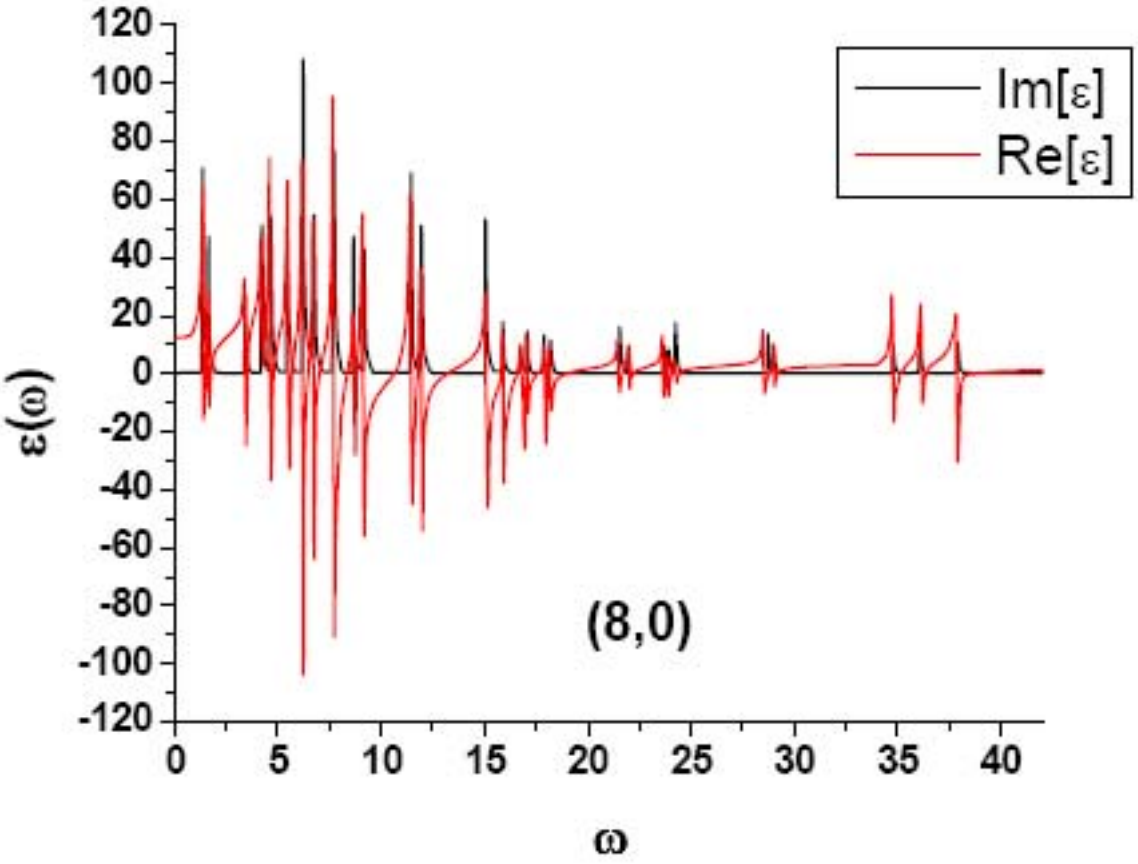

Figure 8.4 Dielectric Response of the (8,0) CNT. Frequency is measured in eV and the dielectric function is dimensionless.

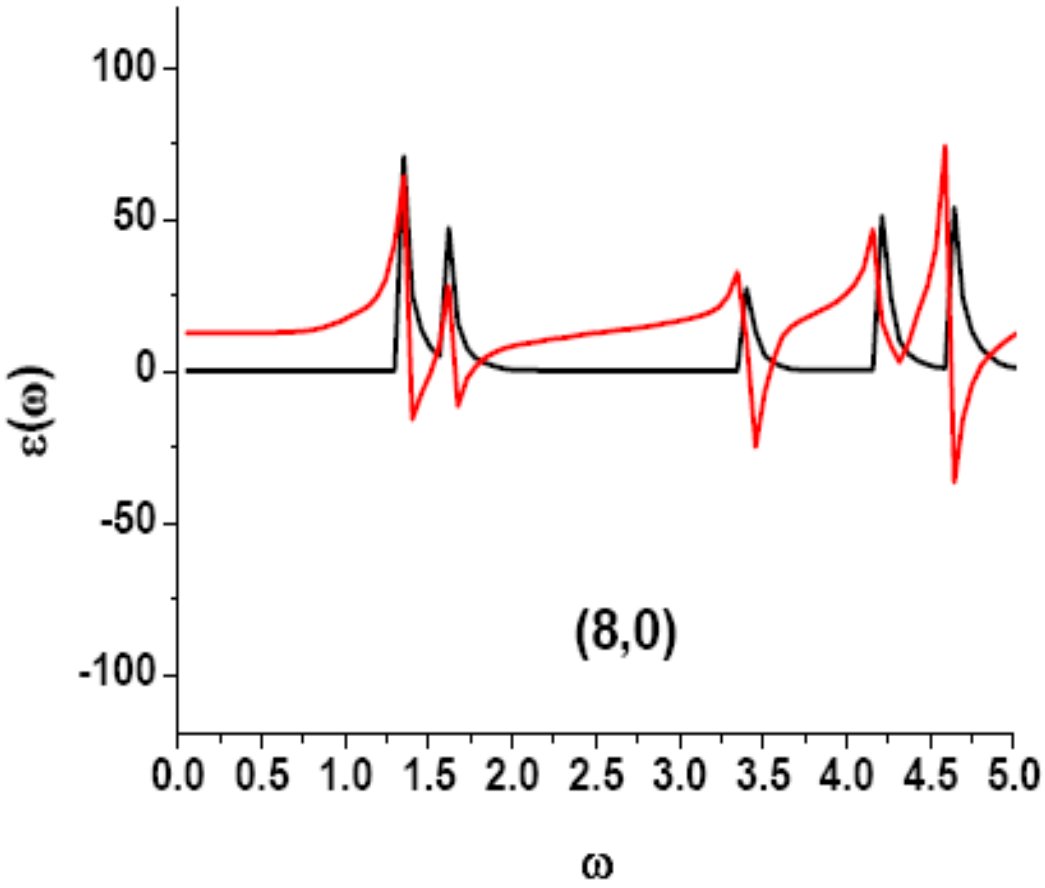

Figure 8.5 Dielectric Response of the (8,0) CNT in the low energy regime. Frequency is measured in eV and the dielectric function is dimensionless.

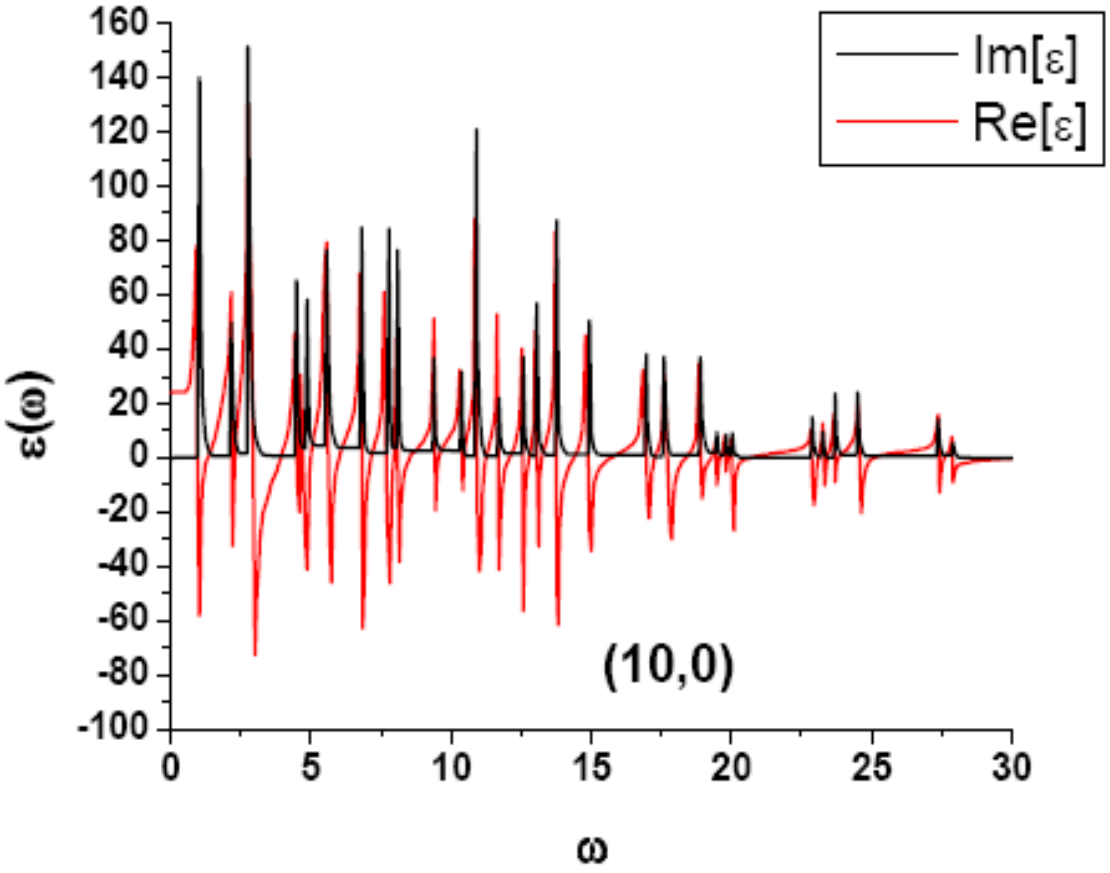

Figure 8.6 Dielectric Response of the (10,0) CNT. Frequency is measured in eV and the dielectric function is dimensionless.

8.4 Exciton-Plasmon Interaction in Semiconducting Single Wall CNTs

After obtaining the dielectric response of the semiconducting nanotubes, we can now proceed in demonstrating the exciton-plasmon coupling. In order to do so, we first need to find the conductivity of each nanotube and this is easily obtained from the dielectric function using the Drude relation. The plasmons are then located using the loss function $-\mathrm{Im}(1/\varepsilon)$ or $\mathrm{Re}(1/\sigma)$ measured in the electron energy loss spectroscopy (EELS) experiments to determine the properties of collective electronic excitations in solids [98]. The plasmons are defined by pronounced peaks occurring in the Plasmon density of states. We find that these peaks take place when the two conditions, $\mathrm{Im}(\sigma) = 0$ $(\text{or}\ \mathrm{Re}(\varepsilon) = 0)$ and $\mathrm{Re}(\sigma) \to 0$ $(\text{or}\ \mathrm{Im}(\varepsilon) \to 0)$ simultaneously and this is clearly shown in Figures (8.7) and (8.8) for the (11,0) and (10,0) nanotube respectively [42].

Figures (8.7) and (8.8) show the dimensionless conductivity as a function of dimensionless energy and it is observed that the plasmon peaks broaden as the nanotube radius decreases as a result of stronger hybridization effects in small diameter nanotubes [99]. The peaks in Figures (8.7) and (8.8) defined by the loss function $\mathrm{Re}(1/\sigma)$ clearly demonstrate the plasmonic nature of the CNT surface excitations.

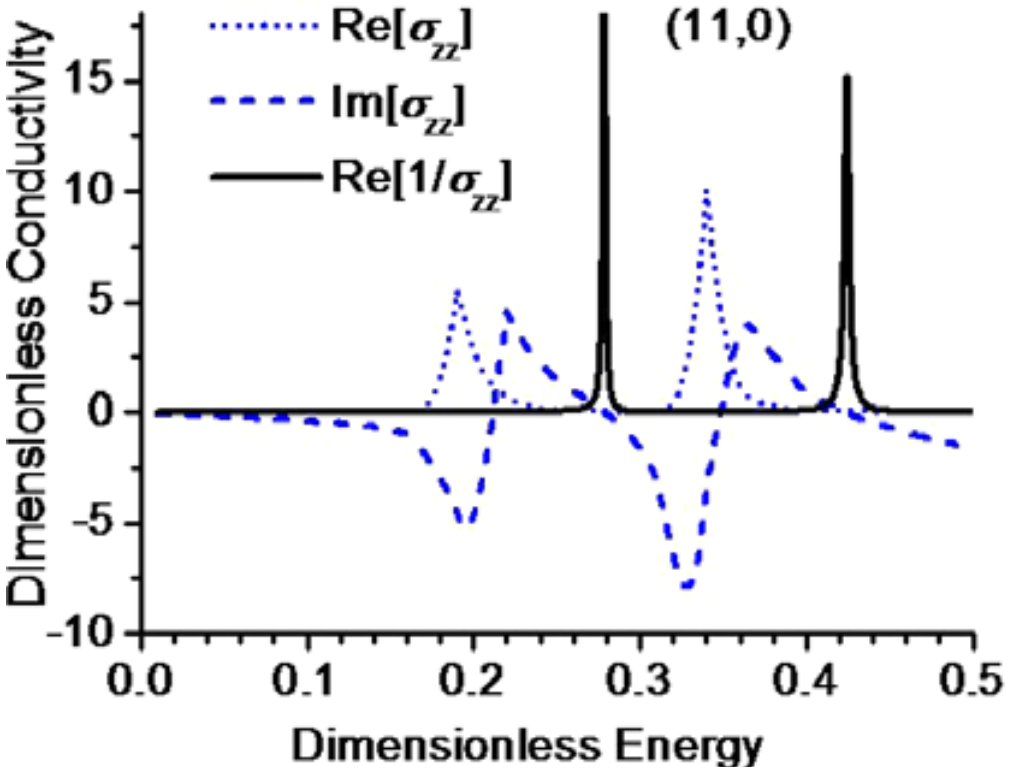

Figure 8.7 Dimensionless conductivity of the (11,0) CNT as a function of dimensionless energy.

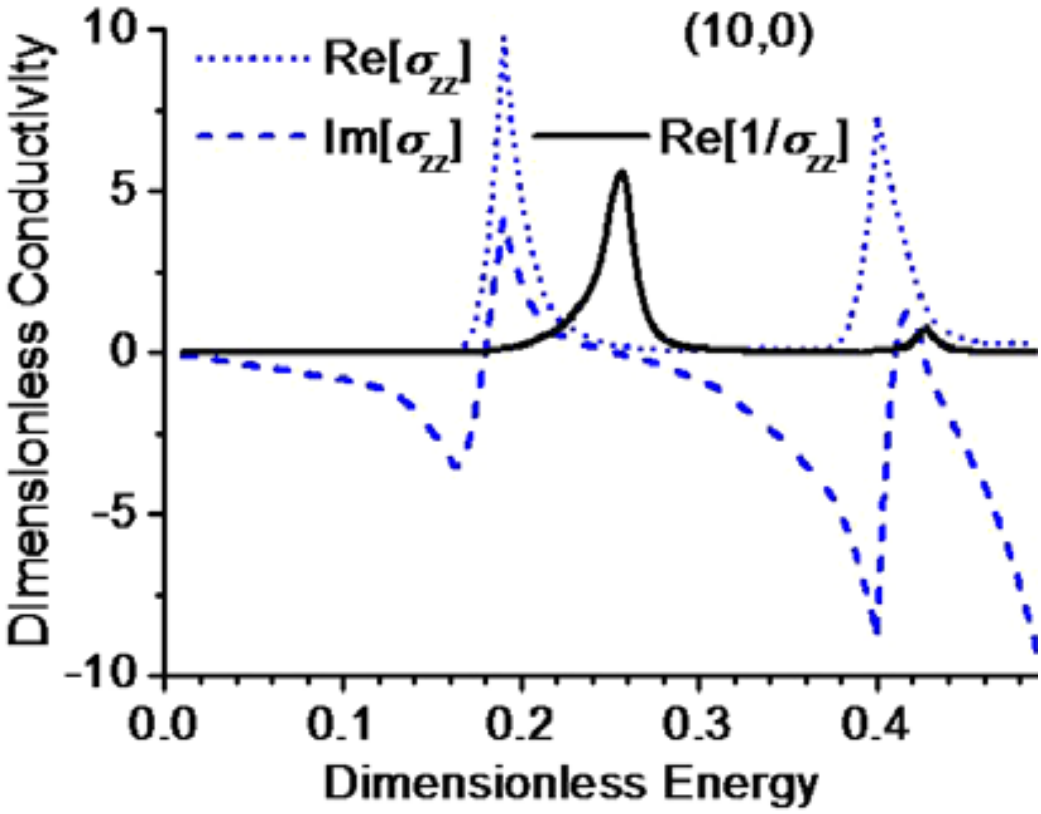

Figure 8.8 Dimensionless conductivity of the (10,0) CNT as a function of dimensionless energy.

Now that the plasmonic nature of the nanotubes is clear, we can proceed to show the exciton-plasmon coupling in small diameter semiconducting nanotubes. In order to examine the exciton-plasmon coupling, we need to examine the dispersion curves of the CNTs. In strong coupling regime, the mixing of exciton and plasmon states modifies the dynamics of the system and this appears as an anticrossing of the two coupled modes [42,43]. The dispersion curves are obtained by solving the dispersion equation as described in Ref. [42,43] and the dispersion curves are shown in Figures (8.9) and (8.10). The corresponding plasmon peaks are also shown in the figures. The upper branches in Figures (8.9) and (8.10) correspond to the plamon dispersion curve while the lower branches correspond to the exciton dispersion curve. Figures (8.9) and (8.10) clearly demonstrate an anticrossing behavior with (Rabi) energy splitting ~0.1 – 0.3 eV, thereby indicating a strong surface plasmon-exciton coupling. This coupling energy is almost as large as the typical exciton binding energies in similar CNTs (~0.3 - 0.8 eV) [100-103], and of the same order of magnitude as the exciton-plasmon Rabi splitting in organic semiconductors (~180 meV) [104]. This plasmon-exciton energy found here for the zig-zag nanotubes are however much larger than the exciton-polariton Rabi splitting in semiconductor microcavities (~140-400 μeV) [105-107], or the exciton-plasmon Rabi splitting in hybrid semiconductor-metal nanoparticle molecules [108]. The formation of the strongly coupled exciton-plasmon states is only possible if the exciton total energy is in resonance with the energy of the surface plasmon mode.

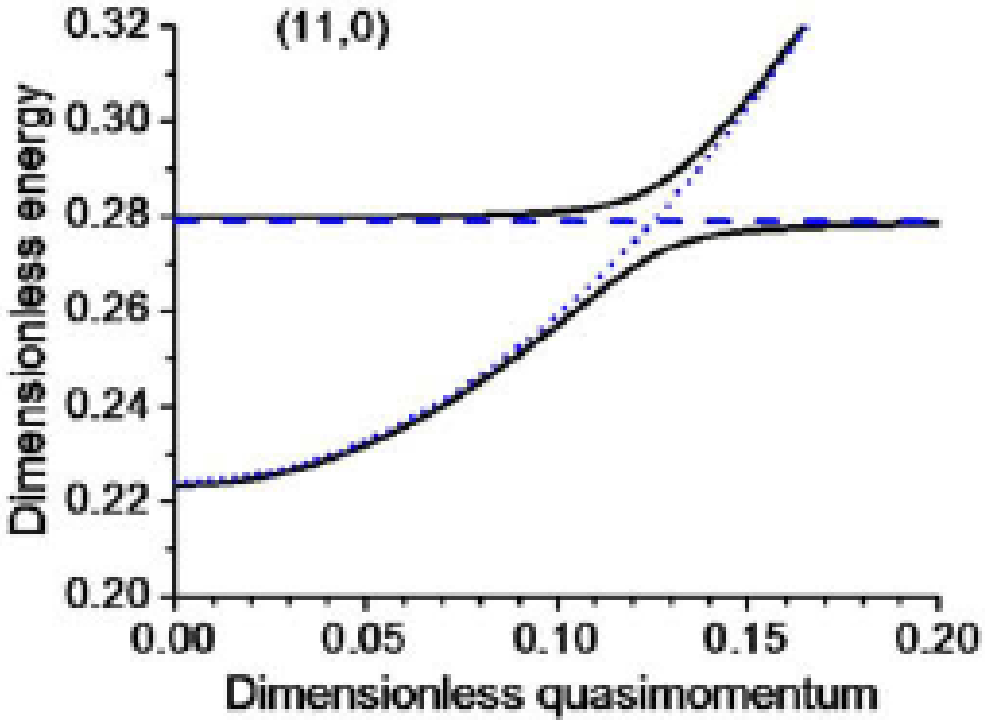

Figure 8.9 Dispersion curves of the exciton and plasmon for the (11,0) CNT.

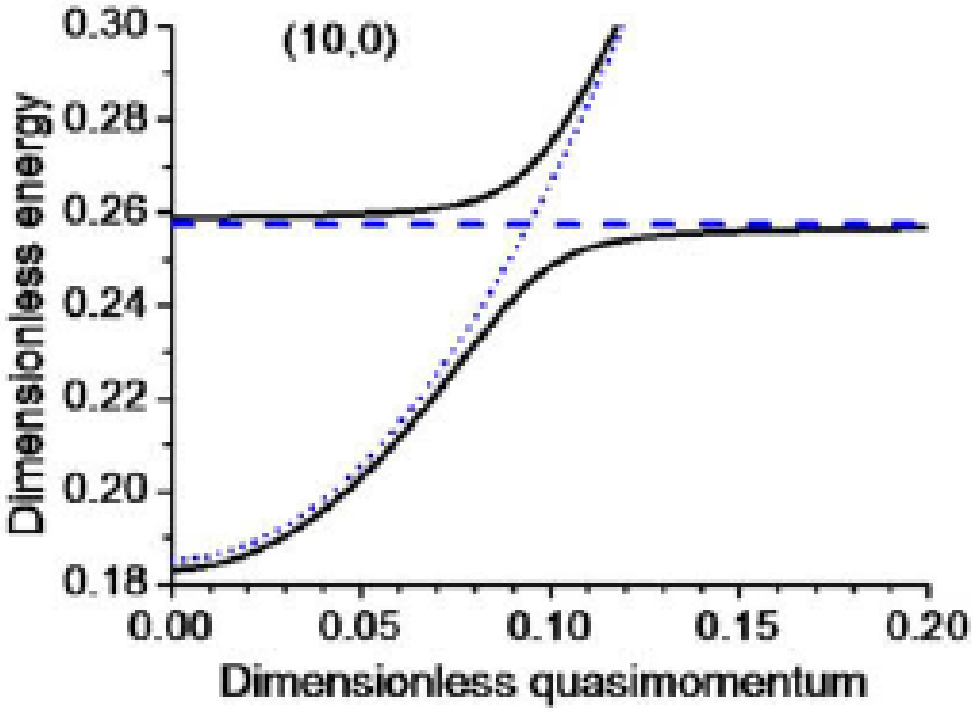

Figure 8.10 Dispersion curves of the exciton and plasmon for the (10,0) CNT.

CHAPTER 9
SUMMARY

9.1 Overview and Conclusion

In this dissertation, we were able to apply the concept of vacuum energy to cylindrical nanostructures using the mode summation method. The mode summation is one of the most convenient and elegant theoretical approaches used when it comes to cylindrical geometries. Although quantum electrodynamics offer a more advanced theoretical technique by taking into account realistic material properties, it becomes far too complicated when dealing with cylindrical geometries because of the large size of the Green's tensor that contains the information of dielectric and magnetic permeabilities. The theoretical challenge of applying the mode summation method to a new set of quasi-one dimensional cylindrical structures proved to be a successful one. In doing so, the Casimir energies of a cylindrical dielectric-diamagnetic layer, multiple cylindrical conducting shells and two straight, parallel dielectric-diamagnetic cylinders were calculated and finite and physically convergent numerical values were obtained. The models developed in this dissertation can provide a very important and novel insight to long range interactions in cylindrical nanostructures such as carbon nanotubes and nanowires. Although qualitative in nature, the models developed here could be of significant interest to experimental studies of cylindrical nanostructures.

In this work, analytical expressions and numerical calculations for various limiting cases were presented in terms of the radial dimension, curvature, and material composition of the cylinder or material. Various limits were investigated and the Casimir energy of certain structures were reproduced such as the Casimir energy of two parallel metallic plates derived by H. G. Casimir was retrieved here. Also, the fundamental effects of long range interactions were studied in the form of exciton-plasmon coupling in small-diameter semiconducting carbon nanotubes. In this section, we briefly mention the results achieved and the conclusions for the different cylindrical models considered.

9.2 Dielectric-Diamagnetic Cylindrical Layer of Finite Thickness

In this model, the Casimir interaction energy for a cylindrical layer with a finite thickness was calculated using the mode summation technique and with the Riemann ζ-function regularization procedure. The dielectric and magnetic properties of the layer and those of the surrounding medium were assumed to be described by real constant dielectric permittivities and magnetic permeabilities satisfying the relationship of constant speed of light across the interfaces. This method proves to be convenient and intuitively easy to follow. It is formulated in terms of only one parameter $\xi = (\varepsilon - \varepsilon_m)/(\varepsilon + \varepsilon_m)$ which allows us to make analytical and numerical evaluations for practically important limiting cases such as a dielectric-diamagnetic cylindrical layer as well as two concentric perfectly conducting thin shells.

The case of a dielectric-diamagnetic layer with $\xi << 1$ was considered and evaluated the first non-zero term $\propto \xi^2$ in the infinite sum representing the Casimir energy per unit length. The Casimir energy is negative, and it is $\propto -1/(R_2/R_1 - 1)^3$ in the limit $R_2/R_1 \to 1$. When $R_2 \to \infty$, the problem becomes equivalent to that of a dielectric-diamagnetic solid cylinder. The Casimir energy $\propto \xi^2$ for such a cylinder is zero [3,5], and here we recover this result for $R_2 \to \infty$. Also recovered was the Casimir energy per unit area of a dielectric-diamagnetic plate [74] in the limit of $R_1, R_2 \to \infty$ when $d = R_2 - R_1 = const.$

Another important case investigated was that of $\xi = 1$ describing two thin perfectly conducting concentric cylindrical shells. We find that the Casimir energy in this case is also negative and it is $\propto -1/(R_2/R_1 - 1)^3$ for $R_2/R_1 \to 1$, whereas for $R_2 \to \infty$ it approaches the limit of a single perfectly conducting cylindrical shell [3,5]. We also recover the well-known Casimir formula for the energy per unit area of two parallel perfectly conducting plates [7] separated by a distance $d = R_2 - R_1 = const$ in the limit of $R_1, R_2 \to \infty$.

9.3 *N* perfectly Conducting Cylindrical Shells

The Casimir energy of a system of *N* perfectly conducting, infinitely long cylindrical shells is also calculated by making use of the mode summation method. We present an expression for the Casimir energy of *N* shells and analyzed various limits for which the analytical expressions are known. The Casimir formula for the energy per unit area of two parallel perfectly conducting plates [7] separated by a distance $d = R_2 - R_1 = const$ in the limit of $R_1, R_2 \to \infty$ was recovered. Also analyzed was various limits in the case of three shells, and it was found that our result agrees with Ref. [84] in the limit of $R_1, R_2, R_3 \to \infty$ and $d_1 = d_2 = const$ where $d_1 = R_2 - R_1$ and $d_2 = R_3 - R_2$, in which case our system corresponds to three parallel plates. The case of *N* perfectly conducting concentric cylinders might be of particular interest as a qualitative model of the Casimir interactions in a multi-wall metallic carbon nanotube system. More thorough and realistic analysis is necessary to describe the Casimir interaction in multi-wall carbon nanotubes, by taking into account realistic electromagnetic properties.

9.4 Two Straight and Parallel Dielectric-Diamagnetic Cylinders

In this model, the Casimir energy for a system of two infinitely long parallel cylinders immersed in medium is calculated using the mode summation method. The analytical expressions derived are of particular importance for the Casimir energy dependence on the dielectric properties of the involved objects. The interaction energy is found to be positive (repulsive force) when the value of the dielectric constant of the medium is between the values of the dielectric constants of the two cylinders. This

particular result may be of significance to research efforts in quantum levitation or reducing friction between nanosized components in devices when cylindrical objects are involved. It is interesting to note that the relation $\varepsilon_1 > \varepsilon_3 > \varepsilon_2$ is the same for a repulsive force between planar systems as described in [38]. These calculations may be viewed as further evidence that the sign of the Casimir force can be manipulated by changing the dielectric response properties of the involved objects regardless of their geometry.

9.5 Exciton-Plasmon Coupling Effect

The fundamental effects of long-range interactions in carbon nanotubes (CNTs) have been studied in the form of exciton-plasmon interactions in CNTs. The interactions of excitonic states with surface electromagnetic modes of small-diameter semiconducting single-walled carbon nanotubes have been shown to produce strong exciton-surface-plasmon coupling. In order to obtain the exciton-plasmon coupling, the dielectric response of the nanotubes was first calculated using the random phase approximation (RPA) and both the real and imaginary parts of the dielectric function of zig-zag nanotubes were obtained. The band structure of the nanotubes was obtained by considering the nearest-neighbor non-orthogonal σ-π tight-binding model. The plasmonic nature of the semiconducting nanotubes was described by pronounced peaks in the plasmon density of state using the loss function. The clear anti-crossing behavior in the dispersion curves of the excitons and plasmons provided the evidence of the strong coupling effect.

REFERENCES

[1] S.Y.Buhmann and D.-G.Welsch, Progress in Quantum Electronics **31**, 51 (2007).

[2] M. Bordag, U. Mohideen, and V. M. Mostepanenko, Physics Reports **353**, 1 (2001).

[3] K. A. Milton, A. V. Nesterenko, and V. V. Nesterenko, Phys. Rev. D **59**, 105009 (1999).

[4] F. D. Mazzitelli, M. J. Sanchez, N. N. Scoccola, and J. von Stecher, Phys. Rev. A **67**, 013807 (2003).

[5] G. Lambiase, V. V. Nesterenko, and M. Bordag, J. Math. Phys. **40**, 6254 (1999).

[6] D. A. R. Dalvit, F. C. Lombardo, F. D. Mazzitelli, and R. Onofrio, Phys. Rev. A **74**, 020101 (2006).

[7] H. B. G. Casimir, Proc. K. Ned. Akad. Wet. **51**, 793 (1948).

[8] Y. Kim, H. Meyer, International Reviews in Physical Chemistry **20**, 219 (2001).

[9] M. C. Heaven, International Reviews in Physical Chemistry **24**, 375 (2005).

[10] R. Schmid, Monatshefte fur Chemie **132**, 1295 (2001).

[11] Y. A. Freiman, H. J. Jodl, Physics Reports **1**, 401 (2004).

[12] U. Tartaglino, T. Zykova-Timan, F. Ercolessi, E. Tosatti, Physics Reports **291**, 411 (2005).

[13] J. R. Henderson, Heterogeneous Chemistry Reviews **2**, 233 (1995).

[14] D. F. Lawler, Water Science and Technology **27**, 165 (1993).

[15] D. N. Thomas, S. J. Judd, N. Fawcett, Water Research **33**, 1579 (1999).

[16] T. Poppe, J. Blum, T. Henning, Advances in Space Research **23**, 1197 (1999).

[17] J. Xiao, B. Liu, Y. Huang, J. Zuo, K. C. Hwang, and M. F. Yu, Nanotechnology **18**, 395703 (2007).

[18] N.G. Chopra, R.J. Luyken, K.Cherrey, V.H. Crespi, M.L.Cohen, S.G. Louie, A. Zettl, Science **269**, 966 (1995).

[19] A. Popescu, L.M. Woods, I.V. Bondarev, Phys. Rev. B **77**, 115443 (2008).

[20] J. Cumings and A. Zettl, Science **289**, 602 (2000).

[21] P. Liu, Y. W. Zhang, and C. Lu, J. Appl. Phys. **97**, 094313 (2005).

[22] F. M. Serry, D. Walliser, G. J. Maclay, Journal of Applied Physics **84**, 2501 (1998).

[23] E. Buks, M. L. Roukes, Phys. Rev. B **63**, 033402 (2001).

[24] E. Buks, M. L. Roukes, Europhysics Letters **54**, 220 (2001).

[25] J. N. Israelachvili, Quarterly Reviews of Biophysics **6**, 341 (1974).

[26] V. A. Parsegian, *Van Der Waals Forces* (Cambridge, New York, 2006).

[27] D. van der Waals, *Die Kontinuitat des Garformigen und Flussigen Zustandes* (Amsterdam, 1881).

[28] F. London, Z. Phys. **63**, 245 (1930).

[29] S. K. Lamoreaux, Phys. Rev. Lett. **78**, 5 (1997).

[30] U. Mohideen and A. Roy, Phys. Rev. Lett. **81**, 4549 (1998).

[31] A. Roy, C. Y. Lin, U. Mohideen, Phys. Rev. D **60**, 111101 (1999).

[32] A. Roy, U. Mohideen, Phys. Rev. Lett. **82**, 4380 (1999).

[33] B. W. Harris, F. Chen, U. Mohideen, Phys. Rev. A **62**, 052109 (2000).

[34] F. Chen, B. Harris, A. Roy, U. Mohideen, International Journal of Modern Physics A **17**, 711 (2002).

[35] F. Chen, U. Mohideen, G. L. Klimchitskaya, V. M. Mostepanenko, Phys. Rev. A **72**, 020101 (2005).

[36] F. Chen, U. Mohideen, Journal of Physics A: Mathematics and General **39**, 6233 (2006).

[37] H. B. Chan, V. A. Aksyuk, R. N. Kleiman, D. J. Bishop, and F. Capasso, Science **291**, 1941 (2001).

[38] J. N. Munday, F. Capasso, and V. A. Parsegian, Nature **457**, 170 (2009).

[39] I. E. Dzyaloshinskii, E. M. Lifshitz, and L. P. Pitaevskii, Adv. Phys. **10**, 165 (1961).

[40] A. M. Fennimore, T. D. Yuzvinsky, W. Q. Han, M. S. Fuhrer, J. Cummings, A. Zettl, Nature **424**, 408-410 (2003).

[41] A. C. Dillon, M. J. Heben, Appl. Phys. A **72**, 133 (2001).

[42] I. V. Bondarev, K. Tatur, L. M. Woods, Optics Communications **282**, 661 (2009).

[43] I. V. Bondarev, L. M. Woods, K. Tatur, Phys. Rev. B **80**, 085407 (2009).

[44] M. S. Dresselhaus, G. Dresselhaus, R. Saito, Carbon **33**, 883 (1995).

[45] F. L. Shyu, C. P. Chang, R. B. Chen, C. W. Chiu, and M. F. Lin, Phys. Rev. B **67**, 045405 (2003).

[46] G. Bressi, G. Carugno, R. Onofrio, and G. Ruoso, Phys. Rev. Lett. **88**, 041804 (2002).

[47] E. Buks and M. L. Roukes, Phys. Rev. B **63**, 033402 (2001).

[48] I. Klich, J. Feinberg, A. Mann, and M. Revzen, Phys. Rev. D **62**, 045017 (2000).

[49] S. G. Mamaev and N.N. Trunov, Sov. Phys. J. **22**, 51 (1979).

[50] S. G. Mamaev and N. N. Trunov, Theor. Math. Phys. **38**, 228 (1979).

[51] Y. Sherkunov, Phys. Rev. A **72**, 052703 (2005).

[52] C. G. Shao, D. L. Zheng, and J. Luo, Phys. Rev. A **74**, 012103 (2006).

[53] K. Tatur, L. M. Woods, submitted to Phys. Rev. A (Rapid Communications).

[54] L. A. Girifalco, M. Hodak, R. S. Lee, Phys. Rev. B **62**, 13104 (2000).

[55] M. Schaden and L. Spruch, Phys. Rev. Lett. **84**, 459 (2000).

[56] R. L. Jaffe and A. Scardicchio, Phys. Rev. Lett. **92**, 070402 (2004).

[57] J. Blocki, J. Randrup, W. J. Swiatecki, and F. Tsang, Ann. Phys. **105**, 427 (1977).

[58] V. V. Nesterenko and I. G. Pirozhenko Phys. Rev. D **57**, 1284 (1998).

[59] M. E. Bowers and C. R. Hagen, Phys. Rev. D **59**, 025007 (1998).

[60] E. Abdalla, M. C. B. Abdalla, and K. D. Rothe, *Non-perturbative Methods in 2 Dimensional Quantum Field Theory* (World Scientific, Singapore, 2001).

[61] M. Bordag, G. L. Klimchitskaya, U. Mohideem, and V. M. Mostepanenko, *Advances in the Casimir Effect* (Oxford, New York, 2009).

[62] L. Dolan and R. Jackiw, Phys. Rev. D **9**, 3320 (1974).

[63] W. Dittrich and M. Reuter, *Lecture Notes in Physics: Effective Lagrangians in Quantum Electrodynamics* (Springer Verlag, Berlin, 1984).

[64] A. Das, *Finite Temperature Field Theory*, World Scientific Publishing, 1997).

[65] J. A. Stratton, *Electromagnetic Theory* (McGraw–Hill, New York, 1941).

[66] T.D.Lee, *Particle Physics and Introduction to Field Theory* (Harwood, New York, 1981).

[67] I. Brevik, J.Phys. A **15**, L369 (1982); I. Brevik, Can. J. Phys. **61**, 493 (1983).

[68] I. Brevik and H. Kolbenstvedt, Can. J. Phys. **62**, 805 (1984); I. Brevik and H. Kolbenstvedt, Can. J. Phys. **63**, 1409 (1985); I. Brevik and H. Kolbenstvedt, Phys. Rev. D **25**, 1731 (1982).

[69] J. Pritz and L.M. Woods, Sol. St. Comm. **146**, 345 (2008).

[70] Bo E. Sernelius, *Surface Modes in Physics* (WILEY-VCH, Berlin, 2001).

[71] I. Brevik, V. V. Nesterenko, and I. G. Pirozhenko, J. Phys. A **31**, 8661 (1998).

[72] K. A. Milton and Y. J. Ng, Phys. Rev. E. **55,** 4207 (1997).

[73] M. Abramowitz and I. A. Stegun, *Handbook of Mathematical Functions* (Dover, New York, 1972).

[74] I. Klich, A. Mann, and M. Revzen, Phys. Rev. D **65**, 045005 (2002).

[75] I.V.Bondarev, G.Ya.Slepyan, and S.A.Maksimenko, Phys. Rev. Lett. **89**, 115504 (2002).

[76] I.V.Bondarev and Ph.Lambin, Phys. Rev. B **70**, 035407 (2004).

[77] I.V.Bondarev and Ph.Lambin, Phys. Rev. B **72**, 035451 (2005).

[78] I.V.Bondarev and B.Vlahovic, Phys. Rev. B **74**, 073401 (2006).

[79] I.V.Bondarev and B.Vlahovic, Phys. Rev. B **75**, 033402 (2007).

[80] K. Tatur, L. M. Woods, I. V. Bondarev, Phys. Rev. A **78**, 012110 (2008).

[81] M. Zdrojek, T. Heim, D. Brunel, A. Mayer, T. Melin, Phys. Rev. B **77**, 033404 (2008).

[82] P.G. Collins, Ph. Avouris, Appl. Phys. A **74**, 329 (2002).

[83] F.D. Mazitelli, D.A.R. Dalvit, F.C. Lombardo, New Journal of Physics **8**, 240 (2006).

[84] H. Cheng, [hep-th] arXiv:0801.2810v1.

[85] Y. Zhang, W. E. Leithead, D. J. Leith, and L. Walshe, J. Comp. and Applied Math. **220**, 198 (2008).

[86] K. Tatur, L. M. Woods, Phys. Lett. A **372**, 6705 (2008).

[87] A. Erdelyi, W. Magnus, F. Oberhettinger, and F. G. Tricomi, *Tables of Integral Transforms*, (McGraw–Hill, New York, 1954).

[88] C.D. Spataru, S. Ismail-Beigi, R.B. Capaz, S.G. Louie, Phys. Rev. Lett. **95**, 247402 (2005).

[89] G. A. Wurtz, P. R. Evans, W. Hendren, R. Atkinson, W. Dickson, R. J. Pollard, and A. V. Zayats, Nano Letters, No.**5**, 1297 (2007).

[90] L. D. landau and E. M. Lifshitz, *The Clasical Theory of Fields* (Pergamon, New York, 1975).

[91] V. Popov and L. Henrard, Phys. Rev. B **70**, 115407 (2004).

[92] J. X. Cao, X. H. Yan, J. W. Ding, and D. L. Wang, J. Phys. Condens. Matter **13**, L271-L275 (2001).

[93] X. Blase, L. X. Benedict, E. L. Shirley, and S. G. Louie, Phys. Rev. Lett. **72**, 1878 (1994).

[94] C. W. Chiu, C. P. Chang, F. L. Shyu, R. B. Chen, and M. F. Lin, Phys. Rev. B **67**, 165421 (2003).

[95] S. C. Chen, W. C. Hseih, and M. F. Lin, Phys. Rev. B **72**, 193412 (2005).

[96] M. F. Lin, D. S. Chuu, and K. W. K. Shung, Phys. Rev. B **56**, 1430 (1997).

[97] M. F. Lin, Phys. Rev. B **62**, 13153 (2000); I. Milosevic, T. Vukovic, S. Dmitrovic, and M. Damnjanovic, Phys.Rev. B **67**, 165418 (2003).

[98] T. Pichler, M. Knupfer, M.S. Golden, J. Fink, A. Rinzler, R.E. Smalley, Phys. Rev. Lett. **80**, 4729 (1998).

[99] X. Blase, L.X. Benedict, E.L. Shirley, S.G. Louie, Phys. Rev. Lett. **72**, 1878 (1994).

[100] T. Pedersen, Phys. Rev. B **67,** 073401 (2003).

[101] T. Pedersen, Carbon **42**, 1007 (2004).

[102] R.B. Capaz, C.D. Spataru, S. Ismail-Beigi, S.G. Louie, Phys. Rev. B **74**, 121401. R (2006).

[103] F. Wang, G. Dukovic, L.E. Brus, T.F. Heinz, Science **308**, 838 (2005).

[104] J. Bellessa, C. Bonnand, J.C. Plenet, J. Mugnier, Phys. Rev. Lett. **93**, 036404 (2004).

[105] J.P. Reithmaier, G. Se_k, A. Löffler, C. Hofmann, S. Kuhn, S. Reitzenstein, L.V. Keldysh, V.D. Kulakovskii, T.L. Reinecke, A. Forchel, Nature **432**, 197 (2004).

[106] T. Yoshie, A. Scherer, J. Hendrickson, G. Khitrova, H.M. Gibbs, G. Rupper, C. Ell, O.B. Shchekin, D.G. Deppe, Nature **432**, 200 (2004).

[107] E. Peter, P. Senellart, D. Martrou, A. Lemaître, J. Hours, J.M. Gérard, J. Bloch, Phys. Rev. Lett. **95**, 067401 (2005).

[108] W. Zhang, A.O. Govorov, G.W. Bryant, Phys. Rev. Lett. **97**, 146804 (2006).

ABOUT THE AUTHOR

Kevin Tatur was born in the island of Mauritius in the Indian Ocean. He received his BS with honors in Physics at the University of Mauritius and his MS in Computer Science from the Griffith University in Australia. Kevin then joined the University of South Florida in 2006 where he received his MS in Physics and worked towards his Ph.D. degree in Physics. His work in the field of long range interactions has been published in high impact journals such as Physical Review A (Rapid Communications), Physical Review B, Physics Letters A, Optics Communications. Kevin also has various conference proceedings and has given presentations at important conferences. Kevin did an internship at the MOFFITT Cancer Center and Research Institute in a medical physics. He was trained in various aspects of medical physics and assisted board certified medical physicists in various duties.